

GENERATION OF REPUMPING LIGHT FOR ULTRACOLD STRONTIUM EXPERIMENTS

Bachelor's Honors Thesis

Erica Mason

Principal Investigator:
David M. Weld

University of California, Santa Barbara
Department of Physics
June 2013

I certify that this dissertation fulfills the requirements for the Bachelor's Honors Thesis in partial fulfillment of the requirements for the degree of Bachelor of Science in Physics from the University of California, Santa Barbara.

David M. Weld

I certify that this dissertation fulfills the requirements for the Bachelor's Honors Thesis in partial fulfillment of the requirements for the degree of Bachelor of Science in Physics from the University of California, Santa Barbara.

Carl Gwinn

I certify that this dissertation fulfills the requirements for the Bachelor's Honors Thesis in partial fulfillment of the requirements for the degree of Bachelor of Science in Physics from the University of California, Santa Barbara.

Ben Monreal

Abstract

Novel experimental capabilities have been introduced with the expansion of ultracold atomic experiments from alkali atoms to alkaline earth atoms, which boast a more complex electronic structure. However, laser cooling and manipulation of these atoms requires narrow light sources at a large number of wavelengths. In this undergraduate senior honors thesis I report the development of an architecture for flexible, stable, narrow-line external-cavity diode lasers (ECDLs) and a separate frequency-doubling module, both of which will be used to produce light at a variety of wavelengths for driving transitions in ultracold strontium. I describe the features of the ECDL design, the construction of the first such light source in our group (at 994nm), and the design of a resonant frequency-doubling setup for producing light at 497nm.

Acknowledgements

I will forever esteem and appreciate Dr. David M. Weld, unquestionably one of the smartest people I know. From teaching us that physics jargon can quite cleverly be used in colloquial conversation, to working through specific details of our projects, to teaching us life skills such as how to stand around awkwardly in order to encourage others' productivity, Dr. Weld has shared with my fellow undergrads and me his apparently infinite knowledge and wisdom. He trusts his undergraduate students beyond our wildest expectations. In providing me the opportunity to do this research and work in his lab, he has given me an experience that has become the absolute highlight of my undergraduate career.

My research during the summer of 2012 would not have been possible without the support of the Worsters. Thank you for supporting the Physics program and undergraduate summer research, and for giving me the opportunity to immerse myself in this project.

Vyacheslav “Slava” Lebedev began teaching me valuable lessons from the minute he joined the group; the first of these was that sometimes one must simply take a wrench to one's experiment. Although this destroyed a diffraction grating arm, learning to let go of my timidity and hesitation was a beautiful lesson. Slava's passion and enthusiasm about his newest finds or ideas and his eagerness to teach others is inspiring and greatly appreciated.

I want to thank Zach Geiger, who was a wonderful mentor throughout my summer of the Worster Fellowship. He is always available to answer questions or lend a hand. He also has excellent taste in humorous t-shirts. Ruwan Senaratne has likewise graciously shared with me his graduate student's experience and insight. Additionally, even though it's only been a short time, Kurt Fujiwara has already passed on wisdom and shared his support.

Very likely the hardest working and kindest person I've ever met, Shankari Rajagopal has been my confidant, friend, and commiserator. She has listened to me vent and worry, selflessly donated much of her time and energy to help me any time I got stuck or had a question, and even shared her graduate student library privileges. On top of this all, Shankari works magic with Mathematica. I will always look up to and be inspired by her.

Anne Hébert, who shares my deep love of coffee, chocolate, and \LaTeX , has been my partner in crime around Broida ever since we met in lab meeting one year ago.

Only together could we have made it through the early Saturday mornings in analog lab, the long evenings of particle homework sets, or the solid month of poring over GRE practice tests. I hope she knows what a true inspiration she is: Anne cares for and listens to others in the truest way, remains calm and composed no matter what happens, and is intelligent and accomplished beyond her years.

Alexander “Shura” Kotlerman, the recipient of blame for every misplaced tool in the lab, is a curious scientist, a caring friend, and a dedicated adventurer. From “trough” to “Campbell,” he is always an appreciated source of laughter.

The presentation skills and stage presence of Robert Salazar are awe-inspiring. Robert is friendly, kind, and truly brilliant. I appreciate Erik Anciaux for having been my thesis-writing sympathizer, and for sharing my appreciation of a good physics joke. Max Garber is an incredible machinist, and was a pleasure to work with in lab.

I am endlessly grateful for and appreciative of Dave Prine, and I am certainly not a lone holder of that sentiment. I have never seen anyone accomplish their job with such dedication. He is so attentive to each PO, he can recall the status of a specific order and frequently relays such details when we run into each other around Broida. Plus, an email from Dave Prine is a guaranteed day maker.

During the past summer, Eric Miller also constructed an ECDL for Dr. Ania Jayich’s lab. Thank you to both Eric and Dr. Jayich for their collaboration.

Of Dr. Ben Monreal, I am grateful for many things: for leading the Worster program and helping the other Worster fellows and me develop our presentation skills, for opting to be an additional faculty member at my thesis defense, and most importantly, for being a dedicated professor who cares deeply about his students’ educations.

The other faculty member of my thesis defense committee was Dr. Carl Gwinn, whom I would like to thank for his presence and his questions.

My sincerest appreciation to the Steck Group at the University of Oregon, not only for developing such a successful ECDL design, but also for both making it available for others to utilize, and being open to communication during my construction process.

A strength of the Physics Department at UCSB is its sense of community and collaboration, the benefits of which I was given the opportunity to experience multiple times. Thank you to both the graduate students of the Hansma Lab, who used their laser etching printer to create the acrylic prism alignment etching for my ECDL, as well as to the graduate students of the Bouwmeester Lab, for offering their time and equipment in allowing Zach and me to use their specturm analyzer.

Dr. David Cannell generously shared his laboratory space while the Weld Lab rooms were under construction. Incidentally, Dr. Cannell was the professor for my introductory physics courses during my first year at UCSB, and was one of the reasons I became inspired to study physics.

I wish to extend my gratitude to David Low, for his Mathematica and \LaTeX help, and for his sharing my enthusiasm at the beauty of a properly formatted plot.

To Jean Dill from her biggest fan: thank you for the support throughout my entire

undergraduate career, and for helping me navigate the registration difficulties, course requirement details, and especially completion of this thesis. I'd also like to thank the student administrative employees in the Physics Department office for not being bothered by my stopping by the office multiple times every day to take free chocolates (the chocolates made the many hours in Broida much more enjoyable).

Most deserving of my gratitude are my Mom, Dad, and sister. The past four years would have been impossible without their support, presence, love, and belief in me. Also, thank you Dad for helping edit this very, very long document. Thank you to my friends and to especially to Zack, for our undergraduate experiences both in and out of class and schoolwork.

Finally, my appreciation goes to all of the new members of the Weld Lab, for carrying on this exciting research.

Contents

Abstract	ii
Acknowledgments	iii
1 Introduction	4
2 ECDL	6
2.1 Theory	6
2.1.1 External Cavity Diode Lasers	6
2.1.2 Littrow Configuration	6
2.1.3 Feedback and Diffraction Gratings	7
2.1.4 Unibody Design	8
2.1.5 Components and Supplies	10
2.2 Construction	23
2.2.1 Machining	24
2.2.2 Wiring and Soldering	25
2.2.3 Cleaning	27
2.2.4 Other Pre-epoxy/Bake Tasks	28
2.2.5 Vacuum Safe Epoxying and Baking	29
2.2.6 Assembly	30
2.2.7 Testing	33
2.3 Results/Data	39
2.4 Future ECDL Work	40
3 Frequency Doubling Cavity	43
3.1 SHG Theory	43
3.1.1 Nonlinear Optics Overview	43
3.1.2 Gaussian Beams	46
3.1.3 Phase Matching	47
3.2 Cavity Design	52
3.2.1 The Nonlinear Crystal	52
3.2.2 Resonant Cavity	57
3.2.3 Spectral Parameters	57

3.2.4	Cavity Power Enhancement	59
3.2.5	Choice of Bow-tie Design	60
3.2.6	Impedance Matching	61
3.2.7	Astigmatism	66
3.2.8	Thermal Lensing	73
3.2.9	Acceptance Bandwidths	75
3.2.10	Optimizing the Cavity	76
3.3	Cavity Components	78
3.4	Future Doubling Cavity Work	78
4	Conclusions	80
A	Product numbers for ECDL components	81
A.1	Epoxies	81
A.2	Diffraction gratings	82
A.3	Electrical: protection circuit and wiring	82
A.4	Diode laser	83
A.5	O-rings	84
A.6	Screws/nuts/washers	84
A.7	Cleaning supplies	85
A.8	Piezo modulation	85
A.9	Temperature control	85
A.10	Components for beam output	86
A.11	Vacuum	86
B	Product numbers for cavity components	87
	Bibliography	89

List of Figures

1.1	Stontium level diagram [1]	5
2.1	Littrow configuration [2]	7
2.2	Diffraction grating diagram	7
2.3	Wavelengths accessible to the unibody design. [3]	9
2.4	Cavity body part drawing. [4]	10
2.5	Cavity body with components. [4]	11
2.6	Part drawings of baseplate and cavity body [3]	12
2.7	Photograph of bare aluminum unibody.	13
2.8	Photograph of ECDL body; diffraction grating.	15
2.10	Protection circuit diagram. [3]	17
2.9	Printed circuit board diagrams	17
2.11	Photograph of soldered and installed protection circuit.	18
2.12	Prism placement etching design. [3]	23
2.13	Photograph of wiring box	24
2.14	Diagrams of different laser diode pinouts	26
2.15	Diagram indicating wiring designation	27
2.16	Photograph of sonication.	28
2.17	Photograph of ECDL cavity; close-up of inserted piezo.	32
2.18	Photograph of ECDL cavity.	36
2.19	First order feedback using IR viewing card.	37
2.20	Photograph of oscilloscope power output vs. current applied.	38
2.21	Diagram of laser diode pinout for Power Technology laser diode.	39
2.22	Unibody ECDL with silicone cover. [4]	40
2.23	Photograph of completed ECDL and Arroyo controller	41
2.24	Photograph of Arroyo controller and wavemate readouts.	42
3.1	Gaussian beam incident on a crystal. [5]	47
3.2	Diagram of crystal axes. [6]	49
3.3	Diagram of birefringent walk-off. [7]	50
3.4	Diagram of periodic poling. [8]	51
3.5	Plot of amplitude of generated second harmonic field as a function of distance in the crystal. [8]	51

3.6	Refractive indices of KNbO_3 for noncritical phase matching.	53
3.7	Covesion, Inc. crystal [9]	55
3.8	Plot of spectral transmission as a function of wavelength, for different values of the finesse \mathcal{F} [5].	58
3.9	Plot of spectral transmission plot indicating the FSR and the FWHM [10].	58
3.10	Ring resonator [11]	61
3.11	Bow-tie cavity [5]	62
3.12	Plot of power reflected from cavity vs. reflectance of incoupling mirror.	63
3.13	Diagram of bow-tie cavity.	64
3.14	AR curve for MgO:LN [9]	65
3.15	Bow-tie cavity reduced to equivalent setup of lenses. [5]	67
3.16	Bow-tie cavity reduced to equivalent setup of lenses and mirrors. [5]	67
3.17	Plots of beam waists vs. distance between spherical mirrors.	70
3.18	Plot of beam waist in the crystal for different cavity geometry; fold beam path to minimize astigmatism.	71
3.19	Plot of beam waist between the spherical mirrors with and without crystal.	71
3.20	Diagram of bow-tie cavity reproduced.	72
3.21	Diagram of thermal lensing modeled by 8 thin lenses along crystal.	74
3.22	Flowchart for optimizing the cavity.	77

Chapter 1

Introduction

Ultracold atoms serve numerous purposes in experimental physics. They act as a controlled, precise analog to electrons in ionic lattices, allowing the study of many-body quantum mechanical systems. Ultracold atom systems are also ideal for investigating the quantum dynamics of single- and multi-component systems. Additionally, they can be used in quantum-limited force sensing, applicable to the study of non-Newtonian gravitational interactions at small length scales.

Until recently, these types of ultracold atom experiments have mainly utilized single-valence-electron atoms; lithium is a primary example. Experimentalists have lately broadened their toolboxes to include multi-valence electron atoms, such as strontium. By nature of having more complex electronic structure, these multi-valence electron atoms come with more complicated requirements for cooling, trapping and imaging; there are more electronic transitions to address. Numerous finely tuned lasers are used to address these transitions.

The $^1S_0 - ^1P_1$ transition, which is used for optical cooling, is not completely cyclic. The excited state exhibits some loss to the metastable 3P_J states. The atoms must be returned to the 1S_0 state, and there are multiple methods for doing so. One option is a two-laser system of a 707nm and a 679nm laser with resonant transitions $^3P_J - ^3S_1$. Another option is a 3.0 μ m laser addressing the $^3P_2 - ^3D_2$ transition. The third option, which the Weld Lab has utilized, is a 497nm laser addressing the $^3P_2 - ^3D_J$ transitions [12]. This 497nm repumper has the benefit of being a single-laser system, but has the disadvantage that it isn't a commercially available laser diode wavelength. Instead, a 994nm laser can be frequency doubled to achieve the 497nm resonant wavelength. This is the method we opted for, and the development of this 497nm light is the ultimate goal of the project described by this thesis. The level diagram for cooling strontium, using the 497nm repumping transition, is shown in Fig 1.1.

The linewidth of this transition is $\Gamma/2\pi=2.3\text{MHz}$, and its intensity of saturation is $I_{sat}=2.4\text{mW}/\text{cm}^2$ [13]. Therefore, only a few milliwatts of 497nm light are needed, but the source must be precise and stable, and have linewidth narrower than 2.3MHz.

Free-running laser diodes are too imprecise for a repumping source. Gas lasers

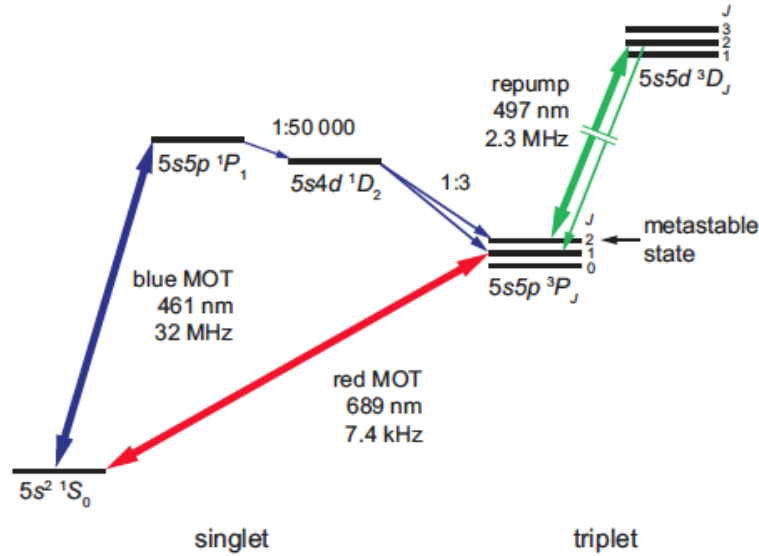


Figure 1.1: Strontium level diagram [1]

exist at limited wavelengths, and these often differ from those required for atomic cooling. Therefore, a common solution for attaining lasers of the necessary precision and stability is to use a grating-stabilized external-cavity diode laser (ECDL). ECDLs can achieve sub-100kHz linewidth by feeding a portion of the laser’s output back into itself. They also incorporate electronic control and stabilization into their design.

ECDLs can be purchased, but are often expensive. Considering that the Weld Lab needs multiple ECDLs at varying wavelengths in the foreseeable future, it is beneficial to develop a design and process for in-house, wavelength adaptable construction.

The ECDL design chosen is the “unibody” design, developed by and freely available from the Steck Group at the University of Oregon [4]. Their design provides numerous benefits, including long- and short-term stability, reduced sensitivity to acoustic perturbation, and a sufficiently narrow linewidth.

The first chapter of this thesis describes the construction of the Weld Lab’s first in-house built ECDL for 994nm light, to be frequency doubled to address the 497nm strontium repumping transition. It is meant to provide instructive information and suggestions for future ECDL projects.

The second chapter of this thesis describes the research, design and calculations for the frequency doubling of this 994nm light. Due to limitations on time, the construction and testing of this nonlinear optical cavity were not reached, and are not covered in this thesis. The second chapter serves as a presentation of the theory of Second Harmonic Generation (SHG) and as an explanation of doubling cavity design and calculations. It is hoped that this chapter can serve as a foundation for future frequency conversion processes in the Weld Lab.

Chapter 2

ECDL

This chapter documents the construction of a Littrow-configuration grating-stabilized ECDL based on the unibody design by the Steck Group [4]. This 994nm ECDL is the first of its kind for the Weld Group, and serves as instruction for constructing future ECDLs based on this design at other wavelengths.

2.1 Theory

2.1.1 External Cavity Diode Lasers

Narrow linewidth light sources tuned to specific atomic transitions are necessary for many atomic physics experiments. ECDLs are a suitable solution; they are stable, tunable, and can achieve low spectral linewidth through optical feedback, temperature control, and locking.

2.1.2 Littrow Configuration

Many frequency selective feedback lasers utilize diffraction gratings in either the Littrow configuration or the Littman-Metcalf configuration. The design that I use is in the Littrow configuration. As illustrated in Fig. 2.1, the Littrow configuration entails that the cavity is bounded by the laser diode on one end and the diffraction grating on the other; the first order diffracted beam from the grating is coupled back into the laser diode to achieve optical feedback. The directly reflected beam provides the output. Changing the length of the cavity, which can be done in this design by changing the angle of the grating arm, tunes the wavelength of the emitted light.

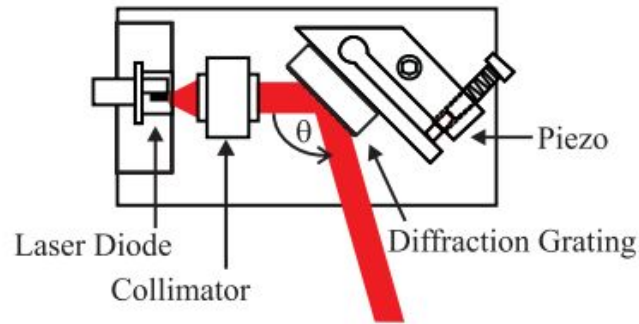


Figure 2.1: Littrow configuration [2]

2.1.3 Feedback and Diffraction Gratings

A beam incident on a diffraction grating has a specularly reflected beam, as it would from a reflecting surface ($\alpha_{incident} = \alpha_{reflected}$), and also has diffracted beams at angles $\beta_1, \beta_{-1}, \beta_2, \beta_{-2}...$ from normal to the grating surface. This is illustrated in Fig. 2.2.

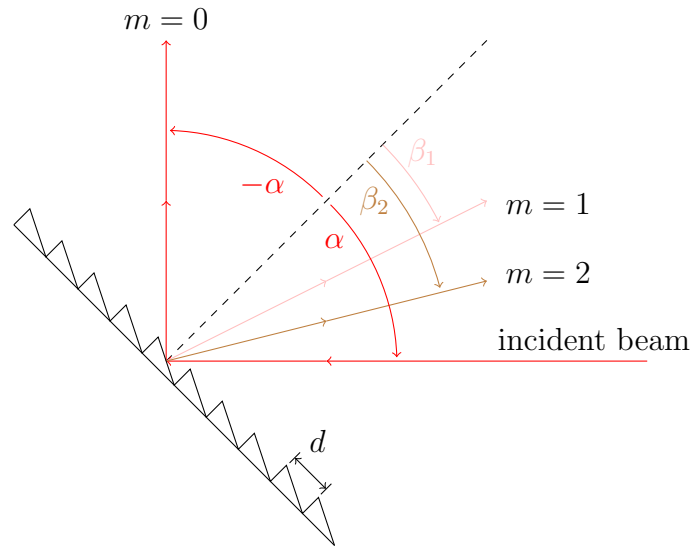


Figure 2.2: Beams reflected and diffracted from a diffraction grating.

The diffraction grating equation is: $m\lambda = d(\sin\alpha + \sin\beta_m)$, where d is the grating spacing, α is the angle of the incident beam from normal to the grating surface, and β_m is the angle of the m^{th} order diffracted beam from normal to the grating surface [14]. In the Littrow configuration, $\alpha = \beta$ for the first order ($m = 1$), so the equation simplifies to:

$$\lambda = 2d\sin\alpha \quad (2.1)$$

The cavity body is designed with the grating arm positioned at $\alpha = 45^\circ$, and can withstand only small deflections. Therefore, the ideal grating spacing ($1/d$) is calculated for $\alpha = 45^\circ$: $1/d = \sqrt{2}/\lambda$ (Eq. 2.1 rearranged). Diffraction gratings are not available with spacings in a continuous range, and so the closest to this ideal grating spacing is purchased, and the arm angle adjusted accordingly.

Diffraction gratings can be manufactured in two ways: ruled or holographic. Ruled gratings are mechanically manufactured by burnishing individual grooves with a diamond tool against a thin coating of evaporated metal applied to the surface. Holographic gratings are manufactured non-mechanically, by recording a stationary interference fringe field in photoresist. These are also known as “interference gratings” [14]. Either can be used, but often certain spacings are only available in one type.

2.1.4 Unibody Design

There are many existing designs for ECDLs that can be built in-house, yet the design by the Steck Group [4] provides numerous features and benefits unmatched by other designs. The Steck Group’s design, fully documented and publicly accessible, is set apart by its “unibody” design: the body is machined from a single aluminum block, a feature which renders it robust against temperature changes and mechanical vibrations. Even the diffraction grating arm is machined as part of the main cavity aluminum block, making it stiff and light so that it suppresses low-frequency mechanical resonances.

The design includes vacuum seal capability in order to prevent condensation and reduce sensitivity to humidity and pressure fluctuations [4]. It also integrates beam shaping optics, an optical isolator, and fiber coupling into the unibody design. Data from the Steck Group’s ECDLs shows that the design is capable of exceeding the specifications of similar commercial ECDLs [4].

This design is stable, has a low passive spectral linewidth, and is adaptable to wavelengths common to ultracold atom experiments; the only alterations necessary are a different diffraction grating and different beam-shaping prisms. The ECDL body is designed such that gratings relevant to common atomic physics wavelengths are compatible with the geometry of the cavity [4]. Fig. 2.3 shows the wavelengths for which this design is possible.

Finally, the design is inexpensive and designed for ease of in-house construction. Fig. 2.4 shows the main cavity body component of the unibody design, and Fig. 2.5 is a diagram of the assembled body and additional components.

The Steck group’s unibody ECDL design includes the option for either a long or short cavity, identical except for the cavity extension. The benefit of the long cavity is reduced white noise to the linewidth, but it also causes a decreased free spectral range (FSR), which reduces the mode-hop free tunability [4]. Therefore, the Steck group suggests to use the short design unless an exceptionally narrow linewidth is required [3].

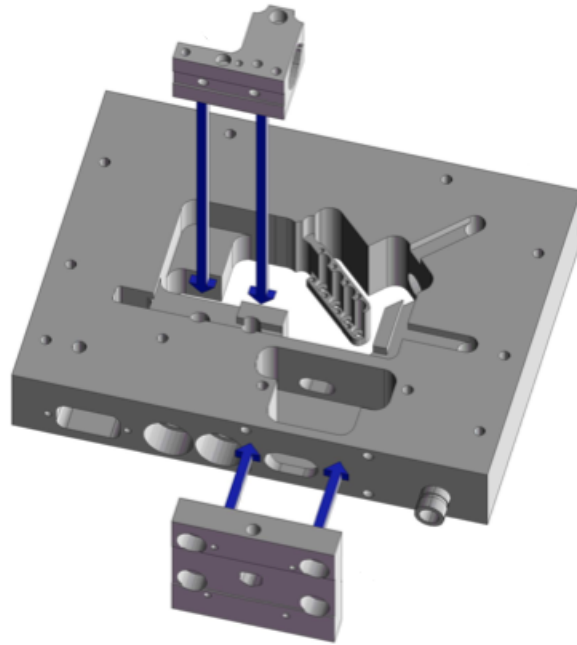


Figure 2.4: Part drawing of the cavity body, optical isolator housing, and laser diode housing, from Steck et. al. [4].

2.1.5 Components and Supplies

The following is a comprehensive list of the peripheral components and supplies that go into this ECDL design. Within this list, the use, purpose, component details, practical issues and suggestions for each component will be discussed and explained. See Appendix A for the part numbers and further specifications for all the ECDL components.

Aluminum body:

The aluminum body consists of six parts: the base plate, bottom cover, cavity body (see Fig. 2.4), top cover, laser diode housing, and optical isolator housing. All are machined from 6061-T6 aluminum. Note: This ECDL uses the Steck group’s short cavity design. Machine drawings can be found on the Steck Group webpage [3] or through links on the Weld Group “ECDL Project” wiki page.

After having constructed an ECDL, I would suggest a few potential design improvements for the baseplate and for the cavity body. The baseplate and cavity body part drawings can be found in Fig. 2.6. Fig. 2.7 shows a photograph of a base aluminum body.

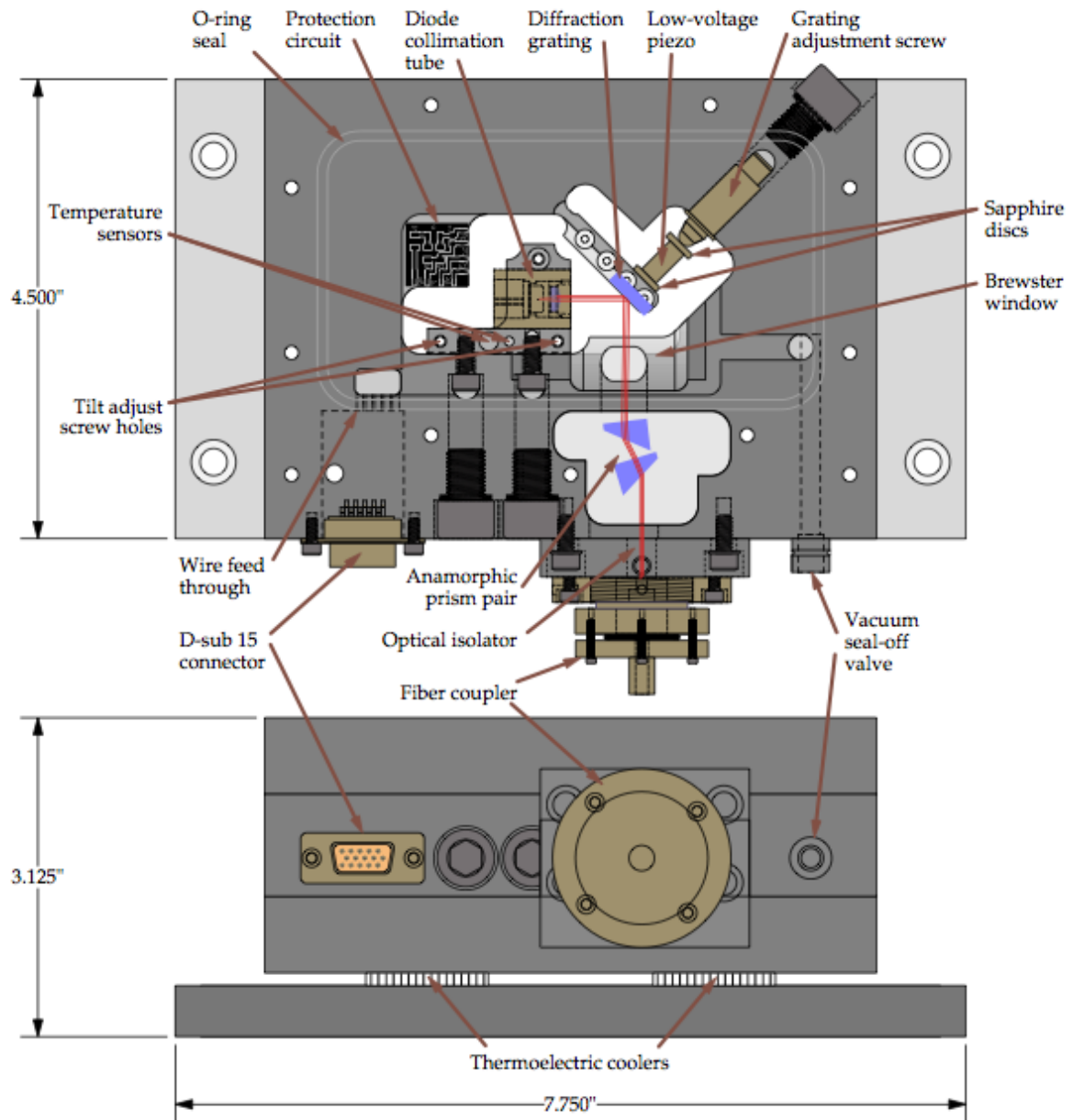
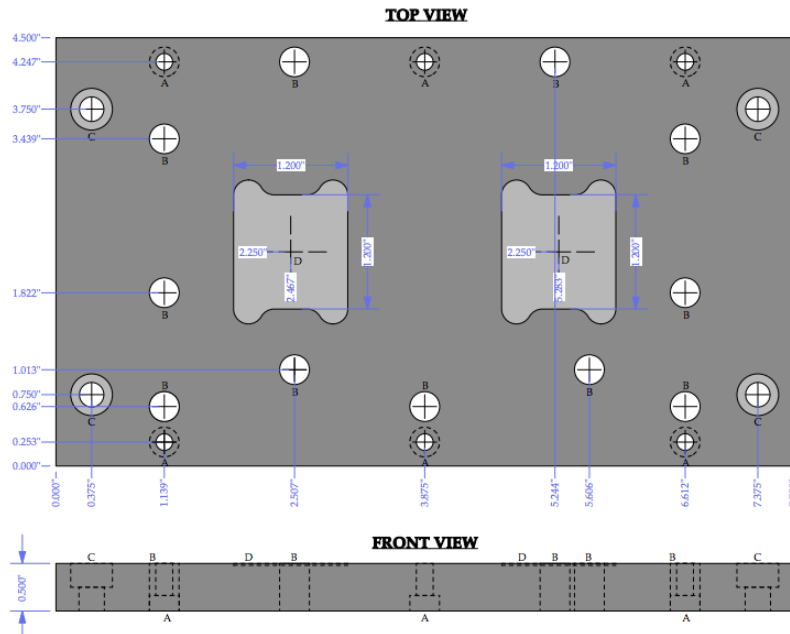
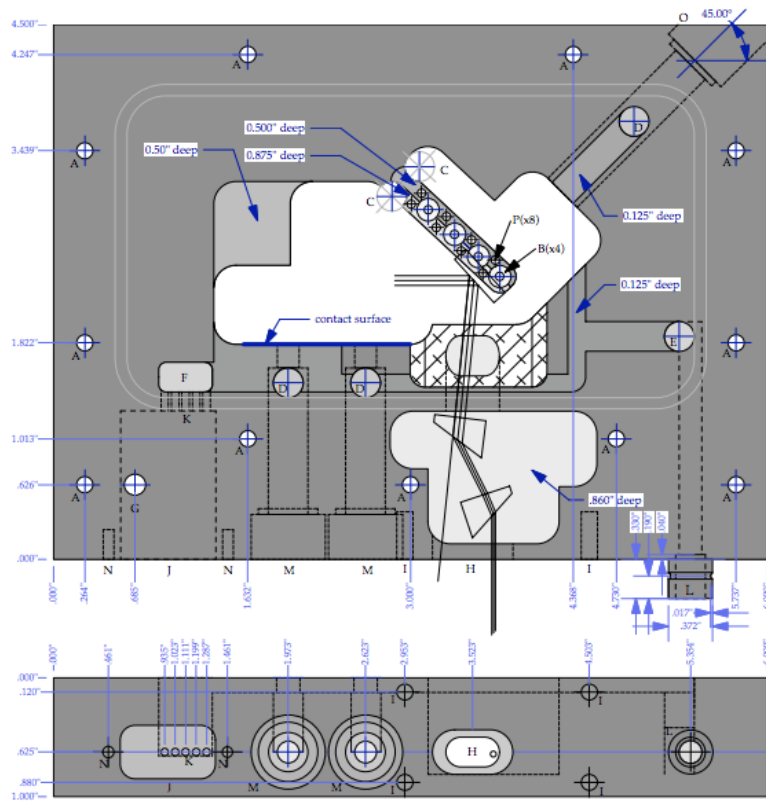


Figure 2.5: Steck design cavity body with components [4]



(a) Baseplate part drawing [3]



(b) Cavity body part drawing [3]

Figure 2.6: Baseplate and cavity body part drawings [3]. Suggested design changes are to these parts of the aluminum body.

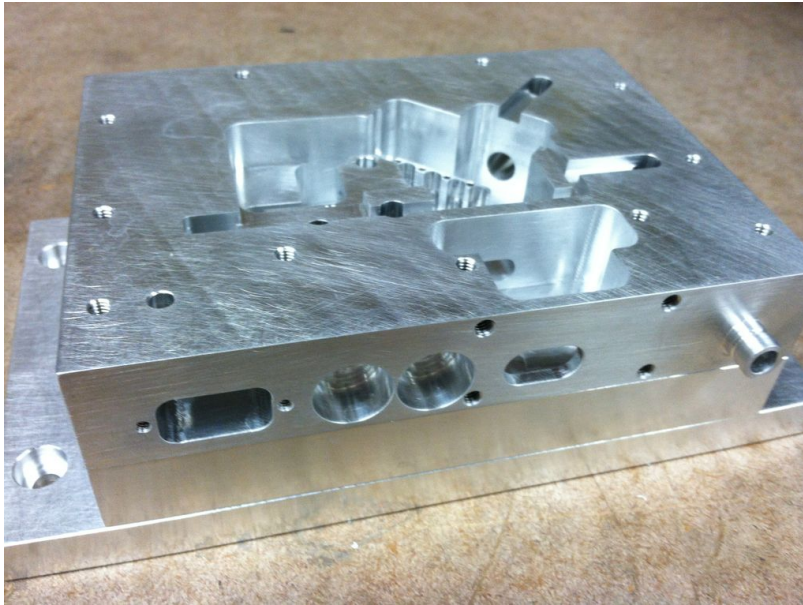


Figure 2.7: Photograph of bare aluminum cavity body, back from the machine shop.

Baseplate suggestions:

- TEC grooves in the baseplate are designed to exactly fit the TECs. Wider grooves would allow for greater ease in aligning the TECs when the baseplate is screwed onto the bottom cover. Another way to make that process easier would be to put the grooves on the bottom of the bottom cover rather than the top of the baseplate (or both would be fine).
- It would be helpful to widen the countersinking of the holes for the nylon screws on the bottom of the baseplate. This way the heads of the nylon screws wouldn't need to be trimmed for you to be able to fully screw them in.
- Add a groove to the bottom cover for the TEC wires. The baseplate and bottom cover need to be screwed in so that they sandwich the TECs as flush as possible; we want maximum contact between aluminum and TECs. The thickness of the wires is a limiting factor here. Also, the wires can easily get in the way of screw holes and make aligning the baseplate and bottom cover more complicated.

Cavity body suggestions:

- I would suggest extending the space where the DB15 wires enter the cavity so they can be more easily potted in epoxy and threaded through the holes without scratching the coating on the wires.
- The space inside the cavity is really tight. I would either heighten the cavity to make more space for the wiring, or lengthen the cavity slightly so it's easier

to remove and replace the diode laser (or you could implement some of both adjustments).

- Additionally, I would relocate the circuit ledge a little farther away from the central area of the cavity. (To do this, there's no need to lengthen the entire cavity and remove so much aluminum, but rather just mill a shelf a short depth into the aluminum creating a new ledge that is located higher and farther back than the current ledge.)

Epoxies: (Appendix A.1)

There are specific epoxies used for different tasks, including Epo-Tek 353ND from Epoxy Technology, Inc., Torrseal (Loctite brand 1C Hysol), Quik Stik 5 minute epoxy. See Appendix A.1 for product numbers.

Seeking an epoxy that would set quickly but easily be snapped off for realignment, UV-cured epoxy was substituted for both the Epotek-353ND to glue the diffraction grating to the grating arm, and for the 5-min epoxy to attach the prism pair to the acrylic etching. However, the UV-cured epoxy degasses significantly, which ruined the optical surface of the diffraction grating. Thus it is no longer a suggestion for construction.

A lab scale is very useful for mixing epoxies, which require precise ratios of their constituents. I purchased a lab-quality high-precision scale specified for $125\text{g} \times .01\text{g}$. For some epoxies, such as the Epotek 353ND, it is important to mix with plastic mixing sticks rather than wooden sticks because the wood can splinter off and contaminate the epoxy. Plastic syringes are useful for squirting the epoxy into harder to reach areas, such as into the wire port of the cavity body once the wires are in.

The Epotek 353ND in particular has a very long cure time at room temperature. Therefore, a curing oven allows the epoxy to be cured on a minute-hour time scale. (On the recommendation of the Steck Group, such a “reflow oven” can simply be substituted by a conventional toaster oven, and so I purchased a toaster oven for the Weld Lab. The only downside to the toaster oven is that the temperature selection is not very accurate, but for epoxy curing this is fine. The Steck Group recommends baking at approximately 80°C . The Epotek 353ND specification sheet, where you can find the curing times for various temperatures, can be found on the Weld Group wiki page.)

Diffraction grating: (Appendix A.2)

I explained in Sec. 2.1.3 the physics that describes the diffraction grating you'll use. Using the rearranged diffraction grating equation, I calculate that the grating spacing for a 994nm ECDL with the grating angle α set to 45° is 1422.75 g/mm. The closest to this available from Newport Corporation Richardson Gratings was a 1350 g/mm holographic grating and a 1200 g/mm ruled grating. Fig. 2.8 shows a close-up photograph of the cavity body with an inserted diffraction grating.

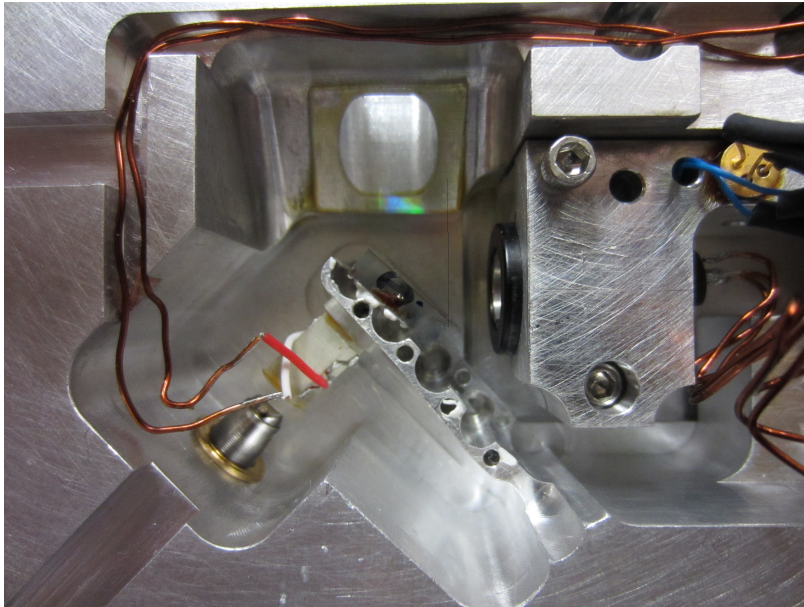


Figure 2.8: Photograph of cavity body to show a close-up of the inserted diffraction grating.

Since I wasn't sure if either holographic or ruled might have benefits over the other, I decided to purchase one of each. (This way, if any issues came up with one of them, I wouldn't have to wait weeks for an alternative order to process and ship.) Without having the experience of deflecting the diffraction grating arm on a unibody ECDL previously, I did not know how much deflection the arm could withstand and remain elastic (i.e. be able to return back to 45°). Note that there is no way of pushing the arm back once it has been deflected past the point at which it remains elastic. This was a critical problem I encountered in my construction, as I will discuss in Sec 2.2.7.

I purchased a holographic reflection grating with 1350 g/mm and a ruled reflection grating with 1200 g/mm, both gold-coated (which the Steck Group recommends for longer wavelength ECDLs [3]), and both 3.2mm thick \times 6mm length \times 12mm width (the custom size chosen by the Steck Group).

The 1350 g/mm grating corresponds to $\alpha = 42.14^\circ$. Therefore, the arm must be deflected 2.86° from its starting point of 45° . The 1200 g/mm grating corresponds to $\alpha = 36.61^\circ$. The necessary angular deflection of 8.39° is far too great an angle to bend the grating arm, and additionally would not allow the specular beam to exit the Brewster window. 1350 g/mm is reasonable, and is the closest sold by the vendor to the desired grating spacing of 1422.75 g/mm.

Even with this 2.86° deflection, in our initial alignment attempts we pushed the grating arm far enough that it was no longer elastic (in other words, it remained deflected even when I tried to allow it back to 45° by loosening the fine-adjust screw

behind it, causing the piezo to fall out from between the grating arm and the fine-adjust screw). This led to the complication I discuss in Sec 2.2.7.

Since the 1350 g/mm grating required so much angular deflection of the grating arm, the 1200 g/mm certainly wouldn't work, so I never ended up trying the 1200 g/mm and finding out how the ruled grating differed in practice from the holographic grating.

Eventually, the 1350 g/mm holographic grating had been experimented with so much that its optical surface became significantly dirtied by fingers near the edges, dust, epoxy, etc. Therefore I purchased a second 1350 g/mm holographic grating. The only change I made to this was the size of the grating. Due to the complications that arose with the L-shaped diffraction grating jig (See Sec. 2.2.1), I wanted to simplify the installation of the new diffraction grating by sizing it to be tall enough to sit on the grating arm's shelf and still have its center reached by the laser. I decided that the additional mass of the taller grating would likely be a negligible addition to the overall mass of the grating arm, and it was a sacrifice worth making. So the second 1350 g/mm holographic grating I purchased was identical except that its dimensions were 3.2mm thick \times 10mm length \times 12mm width.

An additional component which is suggested by the Steck Group [3] in order to avoid over-deflecting the arm is a shim, placed behind the grating to angle the diffraction grating with respect to the arm. I attempted this shimming technique, but found that the diffraction grating could be glued at an angle with respect to the arm without the use of the shim. In some respects, gluing without the shim is easier: while calculations of the size of shim needed are straightforward, in practice, using that shim to achieve the needed angle is not simple. The point from which the grating is angled by the shim is not a defined point on the grating arm (particularly since the arm has semicircular cutouts along it, and so there is not a flat surface against the back of the grating). Therefore, small adjustments of the grating's location along the arm can drastically change the grating's angle with respect to the arm, and therefore with respect to the beam.

Electrical: Protection circuit and wiring (Appendix A.3)

For laser diode current control and temperature control, I decided to purchase a combination controller. I found one from Arroyo Instruments, LLC.: their 6305 ComboSource Controller, 500mA, and have been very satisfied with its performance. It is straightforward to interface and operate.

The protection circuit requires multiple components and a 1" \times 1" printed circuit board. Our circuit boards were ordered from Avante Circuits by Eric Miller, a member of the Jayich Lab, who constructed a similar ECDL during the summer I was constructing mine. Eric ordered circuit boards printed with the design from the Steck Group, which is illustrated in Fig. 2.9. The Osmond PCB file for this protection circuit can be found on the Steck Group webpage [3].

The components, all 1206 package except the Schottky diode, include a 10 Ω

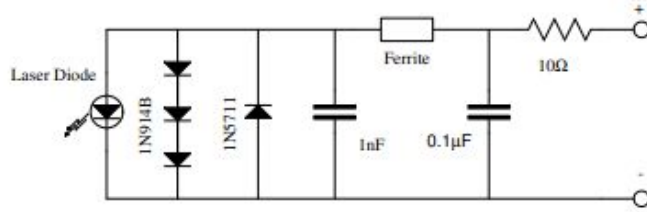


Figure 2.10: Protection circuit diagram [3].

resistor, a $0.1\mu\text{F}$ capacitor, a 1000pF (1nF) capacitor, an EMI filter Murata ferrite bead, and an SOD-323 pkg 1N5711 schottky diode.

Note: When running the protection circuit at around 300mA (370mA is the operating current for the Power Technology, Inc. laser diodes I used), the protection circuit got so hot that the solder on the resistor melted. In calculating that a few hundred mA of current through a 10Ω resistor was enough current to generate this amount of heat dissipation, we replaced the 10Ω resistor with a 2Ω resistor.



(a) printed circuit board components layout

(b) printed circuit board connections layout

Figure 2.9: Printed circuit board diagrams. (Note that these two diagrams are mirror images of each other. (b) shows a top view of the printed circuit board, (a) is its chiral image.)

As for electrical connections, the ECDL aluminum body needs to be connected to the temperature control, the laser diode current control, and the function generator (which will be used to control the piezo). The Arroyo controller controls both the temperature and the laser diode current. It has a 15 pin D-sub connector for the temperature and a 9 pin D-sub connector for the laser diode current control. The ECDL body is designed to fit a 15 pin HD (high density) D-sub connector. To connect the ECDL to both the Arroyo and the function generator, I purchased a small metal box from the UCSB Physics Storeroom, along with the necessary solder cup connectors and D-sub extension cables, using the metal box in which to solder between the 15 pin HD and each of the other connectors. I purchased two 15 pin

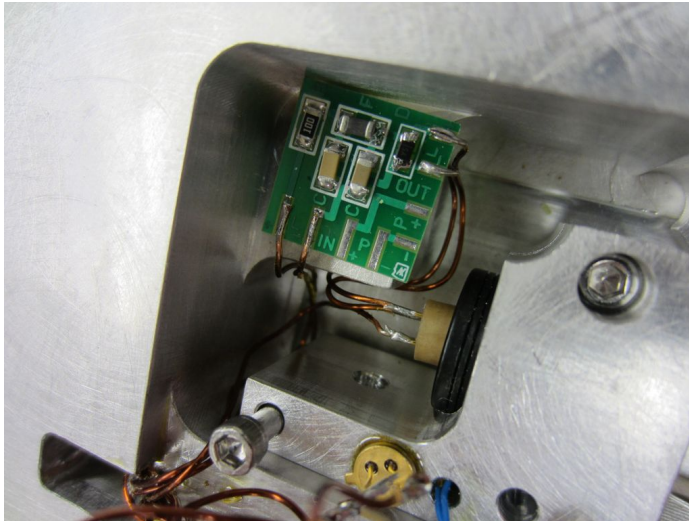


Figure 2.11: Protection circuit soldered onto printed circuit board and install in cavity.

HD D-sub (DB15HD) solder cup connectors (one for the aluminum body, and one for the metal box), and a 15 pin D-sub (DB15) solder cup connector, a 9 pin D-sub (DB9) solder cup connector, and a BNC connector for the metal box. I also purchased D-sub extension cables and a BNC cable, all with the proper pinouts and male/female connectors to connect them.

For soldering, you'll need various soldering tools and supplies, including a soldering iron with fine-point tip (the fine-point tip is immensely helpful for the surface mount soldering), solder, solder wick, a solder fume extractor so you aren't breathing harmful fumes (optional, the Weld Lab has one), and a helping hands mount with flexible arms (one with a magnifying glass is useful). Additionally, one of my most valued tools when surface mount soldering and in general has become a pair of high grade, tapered, bent fine-tipped tweezers.

The wire to be used in all of the intra-cavity wiring will be 23AWG heavy-build Kapton-coated (polyimide) round magnet wire. For wiring that will be external to the cavity, (i.e. within the metal box), any 22 or 23 AWG standard PVC-insulated electrical wire should work. The 22 gauge wire is fine for fitting in the solder cups of the 15 pin and 9 pin D-sub connectors, but is a little big and harder to fit in the solder cups of the 15 pin high density (HD) connector, so I'd recommend the 23 gauge.

Any soldered connections that are liable to touch and make electrical shorts (especially when the cover is on and all the wires get compressed into the small space of the closed cavity) should be covered in heat shrink tubing (also known as shrink wrap). You'll need a heat gun for shrinking this heat shrink tubing.

Diode laser: (Appendix A.4)

I purchased a few different diode lasers, from different vendors and at varying prices. This way, I had a few cheaper ones to start out with, and then I could use my more expensive one once everything else was working and I had gotten some practice with

them. The closest wavelength to 994nm that is commercially available is 985nm. Each diode laser outputs a Gaussian distribution of wavelengths that peaks at a slightly different wavelength; each particular diode isn't guaranteed to come off the shelf with its Gaussian distribution of wavelengths centered at exactly 980nm. Thus, having a few extra diodes gives me more chance of finding one with its Gaussian distribution of wavelengths shifted toward longer wavelengths, closer to my goal of 994nm. The most expensive diode I purchased was from Eagleyard, a 980nm ridge waveguide AR coated diode laser with a quoted 50mW of power. I also purchased a single mode 980nm laser diode from QPhotonics, with a much higher power of 300mW. Additionally, (because they were only \$11.00 each) I purchased three 100mW 980nm laser diodes from the vendor Egismos, with the intention that these inexpensive diodes would be for practice installing and for testing my circuitry and construction. Ultimately, these were unable to lase at 994nm with sufficient power. I purchased 200mW 985nm laser diodes from Power Technology, Inc.

The diode laser is electrically connected to the protection circuit and the current supply using a laser diode socket. This socket can be soldered into the wiring so that the laser diode does not have to be soldered directly, and can be easily removed if it dies. Depending on the laser diode(s) you purchase, you'll need either a 3-pin or 4-pin socket for either a 9mm or 5.6mm diameter laser diode.

The diode laser will be situated within a collimation tube with optic, an M9×0.5 optical housing that will fit in the aluminum diode laser housing. The optic is a collimating lens inside the collimation tube. Collimation is achieved by adjusting the lens's position relative to the diode laser using a spanner wrench. The M9×0.5 size housing requires the SM9 spanner wrench (both of which can be purchased from Thorlabs).

O-rings: (Appendix A.5)

This ECDL design utilizes six o-rings made of Viton material. Three 3³/₈" inner diameter (ID) o-rings are used for sealing at each of the three 3/8 – 24 screws. Two 4.5" ID o-rings are used for sealing between the bottom cover and cavity body and between the cavity body and top cover. A final 5/64" ID o-ring is used for damping of the diffraction grating arm, placed beneath the tip of the grating arm and the bottom cover on which it sits. See Appendix A.5 for part specifications and product numbers.

Screws/nuts/washers: (Appendix A.6)

- Eight 4-40 jack screws (male-female threaded hex standoff screws), with male thread, 3/16" hex length, 3/16" or 1/4" screw length. These are for attaching the D-sub connectors: one to the laser body, three onto the small metal box (two jack screws for each connector).
- The three D-sub connectors that will go in the metal box will also need two 4-40 hex nuts each (six total) to screw the jack screws into.

- Two 8-32 \times 3/8" ss (stainless steel) socket head screws, are used for attaching the laser diode housing into the cavity body.
- Fifteen 8-32 \times 1" ss socket head screws. Eleven of these will be used for attaching the top cover onto the completed ECDL. Another four will attach the optical isolator housing to the completed ECDL.
- Two flat profile washers, made of stainless steel 301/302/304, with outer diameter (OD) 0.310", and inner diameter (ID) 0.206" will be used with the previous four screws for optical isolator housing mounting.
- Three 3/8"-24 \times 1/2" ss socket head screws to seal the two holes that allow you access to attach the diode laser housing to the cavity body, and for the hole for the fine adjust screw.
- One 4-40 \times 1/4" ss socket head screw for tightening the diode laser in its collimation tube into the diode laser housing and fix it at the proper orientation.
- Six 8-32 \times 1" nylon screws for attaching the baseplate to the bottom cover. Nylon screws are used here to keep the base plate and bottom cover thermally isolated and only thermally connected via the TECs. I used flat head nylon screws, but these slip easily and make tightening difficult. I would instead recommend finding nylon phillips head screws. Additionally, the head diameter of the nylon screws I used was too large to fit in the countersunk holes in the base plate. I had to clip them (easy enough since they are nylon). If you can find them, I'd recommend purchasing nylon screws with a smaller head diameter.
- Two 4-40 \times 1" ss socket head screws (length arbitrary provided they are longer than 0.78) with a fine point tip. These are for tilt adjustment of the laser diode housing, and you'll need to round the fine point tips (as I'll discuss in Sec. 2.2.1) so they don't screw into the bottom cover when you tighten them in adjusting the tilt.
- To mount the ECDL to the optical table or breadboard, you'll need four screws. The optical tables in the Weld Lab use 1/4 - 20 ss socket head screws. (Any length is fine.)
- The fine adjust screw, which is used for angular adjustments of the diffraction grating arm, is a 1/4-100 hex adjustment screw with screw receptacle.
- If you decide to machine an L-shaped grating jig, as I will discuss in Sec. 2.2.1), you'll want one 1-72 ss socket head screw to use as a jig handle that won't slip. The length for this "handle" just must be greater than 0.37". As I'll explain in Sec. 2.2.1, I found an alternate method for inserting the diffraction grating, and ended up discarding the jig I machined, in which case this screw is unnecessary.

Cleaning supplies: (Appendix A.7)

Since the ECDL will ultimately be under vacuum, sonication, which uses ultrasound

energy to agitate particles for more thorough cleaning, is an important process for cleaning the aluminum body and any components that will be in the vacuum. I purchased a sonicator with a tub large enough to hold the biggest pieces of the ECDL's aluminum body. The Steck Group suggests doing a multi-stage sonication process for most thorough cleaning, doing a wash in each: Alconox, acetone, water, DI water, methanol, and ultrapure methanol (I substituted isopropanol). Rather than have to fill the entire tub with each of these chemicals, I followed the Steck Group's suggestion of filling plastic bags with the chemical and the part to be washed, and sitting that in the tub full of water. The problem I encountered was that the Alconox, acetone, methanol and isopropanol all ate through the glued seams of the plastic bags I purchased. Any pieces that are small enough should therefore be placed in a glass beaker of the chemical, and the beaker placed in the water bath. For those pieces that were too large to fit in beakers, I had to find a way to use bags – since the ECDL won't be put under ultra-high vacuum, I determined that it would be sufficient to clean the parts in diluted mixtures of the chemicals within the bags. Diluting the chemicals ensured that they weren't strong enough to eat through the bags. However, maximal cleanliness would be better achieved using the undiluted chemicals. Ideally, try to find plastic bags that won't deteriorate in order to sonicate the large components.

You'll also need chemical waste disposal jars to safely dispose of your used chemicals. See Sec. 2.2.3 for more details on the sonication process. Of course, other common lab supplies including lens cleaning wipes, Kim wipes, and gloves are always useful for handling chemicals, cleaning, etc.

Piezo modulation: (Appendix A.8)

The piezo actuator is used to modulate the angular deflection of the diffraction grating arm, and fits between the fine-adjust screw and the back of the grating arm. It is a low-voltage, 5mm×5mm×10mm stacked ceramic multilayer piezo, specified for 60V max and 1000N blocking force.

To control the piezo, I purchased a 4 MHz sweep function generator. The selection of function generator was based on Slava's suggestion.

Two sapphire windows will be epoxied to the piezo, one on each end. This ensures that the force from the fine-adjust screw on the piezo and the force from the piezo on the grating arm is applied evenly. I found it useful to clamp the sapphire discs while baking the epoxy, but clamps often have rotating and non-smooth clamping pads, which rendered it difficult to get a gentle, 90° grip on them. An ideal solution would be to purchase a small clamp with large and flat pads.

Temperature control:(Appendix A.9)

Two ceramic plate Peltier solid-state thermoelectric coolers (TECs) are sandwiched between the baseplate and the bottom cover, allowing the temperature of the body cavity to be thermally isolated and controlled.

Thermal paste (I used Arctic Silver 5, as did the Steck group) is used to ensure

excellent thermal contact between the TECs and both the bottom cover and the baseplate.

The temperature can be measured and read by the Arroyo temperature controller using either a 50k Ω thermistor or an AD590 temperature transducer. I purchased and installed both, so that I could use either and have the option in case I ran into problems with one down the road. I used the AD590, and encountered no issues and so never needed to solder and use the thermistor.

Components for beam output: (Appendix A.10)

The Brewster window is a 0.7" \times 0.7" piece of glass, and can easily be made out of a microscope slide. To cut the microscope slide into the Brewster window, I used a fixed point diamond-tipped scribe. (Any method of glass cutting is suitable to the task. For instance, the Steck Group [3] used a diamond impregnated copper-beryllium blade.) See Sec. 2.2.4 for an explanation of the method I used for scribing and breaking the glass.

A pair of anamorphic prisms is used to convert the elliptical beam shape to circular before it exits the cavity body. These are unmounted, AR-coated, with B coating (the coating for 650-1050nm).

The Steck group has calculated and created drawings for the placement of the anamorphic prisms for a few common wavelengths. This drawing can be etched onto a piece of acrylic and cut around the etching so the acrylic piece fits in the t-shaped cavity after the Brewster window. Making this acrylic prism-alignment etching will greatly simplify your prism alignment process. The Hansma lab at UCSB owns and operates a laser cutter, and they were kind enough to take my design (which I converted to CorelDraw X6 files, to be compatible with their laser cutting software), and laser etched and cut a piece 1/8" thick acrylic for me. ".EPS" files for prism alignment for common wavelengths can be found on the Steck Group webpage [3]. The drawing for the prism placement for 994nm light is shown in Fig. 2.12

The unibody ECDL is designed to include an optical isolator. The isolator is to be secured in an aluminum housing that attaches directly to the unibody at the output window. The Steck Group [3] designed the housing to fit isolators by the vendor OFR (Optics for Research), which is now a division of Thorlabs, Inc. The body type must fit the chosen housing size (the Steck group provides two designs, a larger size and an "aspirin tablet" size (which fits body type D isolators). I purchased the 2.5mm aperture, body type II (to fit in the larger housing) fixed band isolator. The OFR/Thorlabs isolator website is linked on the Weld group wiki page.

The unibody optical isolator housing is machined with screw holes to attached a fiber couple assembly from Oz Optics, Inc. The screw holes are placed to fit the non-contact style laser to PM fiber coupler, which couples to a 3 mm outer diameter jacket polarization-maintaining fiber patchcord. Specification sheets and other Oz Optics, Inc. information can be found on the Weld Group wiki page.

A viewing card is useful if your light is not in the visible spectrum. I purchased

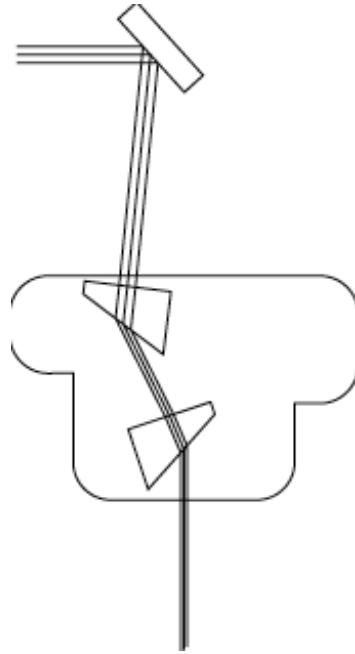


Figure 2.12: Drawing for the prism placement etching for 994nm [3].

an IR viewing card for my 994nm light.

Various optomechanical components, such as clamping forks, optical table screws ($1/4 - 20$ for the Weld Lab tables), mounts, mirrors, lenses, etc. are useful for collimating your beam, measuring the wavelength and power and other such tasks. For collimating the diode laser within its collimation package, a small optomechanical v-clamp with a PM3 clamping arm allows you to easily mount the round collimation package on the optical table. Additionally, when handling optics, (especially the anamorphic prisms), plastic tweezers are an important tool to use so as not to scratch the surfaces with metal tweezers or get oils on the surfaces from your hands.

Vacuum: (Appendix A.11)

In order to put the cavity under vacuum, you'll need to purchase a vacuum seal-off valve of $1/4$ " aluminum and a 25mm ISO flange valve operator.

2.2 Construction

As this chapter is an account of my project as well as instructions for other ECDL construction, I have rearranged the process into categories of like tasks to maximize construction efficiency (thus the ordering and organization of my instructions differs from that available on the Steck Group web page). These categories are: machining (Sec. 2.2.1), soldering (Sec. 2.2.2), cleaning and sonication (Sec. 2.2.3), steps to do before epoxying and baking, (Sec. 2.2.4), the process for epoxying and baking



Figure 2.13: Wiring box; the wires connect the DB15HD to the DB15 and DB9 solder cup shells.

(Sec. 2.2.5), and finally the assembly and testing processes (Sec. 2.2.6 and 2.2.7). My suggestions for design improvement and procedural efficiency are interspersed throughout.

2.2.1 Machining

Aluminum body: The Weld Lab had its aluminum bodies machined by the UCSB Machine Shop.

Round the 4-40 tilt-adjust screws: The two 4-40 screws will be used in the laser diode housing to adjust the tilt angle of the housing, and thus the angle from horizontal at which the light is incident on the diffraction grating. The length of these screws must be greater than the height of the housing (0.78"). The tips must be rounded so that they do not screw into the aluminum body. The Steck Group rounded these with a lathe. The method I developed was holding the screw in a hand-held electric drill, and spinning it while touching the tip to an electric sander.

Wiring box: "D"-shaped holes, a circular hole for the BNC plug, and screw holes need to be drilled into the small metal box in which the DB15HD plug is electrically connected to the DB15, DB9, and BNC plugs. Fig. 2.13 shows a photograph of the inside of this connector box.

(Optional) L-shaped diffraction grating jig: This jig is a temporary insert that raises the diffraction grating while its epoxy sets, so that it can be glued at a height such that the beam hits its center. This benefits the design by reducing the size of the grating; a smaller grating is lighter and less susceptible to mechanical resonances.

The Steck Group machined this L-shaped insert. I attempted this method, but found that, while it was possible to use, it complicated my process by introducing instability when aligning the grating. It is likely that this was due to machining error on my part. The horizontal surfaces of my jig were not professionally machined and not sufficiently flat. Thus the grating didn't sit stably on the jig, nor the jig stably on the grating arm. This introduces nonlinearities when the arm is adjusted.

After unrelated complications with the grating arm, the grating had been handled and maneuvered too much and its optical surface had become damaged. When purchasing a replacement, I opted to buy a taller grating, so that the grating could sit directly on the arm and I could forgo the use of the jig. I still epoxied to the grating arm a small metal shelf to lift this taller grating slightly, so that the beam hit its center. Both this shelf and the taller grating add to the mass of the overall arm and grating system, which is designed to be as light as possible. We determined that the complications introduced by the jig outweighed the disadvantages of a heavier grating arm and so was a worthwhile compromise.

If the smaller grating and jig method is chosen, a jig can be machined following the SolidWorks part drawing I created, which can be found on the Weld Group wiki page. The hole in the part is tapped with a 1-72 thread to fit a screw to be used as a non-slip handle for ease in removing the jig once the epoxy sets.

2.2.2 Wiring and Soldering

TEC wiring: The TECs are wired in series (the text on the TECs should either all face up or all face down), using heat shrink tubing to cover the soldered connections. To the far wire of the TEC that will be located away from the hole to the DB15HD port, solder extra wire to the TEC's wire so that the connection reaches, and also cover this connection with shrink wrap.

It is important that the connections between these wires are soldered as flat as possible (no thicker than the thickness of a TEC). Otherwise, they will prevent the baseplate and bottom cover from making good thermal contact with the TECs.

D-shell connectors: The D-shell connector that fits in the cavity body is one of the two DB15HDs. Kapton-coated wire, which is vacuum compatible, is soldered in 1-1 $\frac{1}{2}$ ft. long segments into the solder cups of the connector. Three (or four, in the case of a 4-pin laser diode) will connect to the protection circuit which will go to the laser diode, two will attach to the piezo, and either 3 pins for an AD590 or 2 pins for a thermistor (or both, to have the option after the ECDL is constructed) are needed for temperature control. Two of the solder cups must be left empty as these will connect the TEC wires, accessed through a hole in the bottom cover.

The second DB15HD, the DB15, DB and BNC shells can all be inserted into the machined metal wiring box, and the wires can be soldered into their solder cups to

electrically connect them. The connecting schematic I designated is diagrammed in Fig. 2.15. It uses only the AD590, and the pinouts of the Arroyo connectors are specific to the Arroyo controller. Standard PVC-insulated electrical wire can be used here, outside of the vacuum. Once soldered, the connectors can be secured using the jack screws and hex nuts.

Protection circuit: The surface mount components are soldered onto the printed circuit board. This circuit was designed by the Steck Group [3]. A circuit schematic and images of the Gerber files can be found in Fig. 2.9, as well as on the Weld Lab Wiki. To connect the protection circuit to the diode laser, solder three wires of approximately 2" in length between the output solder pads and the pin side of the laser diode socket. Determining which output of the protection circuit should connect to which pin of the laser diode is specific to the pinout of the laser diode. If a new diode laser is used, the socket will need to be resoldered to match the new diode's pinout designation as each may differ, as illustrated in Fig. 2.14.

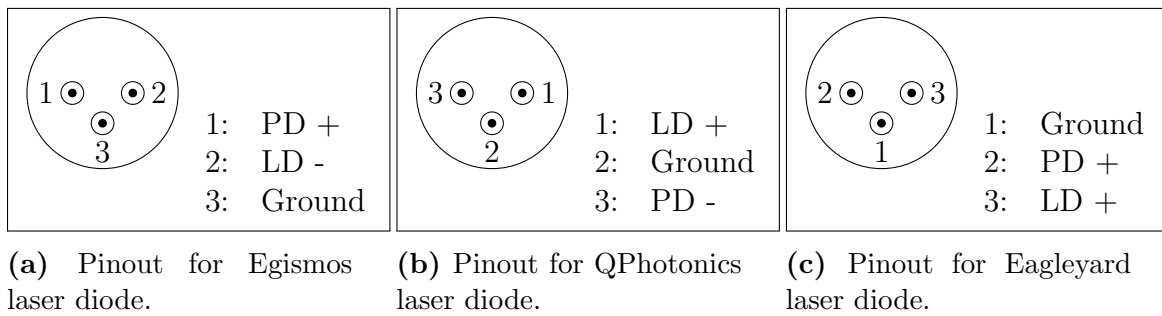


Figure 2.14: Different laser diode pinouts.

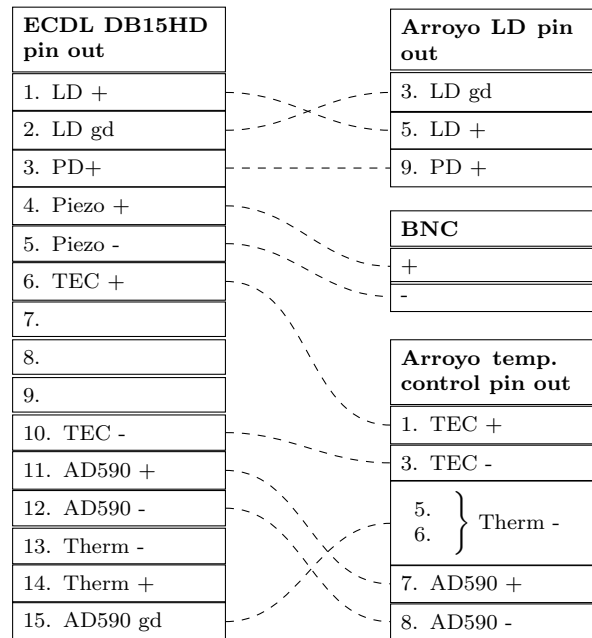


Figure 2.15: Wiring and pinout designation

2.2.3 Cleaning

Sonication Steps [3]:

Wash:	Purpose:
Alconox (detergent)	removes machining oils
Tap water	removes Alconox, debris, chemicals
DI water	removes minerals and tap water remnants
Acetone ^a	removes adhesives, organic compounds
Methanol	removes solder resin, other compounds
Isopropanol (or ultra-pure methanol, as the Steck Group used)	removes contaminants left by methanol

^aWarning: Do not use Acetone on rubber or other sensitive parts.

In a sonicator, the part being washed must be suspended in the tub; it cannot rest on the tub floor. Otherwise, the bottom component will not experience the sonication effects and will not get sufficiently cleaned. One way to do this is to put the part and cleaning chemical in a beaker, and suspend the beaker in the water such that the beaker does not rest on the tub floor. This can be achieved by suspending a beaker by its lip between two wooden dowels. If the component is too large to fit in a beaker, another method for suspending the part is to use a plastic bag, and suspending the part by filling the bag with some of the chemical, the part, and enough air to keep the bag partially afloat in the tub (but so that the part is submerged fully). Fig. 2.16

is a photograph of this plastic bag method of sonication. However, as I discussed previously, some bags are liable to rupture at the seams by the chemicals, and so it is important that bags with stronger seams are used for this method.



Figure 2.16: Photograph of sonication process using plastic bags to suspend the part.

The items that need to be sonicated in all of the cleaning chemicals are any components that will be in or touching the cavity when it is under vacuum. These include the baseplate, bottom cover, cavity body, top cover, and laser diode housing, the thermistor and/or AD590, the fine-adjust screw and receptacle, and the screws to attach the cavity body to the bottom cover. The protection circuit and 3-pin laser diode receptacle will also need to be sonicated in all the steps (omitting the Acetone step, as it can damage the surface mount components). The o-rings and TECs also must also be cleaned, but the o-rings can be wiped in isopropanol and the TECs wiped with acetone.

2.2.4 Other Pre-epoxy/Bake Tasks

Feed wires through wire port: The Kapton-coated wires that have been soldered into the cups of the DB15HD shell are to enter the cavity through the holes in the port in the cavity body. Forceps or fine-tipped tweezers are useful in working the wire through, taking care not to scratch off the Kapton coating if possible. (This is where my design suggestion of enlarging this area would make this process much easier.) Leave approximately an inch of the wires in the port so that the solder cup connections can be accessed if necessary, but only enough so that the connector

shell can still be screwed onto the port with the wires bent in the port into an S-shape.

Brewster window: This is a $0.7'' \times 0.7''$ piece of glass, cut from a microscope slide, and epoxied onto the inside of the cavity body. I used a diamond-tipped scribe to score lines in the glass microscope slide where I wanted it cut, wrapped the slide in lens papers to keep shards of glass from flying out, and snapped the glass. It helps to snap the glass while holding the scored line along a ruler (or other firm, straight edge) to encourage it to break along the scored, straight line. Any sharp edges must be removed, and the slide cleaned with lens cleaning paper and isopropanol.

2.2.5 Vacuum Safe Epoxying and Baking

Both the wire port and the Brewster window need to be epoxied and baked, but the cavity body needs to be tilted at a 45° angle for baking the Brewster window's epoxy, and so it should be epoxied and baked in separate steps. Additionally, the sapphire discs also need to be epoxied and baked to the ends of the piezo, and the AD590 and/or thermistor need to be epoxied and baked into the diode laser housing. The Epo-Tek 353ND vacuum safe epoxy is used for all of these, and should be well mixed and if possible, degassed. A syringe is useful for dispensing the epoxy.

Wire port: About 2 mL will be needed to fill the port at which the wires enter the cavity, to seal the vacuum. The epoxy tends to climb the wires, and once it sets, hardens them in that position, so it is important that the wires are oriented as they will be when the cavity is finished and closed. The epoxy should be applied both from the exterior port as well as from interior side—it is useful to apply to one side, bake, and then apply to the other side and bake again, since the epoxy isn't viscous and will drip out easily. Each time, the cavity can be propped up so that the epoxy covers all the holes.

BEFORE THE EPOXY SETS, a discontinuity check must be done between wires and cavity body. Continuity between any pin in the DB15HD and the bottom cover indicates damaged Kapton insulation and a short to the aluminum body. This can be fixed by coating the damaged wire with the epoxy by jiggling the wires until the epoxy slips in to coat the exposed wire.

Once assuring there is no continuity between the wires and the aluminum body, the epoxy needs to be baked. Propping the cavity up allows the epoxy to cover all holes, but also allows the epoxy to flow into the cavity. Propping it at a low angle helps avoid this, but the epoxy may not cover the very top holes. The cavity body can be flipped over and the process repeated (applying epoxy from the same side of the holes) to cover the rest of the holes.

Bake in order to set the epoxy according to the curing time indicated in the epoxy technical data sheet. (For Epo-Tek 353ND, 80°C is required for a 30 min. cure time.)

Brewster window: To epoxy the Brewster window, the bottom cover will need to be propped up at a 45° angle so that the window is positioned horizontally. A syringe is useful in applying a thin, even ring of epoxy around the window's frame. Position the window, avoiding getting any epoxy on the window where the beam will pass. Something heavy (I used a small piece of brass) wrapped in lens paper can be placed on top of the horizontal Brewster window to apply pressure to the window's seal as it sets.

Sapphire discs to piezo: The sapphire discs are epoxied to the ends of the piezo. A clamp is useful to keep them in place while they bake. Another suggestion is not to attempt to epoxy both at the same time; attaching each sapphire disc individually is much easier.

Thermistor and/or AD590 into cavity body: The thermistor or AD590 (or both, in order to have the option after the cavity assembly is complete) are inserted into the diode housing, using a bit of epoxy, and baked.

Fine-adjust screw receptacle: The receptacle of the fine-adjust screw is coated in epoxy and inserted into its hole in the cavity, from the inside (tweezers are helpful with this). The receptacle should be rotated several times once inserted to ensure that the epoxy makes contact around the entire receptacle with the aluminum body. The receptacle can be clamped in place while the epoxy sets; one way to do this is with a bent paperclip, as the Steck Group did [3]. Another method is to stand the cavity body on its side and place a heavy object on the edge of the receptacle while it bakes, assuming that the oven used is large enough to accommodate this arrangement.

2.2.6 Assembly

Test the wiring: Each pin of the DB15HD must be electrically connected to one (and only one) of the wires fed into the cavity. It is useful to ensure that no shorts between wires have been made or connections interrupted. It is also a convenient time to label the wires by their pin number for connecting to their proper components in the next few steps.

Baseplate set up with nylon screws: The nylon screws that I purchased from McMaster-Carr have too large a head diameter to fit in the countersunk holes of the baseplate, and need to be clipped (wire cutters work well on the nylon). They are inserted into these holes from underneath. The TEC wires need to be passed through the small access hole in the bottom cover.

Thermal paste the TECs: The TECs get coated in a fine layer of thermal paste on both sides. A razor blade is useful for covering the entire surface in a minimally thick layer. (A very small drop of thermal paste will cover an entire TEC surface.)

Tighten the “baseplate-TECs-bottom cover” sandwich: A second pair of hands is helpful for this task. Place the thermal paste-covered TECs in their grooves in the baseplate, and flip the bottom of the bottom cover onto the TECs, so that the screw holes in the bottom cover are aligned with the nylon screws coming up from the baseplate. Ensure that the TECs stay in their grooves so that they make good thermal contact with the bottom cover. (Here is where my design suggestion of widening the TEC grooves and/or adding TEC grooves to the underside of the bottom cover would add significant ease.) Even a small offset of the TECs can drastically affect the thermal conductivity.

It is important at this step to ensure that the TEC wires do not cross any screw holes in the baseplate. These holes will later be used for the screws that attach the cavity body to this “sandwich,” and the wires will not be easily accessible for readjusting their position once the “sandwich” has been tightened. It is helpful to tape the TEC wires onto the baseplate so that their path is fixed and is guaranteed not to shift and cross any screw holes.

It is useful to hold the “sandwich” up to the light to look for gaps between the TECs and the bottom cover. Rather than flipping it over to tighten, which risks allowing the TECs to slip out of their grooves, it is better to have one person hold the “sandwich” up while the other tightens the nylon screws from below. The screws should be tightened in a star pattern (i.e. alternate incremental tightening of diagonal pairs), to ensure that even pressure is exerted on the TECs.

Install protection circuit in the cavity body: Three of the wires in the cavity are to be soldered to the input of the protection circuit. These should be cut so that they reach to the circuit ledge with only a little slack (for when the diode laser needs to be moved outside of the body for collimation and polarization alignment), but not so much that the wiring cannot easily be compacted into the cavity when the cavity is sealed. The ends of these wires should be stripped and soldered to the circuit.

Attach cavity to bottom cover, including o-rings: The cavity body gets attached to the bottom cover (which is now attached to the baseplate in the “sandwich”) with the 11 8-32 x 1 stainless steel socket cap screws. One of the large o-rings fits in the groove in the bottom cover, sealing the cavity. This o-ring should be coated liberally in vacuum-safe grease before being inserted. The tiny o-ring should be placed in its groove in the bottom cover as well (where it will sit under the tip of the grating arm), but this o-ring should be greased. The screws are inserted from the bottom of the baseplate. Therefore, it is most convenient to flip the cavity body over and flip the “sandwich” onto it, aligning the o-rings properly, so that the screws can

be accessed easily. Before tightening, the TEC wires must be fed through the hole into the DB15HD port, so that they can be soldered into the connector cups. The screws can then be tightened, again in a star pattern to distribute the pressure evenly.

Insert the fine-adjust screw into its receptacle: The fine-adjust screw must be coated in vacuum-safe grease (make sure all the threads are coated) and inserted it into the receptacle from outside the cavity body inwards.

Add the piezo: The piezo, with sapphire discs epoxied on the ends, is inserted between the fine-adjust screw and the back of the diffraction grating arm, so that the piezo is centered on the tip of the fine-adjust screw. No epoxy is necessary; it is held in place by friction. Fig. 2.17 shows a close-up of the piezo inserted in the cavity body.

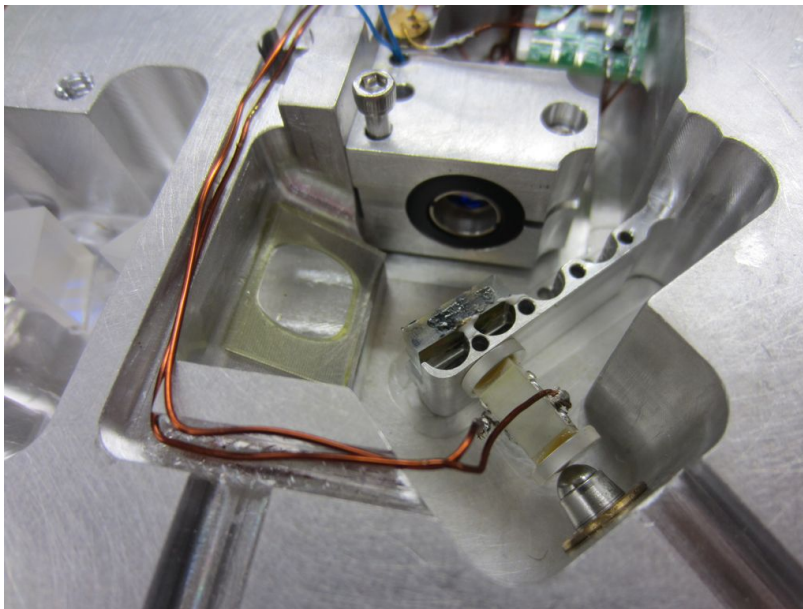


Figure 2.17: Photograph of ECDL cavity: close up of inserted piezo with attached sapphire discs and fine-adjust screw.

Diode laser into collimation package: The collimation package includes a collimating lens and collimation tube, into which the diode laser is placed, as well as a retention ring for securing the diode in the tube. This retention ring should be snug (but tightened by hand). It is critical that you be grounded before touching the diode laser.

Solder wires to AD590 (and/or thermistor): The Kapton-coated wires previously designated for the AD590 can be soldered to its pins. The connections should either be wrapped in heat shrink tubing or coated in Torrseal epoxy to protect the

exposed wire from any accidental shorts.

Solder TEC wires into the DB connector: The TEC wires, accessed through the hole in the bottom cover and into the DB15HD port, must be soldered to their assigned solder cups in the connector. The Steck Group indicates to cover these with shrink wrap, but we deemed this precaution unnecessary. Secure the DB15HD to the cavity body with two of the jack screws.

Connect everything: Finally, the diode can be plugged into its socket, and all connectors attached with their respective extension cords: the laser body to the wiring box and the wiring box to the Arroyo and function generator.

2.2.7 Testing

Test the TECs: The temperature controlling should be tested to ensure that the TECs make a good thermal connection with both the baseplate and bottom cover. To test this, the rate at which the temperature is changed can be observed. We set the Arroyo controller to 20C, and found that after about a minute the body was noticeably cold and the baseplate warm, and the temperature of the body was decreasing at about a hundredth of a degree per second.

Insert the diffraction grating: I opted to include installation of the diffraction grating in this testing section because I found it useful to use the beam when setting the angle of the grating with respect to the arm and epoxying it in place. Before inserting the grating, I glued a shelf on the grating arm to raise the grating slightly so that the beam hit its center. This shelf is the width of the grating.

Installing the grating is a delicate task. First it is important not to touch the optical surface. The grating can be placed on the seat of the grating arm (or the L-shaped jig, if that option is used). Plastic tweezers can aid in placing and moving the grating. If a shim is desired, it can be put in place. If not, the laser itself can be used for setting the angle, and no shim is needed, rendering the previously mentioned complications no longer relevant. The angle of the grating can be determined directly by aligning the first order diffracted beam back into the laser diode, using an IR card with a pin-sized hole. Allow the incoming beam to enter through the hole, and the reflected beam is viewed on the card. The grating's angle can be adjusted until the reflected beam is centered on the hole and no longer visible on the card.

Once the grating is arranged at the proper angle, it can be epoxied in place. The Steck Group uses a small amount of Torrseal epoxy applied to the edges of the grating. Be careful not to get any epoxy underneath the grating, and use only small amounts so that it can be snapped off and realigned if necessary. If a jig was used, it can be removed once the epoxy has set.

Test the laser diode: Make sure you are grounded whenever handling the laser diode, and wear goggles when it is lasing.

Collimate the beam: The collimation tube, which holds the diode laser, plugged into its socket, which is wired to the protection circuit, can be brought outside of the cavity and held in an optomechanical v-clamp while the beam is collimated. (I did not leave enough slack in the wires and so the diode couldn't reach far enough outside the cavity; I had to clamp the diode housing onto the aluminum body, which was sufficient but not ideal.) Aim the beam in a direction in which it can travel unobstructed for quite a few meters. Pointing the beam in this direction, adjust the location of the optic within the collimation tube (using the spanner wrench to adjust the optic's position) while another person walks the IR card along the path of the beam. It is collimated when there is no focus in the beam and it maintains its shape along its entire path. According to the Steck Group, "slight distortions are unavoidable due to aberrations in the lens, but a change from vertical to horizontal ellipticity indicates a poorly collimated beam" [3].

Reinforce soldered connections: Once successful lasing and protection circuit function are confirmed, all soldered connections (the input and outputs of the protection circuit and the pins of the socket) can be reinforced with Torrseal epoxy.

Put collimation tube in the diode housing: Install the collimation tube (now with the diode laser inside and collimated) into the diode housing, and secure the housing to an optics post.

We want our final output beam to be circular (for fiber coupling). To achieve a circular beam after the anamorphic prism pair, we need a horizontally elliptical beam incident on the prisms. Therefore, the collimation tube must be rotated within the diode housing so that the beam is aligned such that the longer axis of the ellipse is horizontal.

To do this, use the polarization of the beam and a polarizing beam splitter (PBS). In a PBS, vertically polarized light is reflected and horizontally polarized light transmitted. The polarization and the elliptical shape of the beam are related such that the polarization is parallel to the short axis of the ellipse. Therefore, you will aim the beam into the PBS, rotating the collimation tube until light transmitted through the PBS is minimized. This will align the long axis of the ellipse horizontally. The Steck Group notes that "It is more accurate to minimize the transmitted (horizontally polarized) light than to maximize the reflected (vertically polarized) light, but they are equivalent operations" [3]. The Steck Group instructs to use a power meter to measure the transmitted beam [3]. However, we determined that minimizing the transmitted beam observation on an IR card was sufficient, since at the time, the only power meter available in the lab was a handheld wand, which would not be able

to continuously display the power reading as we adjusted. Once you are satisfied with the minimization, secure the collimation tube in the diode laser housing with the 4-40 \times 1/4" clamping screw.

Insert the diode housing: Apply a thin layer of the vacuum-safe grease to the contact surfaces of the diode laser housing to help with thermal conductivity, and install the housing into the cavity body with two 3/8" 8-32 machine screws. (Don't tighten them fully yet!) The thermal conductivity is important because the diode housing holds the temperature sensor, the AD590 (and/or thermistor), and so maximal conductivity between the diode housing and the rest of the aluminum body will provide the most accurate reading of the aluminum body's temperature.

Anamorphic prisms: Insert the anamorphic prism pair and etched prism guide. The prism guide was laser etched by graduate students in the Hansma Lab at UCSB.

I placed the prisms on this guide, but did not glue them until the very end. This was a mistake. I achieved feedback and tuned the wavelength, and then positioned the prisms accordingly; while this prism positioning allowed for proper beam shaping and exiting, the beam exits off-center of the exit window. Thus the beam is not aligned with the optical isolator. We should have positioned the prisms first, according to the etching, and then achieved feedback and tuning such that the beam exits with the prisms properly placed, forcing the beam to exit at the center of the exit window. This problem will either need to be fixed by realigning the diffraction grating, re-achieving feedback and tuning, and re-positioning the prisms, or the optical isolator mount will need to be adjusted to reposition it at the exit point of the beam.

The correct method would have been to place the prisms over the prism guides outlines and ensure that the laser beam exits the laser directly over the lines in the guide to ensure that it will pass through the optical isolator, and additionally, to ensure that the beam exits at a right angle to the housing. These prisms could then be fixed with a small touch of the 5-minute epoxy at the edge of the prisms, enough to set the prisms but still allowing for relatively easy removal if minor adjustments are needed later.

Optical isolator: It is critical that the optical isolator is mounted *before* the laser frequency is tuned and feedback achieved. I made the mistake of mounting the isolator after completing these other steps, which led me to achieve feedback and tuning such that the light exits the body off-center, and does not line up with the isolator! Mounting it prior allows one to ensure that the beam exits in alignment with the isolator, and the feedback and tuning are achieved taking this alignment into account.

When mounting the optical isolator, note that there is a powerful magnet and fragile glass inside the isolator, so be careful to keep ferrous tools away so as not to damage anything. Put the optical isolator in the isolator mount so that the white line

on optical isolator is as vertical as possible. Secure isolator with nylon screw on top. Bolt isolator onto body (ferrous material hazard), and use the play in the isolator to align the isolator precisely in front of the beam.

Achieving feedback and tuning wavelength: There are multiple parameters to adjust in order to achieve feedback and to tune the wavelength. These include the tilt angle of the diode housing, the placement of the grating on the arm, the angular position of the grating arm, the current applied to the laser diode, and the temperature at which the cavity is held. Fig. 2.18 is a photograph of the cavity, showing the diode laser properly fixed in its collimation tube and inserted in the diode housing, along with the diffraction grating glued to the arm, and the Brewster window through which the specular beam exits the cavity.

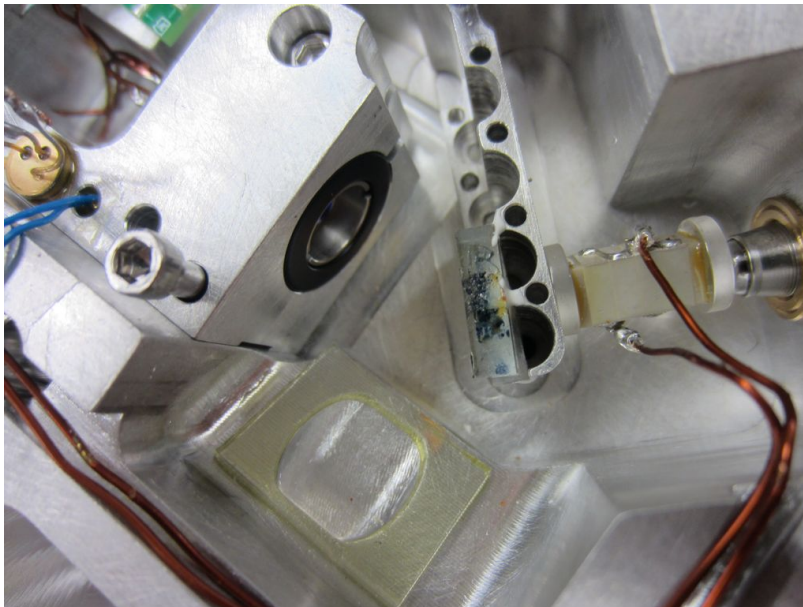


Figure 2.18: Photograph of ECDL cavity: close-up of laser diode in collimation tube in diode housing, diffraction grating, and Brewster window.

Feedback is achieved when the laser is aligned such that the first order diffracted beam of the laser is directed back into the laser diode. This must be achieved while also tuning the wavelength, which can be adjusted by both the angle of the diffraction grating arm (which is further adjusted by the piezo) as well as with temperature control. At the same time, be careful that the grating arm is not deflected so far that the reflected (output) beam does not exit the Brewster window. Fig. 2.19 is a photograph of an infrared viewing card with a hole cut in it for a first order feedback alignment.

Note: This was the first complication I encountered. In pushing the

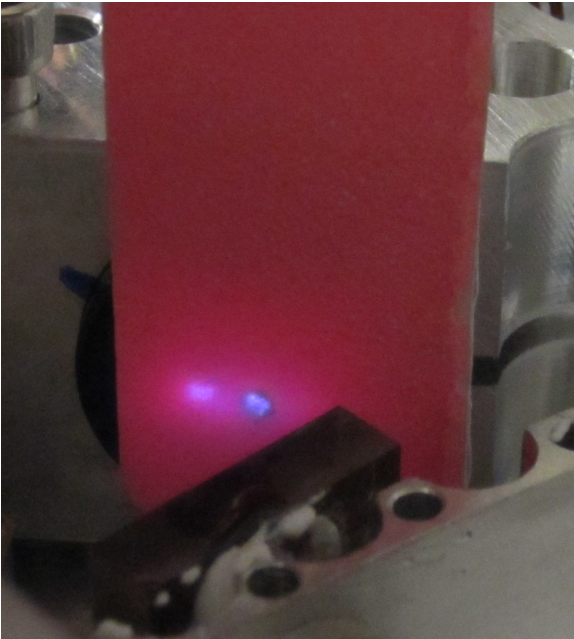


Figure 2.19: First order feedback using IR viewing card. The spot on the right is the hole in the card through which the incident beam passes. The beam to the left is the first order diffracted beam. The grating arm position is adjusted such that this diffracted beam is aligned with the incident beam.

grating arm too far from 45° , the output beam did not exit the Brewster window completely. We had pushed the arm too far, past a critical point from which the arm would not bounce back to 45° . In trying to pull the grating arm back, the arm got bent, losing its linearity. After much experimenting with fixing this arm, I ultimately had to reconstruct the cavity body, since the arm is part of the body and could not simply be replaced. Thus I issue a warning not to deflect the arm past a few degrees. Instead, glue the grating on the arm at an angle with respect to the arm.

It is first necessary to make sure that the first order diffracted beam is aligned back into the laser diode. This is done with fine adjustments of the angle of the grating arm and with the tilt of the diode housing (using the rounded 4-40 screws). It was useful to use an IR card with a pin hole to approximate feedback first. Then fine adjustments can be made until the brightness of the laser increases dramatically, indicating that proper feedback is achieved (this process is known as “thresholding”).

Tuning the laser’s wavelength requires coupling the beam into a wavemeter so that the wavelength can be read as it is adjusted. The fine-adjust screw, which changes the effective length of the resonant cavity, can be used to achieve the approximate desired wavelength. I found that temperature control was the most useful in achieving the approximate wavelength. This adjustment will change the thresholding achieved previously. Oscillation between these adjustments is necessary until you find a balance in which both can be achieved. The Steck group recommends to use the optical isolator for this to avoid feedback from the fiber coupler. However, at this point I had not mounted the optical isolator, and this did not have the fiber coupler attached and aligned (this was a mistake!) I instead directed my outgoing beam into the wavemeter

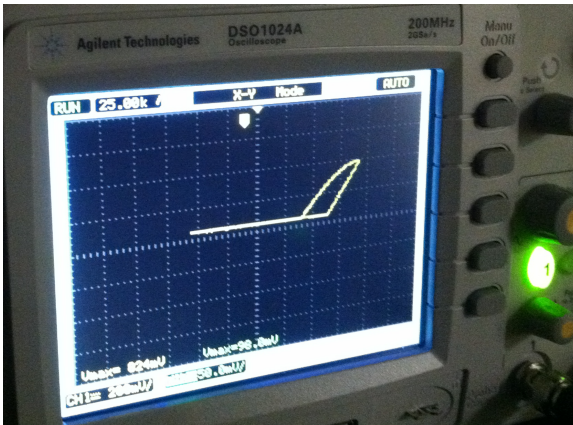


Figure 2.20: Hysteresis observed in power output vs. current applied to the laser diode; viewed on oscilloscope screen.

using various mirrors, which was a more complicated process.

Note: Since I did not have a wavemeter, I attempted to use a spectrum analyzer available in the Bouwmeester Lab. However, since the optical isolator was not mounted, any small change in the angle of the grating arm significantly altered the angle of the output beam. Thus, coupling into the spectrum analyzer needed realignment with every adjustment of the grating arm, which was the method I used for tuning the wavelength. Therefore, this attempt was dismissed.

The Steck group instructs to next modulate the laser current with slow triangle ramp, outputting the beam to a power meter [3]. This modulation of the current should cause the laser to repetitively jump to and from the threshold. I used a photodiode and oscilloscope to implement this early on, however without the optical isolator mounted and the beam output position fixed, it was exceedingly complicated to couple the beam into the photodiode. I instead achieved feedback using IR card alignment. The Steck Group instructs to adjust the tilt screws until thresholding is achieved, observing a plot of diode current versus laser power [3]. The thresholding will have been achieved when minimum current leads to high slope of the output. Fig. 2.20 shows the hysteresis observed in the plot of output power vs. current applied to the laser diode. Feedback is achieved when the power output is maximal for minimal input current.

I first tried the Egismos diode laser. It lased successfully, but at wavelengths near 976nm, and with poor beam quality. However, it was good practice testing a diode laser, collimating the beam, and installing it in the cavity. I then re-soldered my laser diode socket to match the pinout for the QPhotonics laser diode, and tested it. I again achieved successful lasing, but again the wavelength was too low. With increased current and varied temperature, I was able to raise the wavelength to 987nm, but could not achieve any longer wavelength within reasonable temperatures. I additionally tried the Eagleyard laser diode, but determined that its power rating would

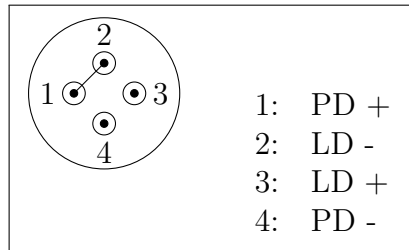


Figure 2.21: Power Technology laser diode pinout. To change into a 3-pin laser diode, pin 1 can be bent and soldered to pin 2, so that the PD+ and LD- function as a common ground.

be insufficient. Its specified 50mW output power, once it lost power to being fiber coupled and frequency doubled, would not be enough to ensure the 5mW needed for the strontium repumping transition.

I therefore researched other diode lasers, and found a 200mW 985nm laser diode from Power Technology, Inc. I purchased five of them (they were very low cost) to increase the chances that one of them would lase close to 994nm. This turned out to be very beneficial because some of the diode lasers did not lase. The other complication with these is that they are 4-pin diodes, while I had only allowed wiring into the cavity for a 3-pin diode. By bending one pin and soldering it to another, I was able to turn this into a 3-pin diode, as detailed in Fig. 2.21.

I achieved successful lasing with a few of the Power Technology diodes, and was able to reach 994nm with temperature control. These laser diodes are no longer being manufactured, and so I purchased eight more from Power Technology's stock, to have as a supply for the lab in case those which lase from my first purchase die or break.

Fix the diode housing's tilt: Once feedback has been achieved and the laser is tuned to the desired wavelength, seal the diode housing screw ports and the fine-adjust screw port with the large machine screws and o-rings.

Close the cavity: Make sure all the wires fit inside the cavity so that the top cover easily closes. Coat the second large o-ring in vacuum grease and insert into the groove in the top cover. Use eleven of the 8-32 screws to screw the top cover onto the body.

Silicone cover: I looked into this option very extensively, but ultimately we decided it was too expensive for something we weren't sure was necessary. However, after creating my own SolidWorks drawing for a mold for the silicone, I got in touch with graduate students from the Steck group who gave me a copy of their SolidWorks design, as well as details about how they constructed the mold. A link to the Steck Group's silicone mold design [3] can be found on the Weld Group wiki page.

2.3 Results/Data

The ECDL lases at 994nm when the applied current is 370mA (operating current for the Power Technology diodes), and the temperature is set to 37°. Figs. 2.23

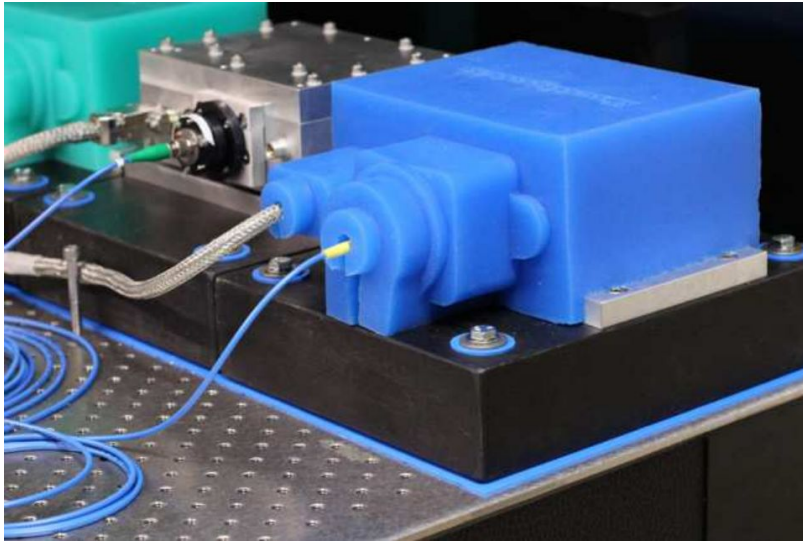


Figure 2.22: Steck Group’s silicone cover for unibody ECDL [3].

and 2.24 show the final cavity and Arroyo controller. Once I reached 994nm at a sufficient power, I moved on to the second stage of my research, the second harmonic generation.

However, as discussed in Sec. 2.2.7, the output light of this ECDL does not exit the cavity in the center of the exit window, and thus does not align with the optical isolator. There are two possible ways to fix this problem. One option is to reposition the diffraction grating and the grating arm, and feedback re-achieved while taking into account the restriction of the exit location. The other is to machine new screw holes in the optical isolator housing, such that it is shifted to align with the current exit position of the laser.

In an attempt to do the first option, the diffraction grating was dismantled. In taking off the grating, it was discovered that the optical surface of the grating had been badly damaged, from what clearly appeared to be degassing of the UV-cured epoxy used to fix the grating on the arm. Based on this result, a new diffraction grating of the same specifications has been ordered. Warnings not to use UV-cured epoxy have been incorporated into the preceding instructions.

2.4 Future ECDL Work

Realign laser with optical isolator: As discussed in the results section of this chapter, a new diffraction grating has been ordered, due to damage done to the previous one by degassing from the UV-cured epoxy. Once this arrives, the ECDL will need to be realigned so that feedback is achieved once again and the wavelength tuned to 994nm.

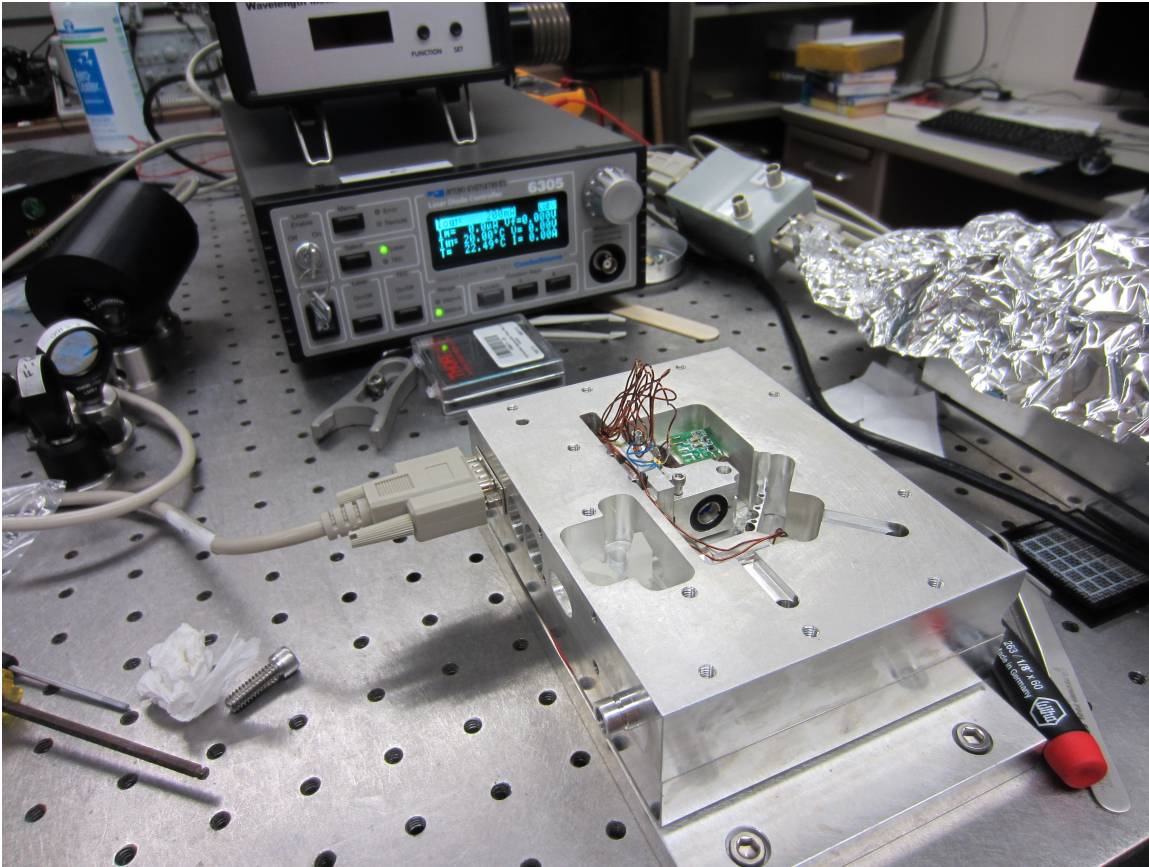


Figure 2.23: Photograph of completed ECDL and Arroyo controller (minus top cover).

Putting the cavity under vacuum: The vacuum valve and valve operator for the ECDL have been purchased. Once the cavity is otherwise ready, the cavity should be put under vacuum to isolate it from temperature fluctuations and mechanical or acoustic noise.

Fiber coupling: The fiber couple assembly is purchased and will attach directly to the optical isolator housing. This has yet to be installed and aligned.

Silicone cover: Although we decided not to pursue this ECDL accessory at the time, it may be determined later that it would be useful for isolation from temperature fluctuations and mechanical and acoustic perturbations. If so, the design and instructions can be followed from the Steck Group's instructions, a link to which can be found on the Weld group wiki page.

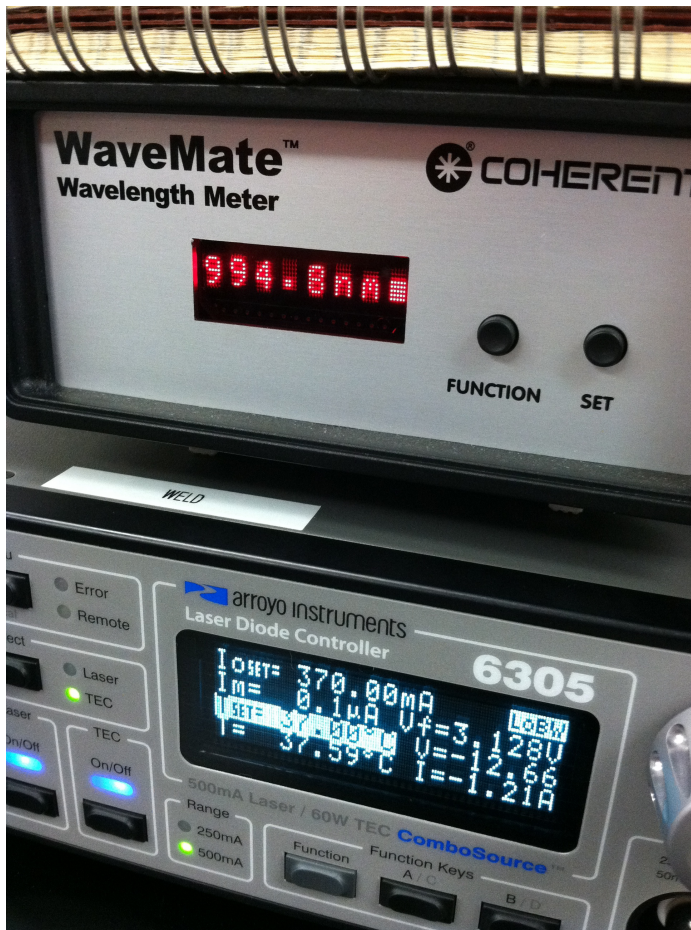


Figure 2.24: Photograph of Arroyo controller readout of temperature current, and wavemate measuring 994nm output.

Chapter 3

Frequency Doubling Cavity

3.1 SHG Theory

3.1.1 Nonlinear Optics Overview

Light has the capability to alter the optical properties of a material in which it is incident, given that the light is sufficiently intense. Nonlinear optics is the study of those alterations in which the material's response is proportional to a power of the strength of the incident electromagnetic field. Such nonlinear effects include second harmonic generation (SHG), sum frequency generation (SFG), and difference frequency generation (DFG), among others. The requirement of intensity of the light typically restricts these nonlinear effects to laser light; according to Falkenau, this threshold is around 2.5 kW/cm^2 [5]. Since the discovery of SHG by Franken *et al.* in 1961, it and other nonlinear phenomena have been exploited to produce light at particular wavelengths [8]. Since laser diodes near 994nm are not commercially available, second harmonic generation is commonly used to frequency double 994nm light to 497nm (diodes near 994nm are easier to come by). This is how I will produce the wavelength needed for the strontium repumping transition from the 994nm ECDL I constructed as described in Chapter 1.

Effectively, SHG is an exchange of photons between different frequency components of an electromagnetic field. As Boyd states it, “2 photons of frequency ω are destroyed and a photon of frequency 2ω is simultaneously created in a single quantum-mechanical process” [8].

What occurs is a nonlinear induced polarization in response to the incident electromagnetic field. The nonlinear effects allow for energy exchange between independent optical inputs [15]. From electrostatics, it is known that the electric field induces a polarization in a dielectric:

$$\tilde{P}(t) = \epsilon_0 \chi \tilde{E}(t) \tag{3.1}$$

where χ is the linear susceptibility of the material (and ϵ_0 is the familiar permittivity of free space). However, this assumes that the susceptibility is independent of the

field strength; in fact, χ is a function of E [15]. To account for this, χ can be expanded in a power series,

$$\chi = \chi^{(1)} + \chi^{(2)}E(t) + \chi^{(3)}E^2(t) + \dots \quad (3.2)$$

which (switching to only the real parts of P and E for simplicity) results in an expansion of the polarization as a power series in E [5, 15]:

$$\begin{aligned} P(E) &= \epsilon_0(\chi^{(1)} + \chi^{(2)}E(t) + \chi^{(3)}E^2(t) + \dots)E(t) \\ &= \epsilon_0(\chi^{(1)}E + \chi^{(2)}E^2 + \chi^{(3)}E^3 \dots) \\ &\equiv P^{(1)} + P^{(2)} + P^{(3)} + \dots \end{aligned} \quad (3.3)$$

The nonlinear phenomena can then be understood by considering the polarization induced by an incident electromagnetic field. Let the incident waves be linearly polarized monochromatic plane waves traveling in the same direction, with frequencies ω_1 and ω_2 . The total incident field is then:

$$E = E_1 \cos(\vec{k}_1 \cdot \vec{x} - \omega_1 t + \phi_1) + E_2 \cos(\vec{k}_2 \cdot \vec{x} - \omega_2 t + \phi_2) \quad (3.4)$$

Plugging this in to the polarization equation (Eq. 3.3), we get:

$$\begin{aligned} P(E) &= \epsilon_0 \left(\chi^{(1)} \left[E_1 \cos(\vec{k}_1 \cdot \vec{x} - \omega_1 t + \phi_1) + E_2 \cos(\vec{k}_2 \cdot \vec{x} - \omega_2 t + \phi_2) \right] \right. \\ &\quad + \chi^{(2)} \left[E_1^2 \cos^2(\vec{k}_1 \cdot \vec{x} - \omega_1 t + \phi_1) + E_2^2 \cos^2(\vec{k}_2 \cdot \vec{x} - \omega_2 t + \phi_2) \right. \\ &\quad \left. \left. + 2E_1 E_2 \cos(\vec{k}_1 \cdot \vec{x} - \omega_1 t + \phi_1) \cos(\vec{k}_2 \cdot \vec{x} - \omega_2 t + \phi_2) \right] + \dots \right) \end{aligned} \quad (3.5)$$

The linear terms can be dropped, since only the nonlinear effects are of interest here. Rewriting the second order terms using trigonometric identities, one can explicitly obtain the second harmonic generation terms for each ω_1 and ω_2 , as well as terms representing an optically rectified field, sum frequency generation (SFG), and difference frequency generation (DFG):

$$\begin{aligned} P^{(2)} &= \epsilon_0 \chi^{(2)} \left[\overbrace{\frac{1}{2} E_1^2 \cos \left(2(\vec{k}_1 \cdot \vec{x} - \omega_1 t + \phi_1) \right)}^{\text{SHG of } \omega_1} + \overbrace{\frac{1}{2} E_2^2 \cos \left(2(\vec{k}_2 \cdot \vec{x} - \omega_2 t + \phi_2) \right)}^{\text{SHG of } \omega_2} \right. \\ &\quad + \underbrace{\frac{1}{2} (E_1^2 + E_2^2)}_{\text{optically rectified field}} + \overbrace{E_1 E_2 \cos \left((\vec{k}_1 + \vec{k}_2) \cdot \vec{x} - (\omega_1 + \omega_2)t + (\phi_1 + \phi_2) \right)}^{\text{SFG}} \\ &\quad \left. + \overbrace{E_1 E_2 \left((\vec{k}_1 - \vec{k}_2) \cdot \vec{x} - (\omega_1 - \omega_2)t + (\phi_1 - \phi_2) \right)}^{\text{DFG}} \right] \end{aligned} \quad (3.6)$$

In the case of the 994nm laser, only one monochromatic wave is incident and so all ω_2 terms drop out including SFG and DFG, and only the SHG term of the fundamental frequency is left:

$$P^{(2)} = \epsilon_0 \chi^{(2)} \frac{1}{2} E_1^2 \cos \left(2(\vec{k}_1 \cdot \vec{x} - \omega_1 t + \phi_1) \right) \quad (3.7)$$

There are a host of subtleties and details that come about when squaring the electric field. These details are beyond the scope of this thesis, however a detailed explanation can be found in *Fundamentals of Nonlinear Optics*, by P. Powers, pgs. 55-66 [15]. The moral of the story is that the second order susceptibility term (χ) is written in terms of a matrix of coefficients of the effective nonlinearity, d_{eff} . Thus, (dropping the subscript from ω_1 , since only one incident frequency—the fundamental—is being considered) the second order polarization for a given cartesian direction goes as:

$$P^{(2)} = \epsilon_0 d_{eff} E(\omega)^2 \quad (3.8)$$

It has now been shown that the incident electromagnetic field induces a nonlinear response in a material, which causes the development of additional frequency components of the material's polarization. Yet how do these new frequency components of the polarization create new frequency components of the electromagnetic field?

The nonlinear polarization response of the material amounts to each atom developing an oscillating dipole moment with a component of frequency at the new frequency (2ω for SHG, $(\omega_1 + \omega_2)$ for SFG, $(\omega_1 - \omega_2)$ for DFG, etc.). As is known from Larmor's theorem, an oscillating dipole exhibits dipole radiation. The dipole radiation from each of these atoms interferes, either destructively or constructively. By designing the system such that the atoms radiate in phase (the phase matching conditions we will consider in Section 3.1.3), the constructively combined radiation can form a well-defined beam [8]. Beginning with $\tilde{D} = \epsilon_0 \tilde{E} + \tilde{P}$, in which \tilde{P} depends nonlinearly on \tilde{E} , Maxwell's equations can be used to derive the optical wave equation (See *Nonlinear Optics*, by Robert Boyd [8]):

$$\nabla(\nabla \cdot \tilde{E}) - \nabla^2 \tilde{E} + \frac{1}{c^2} \frac{\partial^2}{\partial t^2} \tilde{E} = -\frac{1}{\epsilon_0 c^2} \frac{\partial^2 \tilde{P}}{\partial t^2} \quad (3.9)$$

Assuming $\nabla(\nabla \cdot \tilde{E})$ to be negligible, splitting \tilde{P} into its linear and nonlinear components, and simplifying for an isotropic, dispersionless material, this becomes [8]:

$$\nabla^2 \tilde{E} - \frac{\epsilon^{(1)}}{c^2} \frac{\partial^2 \tilde{E}}{\partial t^2} = \frac{1}{\epsilon_0 c^2} \frac{\partial^2 \tilde{P}^{NL}}{\partial t^2} \quad (3.10)$$

This is a driven wave equation, where the driving force is due to the second derivative of the nonlinear polarization response to the E-field. This second derivative of the polarization response, $\partial^2 \tilde{P}^{NL} / \partial t^2$, describes the changing polarization (or in other words, the acceleration of the charges in the material). This acceleration is

responsible for the dipole radiation at the new frequency, which is the produced new frequency component of the electromagnetic field.

Solutions to this wave equation (Eq. 3.10) can be derived, although the algebra will not be reproduced here. The details can be followed in any nonlinear optics text. Recommendations include [15] or [8]. From this algebra, the intensity of the generated wave is calculated to be [8]:

$$I_3 = \frac{2\mu_0 d_{eff}^2 \omega_3^2 I_1 I_2}{n_1 n_2 n_3 c} L^2 \text{sinc}^2\left(\frac{\Delta k L}{2}\right) \quad (3.11)$$

where the quantity Δk is defined to be $\Delta k = k_1 + k_2 - k_3$. Here, k_1 and k_2 refer to the input wavevectors (which have the same frequency in the case of SHG) and k_3 to the output wavevector. In the case of SHG, this equation for the intensity of the generated beam can be simplified by replacing the subscripts 1, 2 with F for fundamental, and 3 with SHG . The SHG intensity is then [15]:

$$I_{SHG} = \frac{2\mu_0 d_{eff}^2 \omega_F^2 I_F^2}{n_{SHG} 2n_{FC}} L^2 \text{sinc}^2\left(\frac{\Delta k L}{2}\right) \quad (3.12)$$

Thus, in the case of a collimated plane wave, it is clear that the condition of perfect phase matching is $\Delta k = 0$, at which the intensity of the second harmonic exhibits a maximum [8]. This occurs because for $\Delta k = 0$, the generated wave and the nonlinear polarization have a fixed phase relation such that the generated wave can most efficiently extract energy from the incident waves, and the generated wave achieves maximum intensity [15]. This ultimately minimizes the amount of destructive interference between the frequency conversion occurring at different locations along the length of the crystal.

Note that Eq. 3.12 is often rewritten in terms of a ‘‘coherence length,’’ $L_{coh} = 2/\Delta k$:

$$I_{SHG} = \frac{2\mu_0 d_{eff}^2 \omega_F^2 I_F^2}{n_{SHG} 2n_{FC}} L^2 \text{sinc}^2\left(\frac{L}{L_{coh}}\right) \quad (3.13)$$

3.1.2 Gaussian Beams

Since nonlinear effects depend on a power of the strength of the electromagnetic field, (E^2 , E^3 , etc....) the nonlinear effects can be drastically increased as the intensity of the beam is increased. Collimated beams cannot achieve high enough conversion efficiency for typical uses [5]. Therefore, it is common practice to reach the necessary conversion efficiencies by focusing the light in the medium.

Lasers have Gaussian beam profiles, and so it is important to understand the properties of Gaussian beams in order to determine the desired amount of focusing and to choose optical components for the cavity (lenses, mirrors) that will achieve the proper focusing.

The Gaussian beam is a solution to the wave equation, for which the amplitude is no longer constant, but rather a function of the transverse coordinate, r , and the propagation distance. Choosing a propagation direction z ,

$$E \sim A(r, z)e^{i(kz - \omega t + \phi)} \quad (3.14)$$

where,

$$A(r, z) = A_0 \frac{w_0}{w(z)} \exp\left(\frac{-r^2}{w^2(z)}\right) \exp\left(-ik \frac{r^2}{2R(z)} + i\zeta(z)\right) \quad (3.15)$$

$$\begin{aligned} w_0 & \text{ beam waist, } w_0 = w(0) \\ z_R = \pi n w_0^2 / \lambda & \text{ Rayleigh range, where } w(z_R) = \sqrt{2} w_0 \\ w(z) = w_0 \sqrt{1 + (z/z_R)^2} & \text{ } 1/e \text{ radius of the field distribution} \\ R(z) = z \left(1 + (z_R/z)^2\right) & \text{ radius of curvature of the wavefront} \\ \zeta = \tan^{-1}(z/z_R) & \text{ Gouy phase shift} \end{aligned} \quad (3.16)$$

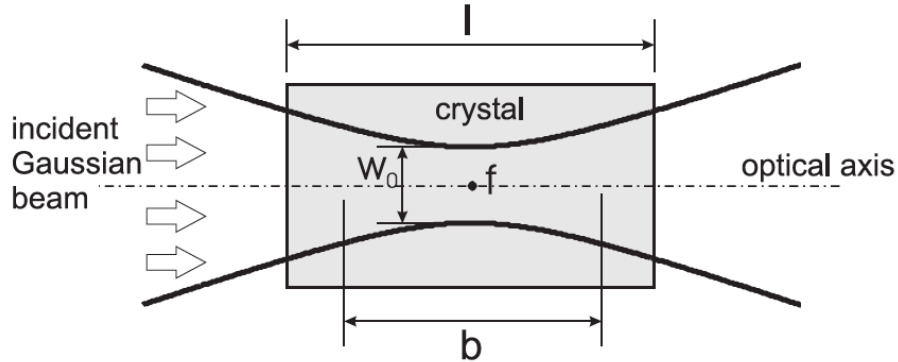


Figure 3.1: Gaussian beam incident on a crystal [5]. In this illustration, f denotes the focal point, w_0 is the beam waist, l is the length of the crystal, and b the confocal parameter.

3.1.3 Phase Matching

As shown in 3.1.1, phase matching is necessary in order to maximize the SHG output. In the case of the plane wave, this is achieved by setting $\Delta k = 2k_F - k_{SHG} = 0$. However, it has been shown by Boyd and Kleinman [16] that optimal phase matching is not in general satisfied by $\Delta k = 0$. Boyd and Kleinman derive [16] the relation between second harmonic power and fundamental power to be:

$$P_{SHG} = \frac{16\pi^2 d_{eff}^2 L}{\epsilon_0 c n_F n_{SHG} \lambda_{vac,F}^3} \hat{h}\left(\frac{L}{2z_R}\right) P_\omega^2 \quad (3.17)$$

where \hat{h} is the Boyd-Kleinman factor, defined as:

$$\hat{h} = \frac{1}{4\xi} \left| \int_{-\xi}^{\xi} \frac{e^{i\sigma\tau}}{1+i\tau} d\tau \right|^2 \quad (3.18)$$

for which,

$$\begin{aligned} L & \text{ length of crystal} \\ f & \text{ focal point} \\ z & \text{ distance in the crystal} \\ z_R & \text{ Rayleigh range} \\ b = 2z_R & \text{ confocal parameter} \\ \xi = L/b & \text{ focusing parameter} \\ \sigma = \frac{1}{2}b\Delta k & \text{ matching parameter} \end{aligned} \quad (3.19)$$

The Boyd-Kleinman factor can then be optimized as a function of ξ . This maximum \hat{h} is achieved for $\xi = 2.84$ [16, 5]. This means that there is a ratio between l and b which allows for optimal second harmonic conversion. This makes sense: in the limit that $b \gg l$, it is a plane wave, in which the fundamental beam is distributed throughout the crystal and so the intensity of the fundamental is not significantly high at any point. In the opposite limit, $b \ll l$, in which the beam is more tightly focused, only a small fraction of the crystal is exposed to high intensity fundamental beam; most of the volume of the crystal is not utilized. Thus it is crucial to find the balance between b and l that maximizes the second harmonic output.

Plotting \hat{h} as a function of $\sigma\xi$ ($= \Delta k L/2$) [5], the maximal \hat{h} can be determined. Falkenau [5] determines this maximum to be achieved at $\sigma_{opt}\xi_{opt} = 1.59$, $\xi_{opt} = 2.84$, and therefore $\sigma_{opt} = 0.56$. Solving σ_{opt} and ξ_{opt} , we can solve for Δk_{opt} :

$$\Delta k_{opt} = \frac{2\sigma_{opt}\xi_{opt}}{L} = \frac{3.18}{L} \quad (3.20)$$

which agrees with Boyd and Kleinman [16] who determine \hat{h} is maximized for $\Delta k = 3.2/L$. According to [13, 16], this maximal value of \hat{h} is 1.09.

The phase matching condition is therefore:

$$\Delta k = 2k_F - k_{SHG} = \frac{3.2}{L} \quad (3.21)$$

where we are assuming the incident and second harmonic beams are propagating in the same direction, so that this is a scalar equation. Continuing this assumption,

$$2\pi \left(2\frac{n_F}{\lambda_F} - \frac{n_{SHG}}{\lambda_{SHG}} \right) = \frac{3.2}{L} \quad (3.22)$$

Critical phase matching

Critical phase matching is also referred to as angle phase matching. The indices of refraction of a medium depend in general on the wavelength of the incident beam, as well as on the temperature of the medium. For birefringent crystals, the indices of refraction additionally depend on the incident wave's direction of propagation. One way, then, to achieve the phase matching condition, Eq. 3.21, is to select an incidence angle for the fundamental beam such that the indices of refraction satisfy phase matching. As is illustrated in Fig. 3.2, the angles θ and ϕ indicate the direction of propagation of the beam relative to the a , b , and c axes of the crystal. For some \vec{k} , there are two directions in the orthogonal plane for which the polarization of the electric field is constant.

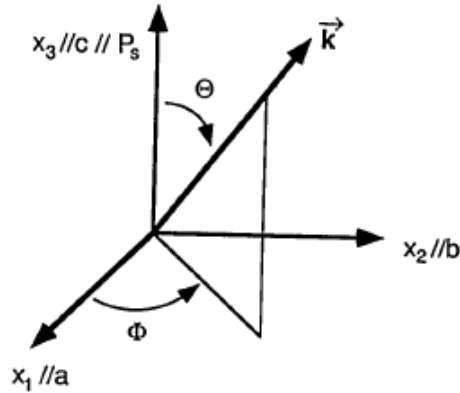


Figure 3.2: Crystal axes [6]

Crystals are classified based on their atomic geometry as biaxial, uniaxial, or isotropic crystals [8]. Uniaxial crystals are characterized by having two of the principal indices the same, $n_x = n_y \neq n_z$, whereas biaxial crystals have $n_x \neq n_y \neq n_z$. Uniaxial crystals thus have a particular axis that exhibits symmetry for all perpendicular directions; this is called the “optic axis.” Light with linear polarizations can be parallel or perpendicular to this axis, and has different indices of refraction depending on its polarization: When light is polarized perpendicular to the optic axis and the plane containing the propagation vector and the optic axis, the beam is said to be ordinarily polarized, and the material has an index of refraction n_o ; light polarized in the plane containing the propagation vector and the optic axis is said to be extraordinarily polarized, and has an index of refraction n_e , which is a function of θ .

The problem inherent in the method of critical phase matching is that walk-off occurs when θ (the angle between \vec{k} and the optic axis) is not 0° or 90° . In this range of angles, the Poynting vector, \vec{S} , and the propagation vector, \vec{k} , are not parallel for extraordinarily polarized rays, as explained in [8, 15]. Thus, the ordinary and extraordinary rays with parallel propagation vectors diverge as they propagate

through the crystal (See Fig. 3.3. The angle δ specifies the amount of walk-off. This limits the spatial overlap of the two waves, which leads to decreased efficiency of nonlinear mixing process [8].

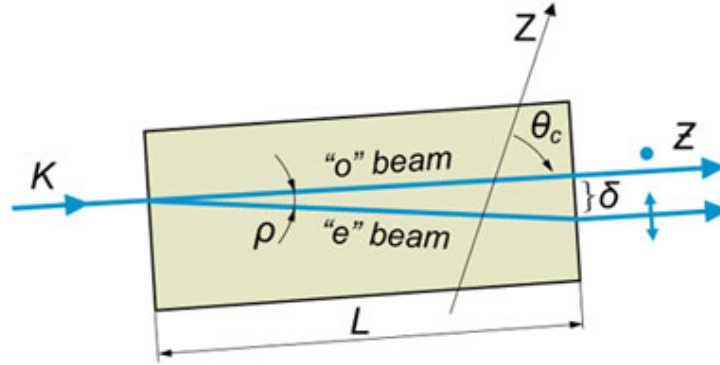


Figure 3.3: Birefringent walk-off [7]

Noncritical phase matching

Noncritical phase matching, which is effectively temperature tuned phase matching, is an alternative method. It is achieved by holding θ fixed at 90° (i.e., the fundamental beam incident along an optic axis of the crystal), and the temperature of the crystal is tuned to a temperature at which the indices of refraction for the fundamental and second harmonic beams in that direction satisfy the phase matching condition, Eq. 3.21.

It is not always guaranteed that a temperature can be found in an achievable range that will satisfy this condition, and thus noncritical phase matching works only for limited configurations. The incident polarization can be chosen to be parallel to one of the axes in order for the walk-off angle to be zero. This type of phase matching requires that the crystal have a high nonlinear coefficient and that there exists a phase matching temperature less than the breakage temperature of the crystal.

Quasi-phase matching

Quasi-phase matching, or QPM, is a third technique often utilized when both critical and noncritical phase matching, which each depend on the birefringence of the crystal, are unsuitable. QPM is achieved by period poling of the crystal, such that the orientation of one of the crystal axes, and thus the sign of the nonlinear coefficient d_{eff} , is inverted periodically as a function of position along the length of the crystal [8]. In QPM, real phase-matching does not occur. Rather, coherence is optimized such that the output achieves high conversion. Fig. 3.4 illustrates this periodic poling.

Fig. 3.5 shows a plot of the generated intensity of the second harmonic as a function of the position along the crystal, in units relative to the coherence length.

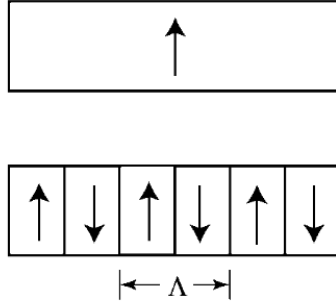


Figure 3.4: Periodic poling (where Λ is the poling period) [8]

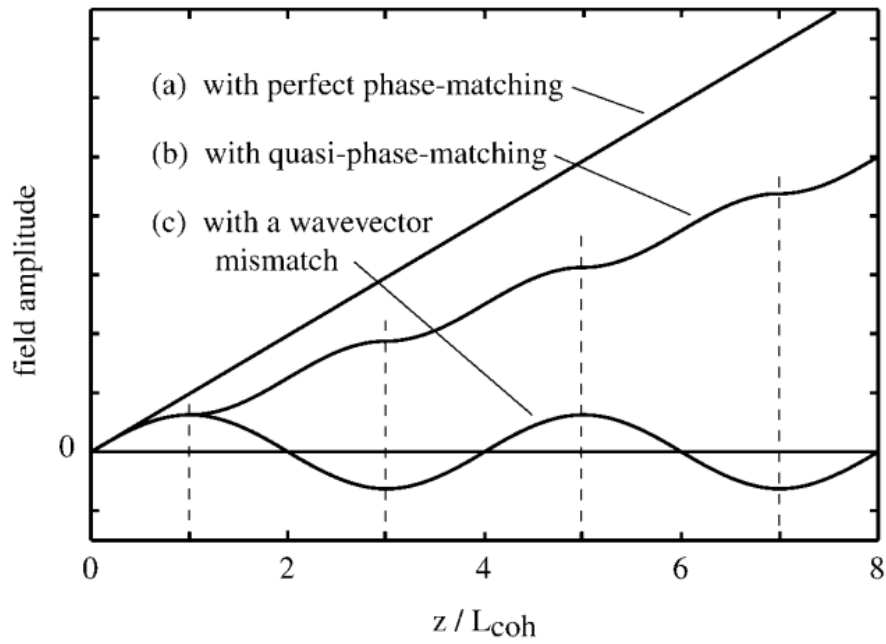


Figure 3.5: Field amplitude of the second harmonic generated beam as a function of distance in the nonlinear crystal, where z is distance and L_{coh} is the coherence length. [8]

3.2 Cavity Design

3.2.1 The Nonlinear Crystal

Choosing the Crystal

The first consideration is that for second harmonic generation, the material must have a nonzero second-order susceptibility ($\chi^{(2)} \neq 0$). After a preliminary assessment of the crystals commonly used for SHG of 994nm light, it was determined that KNbO₃ had strong potential because of its high nonlinear coefficient, $d_{eff} = 16.4pm/V$ [13]. KNbO₃ would be possible to phase match using noncritical phase matching (temperature-tuning), and therefore could be used to sidestep the issue of walk-off. One consideration to note is that KNbO₃ is easily damaged by thermal and mechanical stresses, and so care would need to be taken and the temperature increased slowly.

To determine the temperature at which the phase matching condition would be satisfied for a 994nm fundamental beam and KNbO₃, the indices of refraction as a function of both wavelength and temperature need to be determined. This can be done by fitting data from [17] to a Sellmeier equation of the form:

$$n^2 - 1 = S_1 \frac{\lambda^2 \lambda_1^2}{\lambda^2 - \lambda_1^2} + S_2 \frac{\lambda^2 \lambda_2^2}{\lambda^2 - \lambda_2^2} - D\lambda^2 \quad (3.23)$$

where n is the refractive index at wavelength λ , and S_1 , S_2 , D , λ_1 and λ_2 are determined experimentally at six different temperatures along each axis [17]. λ_1 and λ_2 are the oscillator terms, given in units of energy.

Using these data points, one can solve for the index of refraction at each of the six temperatures along each of the three axes at each of the wavelengths relevant to the experiment in question (in this case, 994nm and 497nm). These 36 data points allow for a computation of the best fit solutions for the index of refraction as a function of temperature, at each relevant wavelength and in each of the three directions. These six best fit lines can be plotted together, as shown in Fig. 3.6. Locating intersections between any one of the 994nm refractive indices and one of the 497nm refractive indices indicates the temperature at which and the axes along which noncritical phase matching is achievable.

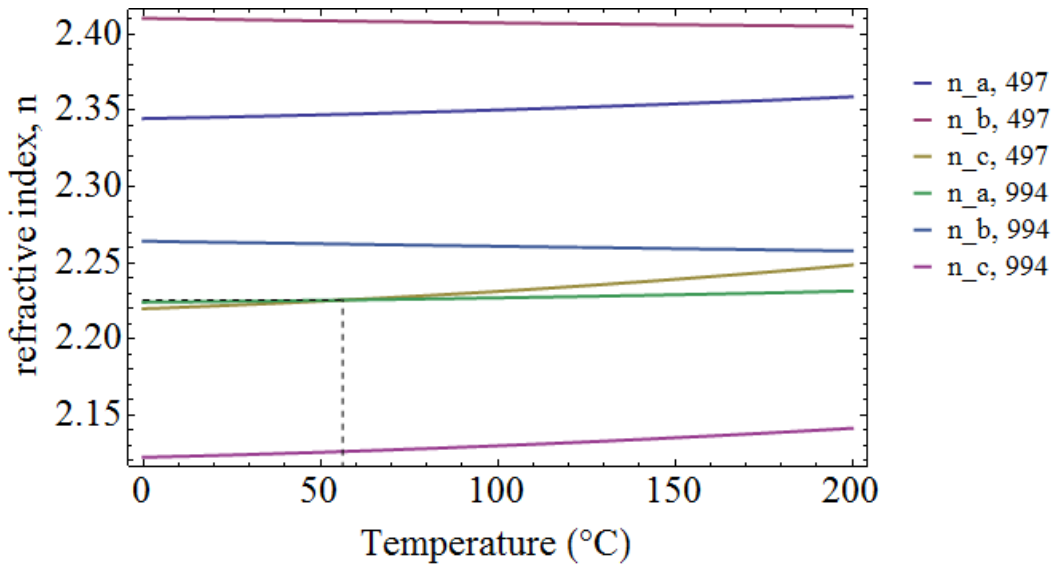


Figure 3.6: Indices of refraction for KNbO_3 for $\lambda_F = 994\text{nm}$ and $\lambda_{SHG} = 497\text{nm}$ along crystal axes a , b , and c , as a function of temperature. The dashed lines indicate the intersection point of the indices of refraction at 994nm and 497nm .

From this plot, noncritical phase matching is determined to be possible at a temperature of 56°C , with the 497nm beam polarized along the c axis and the 994nm beam polarized along the a axis.

However, at the time of investigation into purchasing KNbO_3 , it was unavailable except from a few vendors, and was very expensive and had long lead times. Therefore, an alternative was to choose a different crystal.

The alternate crystal chosen requires quasi-phase matching. Covesion, Inc. manufactures periodically poled lithium niobate (PPLN, i.e., periodically poled LiNbO_3) for quasi-phase matched SHG. A PPLN vendor, Covesion, Inc., quoted the following phase matching conditions for PPLN with an extraordinary-polarized (e-polarized) fundamental beam of 994nm , where Λ is the associated poling period:

$$\begin{aligned}
 T = 267^\circ\text{C}, \quad \Lambda = 5.17\mu\text{m} & \text{ (out of range of Covesion's ovens)} \\
 T = 253^\circ\text{C}, \quad \Lambda = 5.20\mu\text{m} & \text{ (out of range of Covesion's ovens)} \\
 T = 240^\circ\text{C}, \quad \Lambda = 5.23\mu\text{m} & \\
 T = 226^\circ\text{C}, \quad \Lambda = 5.26\mu\text{m} & \\
 T = 211^\circ\text{C}, \quad \Lambda = 5.29\mu\text{m} &
 \end{aligned}$$

While these temperatures are high, Covesion, Inc. sells ovens capable of being pushed to a temperature of 250°C . The oven material is rated up to 300° . The PPLN is not susceptible to damage by high temperatures (and in fact, its damage threshold is actually better at higher temperatures, according to Covesion, Inc.). Nor does the high temperature affect the efficiency of the PPLN, according to Covesion, Inc.

Here are calculations to confirm the phase matching conditions quoted by Covesion, Inc. One must include the effect of the periodic poling on the phase matching condition, which is done according to [18], by including a term in the phase matching equation (Eq. 3.22):

$$2\pi \left(2 \frac{n_e(\lambda_F, T)}{\lambda_F} - \frac{n_e(\lambda_{SHG}, T)}{\lambda_{SHG}} + \frac{1}{\Lambda(T)} \right) = \Delta k_{opt} \quad (3.24)$$

where the indices of refraction are functions of wavelength λ and temperature T , and where $\Delta k_{opt} = 3.2/L$ for a Gaussian beam and 0 for a plane wave, as discussed in Section 3.1.3. Note that n_e denotes the index of refraction for an e-polarized beam. (Also note that [18] defines Eq. 3.24 with the opposite sign convention; here, the sign of $1/\Lambda(T)$ has been changed to match the sign convention consistent with Eq. 3.22.) Rearranging Eq. 3.24, the poling period is calculated by:

$$\Lambda(T) = \frac{1}{\left(\frac{n_e(\lambda_{SHG}, T)}{\lambda_{SHG}} - \frac{2n_e(\lambda_F, T)}{\lambda_F} + \frac{\Delta k_{opt}}{2\pi} \right)} \quad (3.25)$$

The indices of refraction for lithium niobate as a function of wavelength and temperature can be computed from an experimentally determined Sellmeier equation from [18]. The Sellmeier equation to which they fit their data is of the form:

$$n_e(T, \lambda) = \sqrt{a_1 + b_1 f(T) + \frac{a_2 + b_2 f(T)}{\lambda^2 - (a_3 + b_3 f(T))^2} + \frac{a_4 + b_4 f(T)}{\lambda^2 - a_5^2} - a_6 \lambda^2} \quad (3.26)$$

where $f(T)$ is the temperature dependence function, defined as: $f(T) = (T - 24.5^\circ C)(T + 570.83^\circ C)$ [18]. Data points for $a_1, a_2, a_3, a_4, a_5, b_1, b_2, b_3, b_4$ are provided by [18], with which $n_e(T, \lambda)$ can be calculated for LiNbO₃ at any wavelength and temperature.

For the case of $\Delta k_{opt} = 0$, the quasi-phase matching temperature and poling period can be solved (Eq. 3.25). Ignoring the quoted QPM conditions for $T = 267^\circ C$ and $T = 253^\circ C$ since they are out of range of the oven, the phase matching conditions are:

$$\begin{aligned} \Lambda(240^\circ C) &= 5.2478 \mu\text{m} \\ \Lambda(226^\circ C) &= 5.27667 \mu\text{m} \\ \Lambda(211^\circ C) &= 5.30693 \mu\text{m} \end{aligned} \quad (3.27)$$

which are in good agreement with those quoted by Covesion, Inc. In order to do the same for $\Delta k_{opt} = 3.2/L$, the crystal length must be determined.

The crystal from Covesion, Inc. is poled along five different sections with different poling periods. This is shown in Fig. 3.7. This allows the same crystal to be used for more than one SHG process if desired, using different temperatures to achieve phase

matching for different wavelengths.

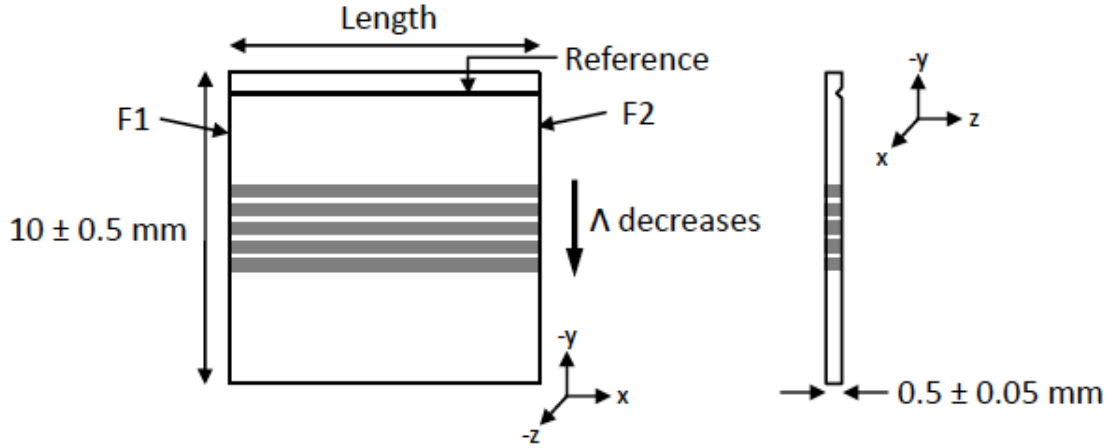


Figure 3.7: Covesion, Inc. crystal, showing the five different sections along which the crystal is periodically poled with different periods (Λ denotes the period). [9]

Determining crystal length

Eq. 3.17 allows one to calculate the second harmonic power achievable as a function of the length L of the crystal. As determined in Sec. 3.1.3, $\hat{h}_{max} = 1.09$. Eq. 3.17 can be easily rearranged to show that it agrees with [18]:

$$P_{SHG} = \left(\frac{L \hat{h} 2 \omega_F^3 d_{eff}^2}{\pi n_F n_{SHG} \epsilon_0 c^4} \right) P_\omega^2 = \gamma_{SH} P_\omega^2 \quad (3.28)$$

where γ_{SH} is the nonlinear conversion efficiency. Plugging in $\hat{h} = 1.09$, $n_F = n_e(211^\circ C, 994\text{nm})$ and $n_{SHG} = n_e(211^\circ C, 497\text{nm})$ from Eq. 3.26, and all known variables and constants (π , c , ϵ_0 , $\omega_F = 2\pi c/994\text{nm}$), the efficiency as a function of the crystal length and the effective nonlinear coefficient, $\gamma_{SH}(L, d_{eff})$, can be computed.

According to Gayer [18], measured values of d_{eff} for lithium niobate range from 9.6 pm/V (for their MgO-doped CLN sample from Deltronic), to 14.9 pm/V (for their MgO-doped SLN sample from HC Photonics). According to the Covesion Inc. website [9], PPLN has a nonlinear coefficient of greater than 14 pm/V. Thus, 14 pm/V is a good estimate of this value.

The Covesion, Inc. product for which the phase matching temperatures were specified is the product: MSHG976. Covesion, Inc. offers this crystal at lengths of 30mm, 20mm, 10mm, or 1mm (however, the 30mm is a non-standard length for the company, and so it would not fit in their mounts or ovens). The 1mm crystal length is not considered because common crystal lengths in SHG experiments tend to be in the 10mm-30mm range.

Plugging $d_{eff}=14\text{pm/V}$ and the different length possibilities (20mm, 10mm) in to Eq. 3.28, values of γ_{SH} at the different crystal lengths can be compared:

$$\begin{aligned}\gamma_{SH}(10\text{mm}, 14\text{pm/V}) &= 0.0252681 \text{ W}^{-1} \\ &= 25.27 \text{ mW}^{-1}\end{aligned}\tag{3.29}$$

$$\begin{aligned}\gamma_{SH}(20\text{mm}, 14\text{pm/V}) &= 0.0505361 \text{ W}^{-1} \\ &= 50.54 \text{ mW}^{-1}\end{aligned}$$

A limiting consideration is the achievable beam waist. As previously defined in Sec. 3.1.3, $\xi = L/b = L/2z_R$, and the optimal phase matching occurs for $\xi = 2.84$. The Rayleigh range, as defined in Sec. 3.1.2, is $z_R = \pi n w_0^2/\lambda$. The condition necessary for optimal phase matching is therefore:

$$\xi = \frac{L}{2(\pi n w_0^2/\lambda)} = \frac{L\lambda}{2\pi n w_0^2} = 2.84\tag{3.30}$$

The beam waist (w_0) can be derived as a function of the crystal length (L):

$$w_0 = \sqrt{\frac{L\lambda_F}{2\pi n_F(2.84)}}\tag{3.31}$$

Plugging in $\lambda_F = 994\text{nm}$ and $n_F = n_e(211^\circ\text{C}, 994\text{nm})$ from Eq. 3.26, the optimal beam waist for different crystal lengths is calculated to be:

$$\begin{aligned}w_0(L = 20\text{mm}) &= 0.0000224181\text{m} \\ &= 22.4\mu\text{m}\end{aligned}\tag{3.32}$$

$$\begin{aligned}w_0(L = 10\text{mm}) &= 0.000015852\text{m} \\ &= 15.9\mu\text{m}\end{aligned}$$

Since a greater γ_{SH} can be achieved with the 20mm, and it also requires the larger beam waist (which will be easier to achieve in practice), the 20mm length crystal is concluded to be the better choice.

QPM calculations with known crystal length

With a known crystal length, $L=20\text{mm}$, one can calculate the quasi-phase matching conditions for the wavevector mismatch $\Delta k_{opt} = 3.2/L = \frac{3.2}{20 \times 10^{-3}\text{m}}$. using Eq. 3.25:

$$\begin{aligned}\Lambda(240^\circ\text{C}) &= 5.2471\mu\text{m} \\ \Lambda(226^\circ\text{C}) &= 5.27596\mu\text{m} \\ \Lambda(211^\circ\text{C}) &= 5.30622\mu\text{m}\end{aligned}\tag{3.33}$$

Thus the effect of the nonzero optimal phase mismatch on the QPM poling period is negligible, and the poling periods calculated are still in good agreement with those quoted by Covesion, Inc. at these indicated temperatures.

3.2.2 Resonant Cavity

A cavity is necessary in a frequency doubling setup to enhance the second order effects. In the absence of a cavity, second harmonic generation in a nonlinear crystal is too small for typical applications. For instance, [5] cites that single pass SHG in a KNbO_3 crystal of a few millimeters only achieves typical conversion efficiency of 1%. For a 100mW fundamental input beam, this would only result in 1mW of second harmonic output. Increasing the length of the crystal can generate more second harmonic power, but comes with many other complications. Enhancement via resonant cavity is the common solution. Using the value I calculated for γ_{SH} in Eq. 3.29 to be 50.54mW, and plugging in $P_\omega = 220\text{mW}$, which is the output power reached by the ECDL, the conversion without a cavity is calculated by Eq. 3.28 to be 2.02 mW. Since at least a few mW of light is needed for the strontium transition, and this 220mW still needs to be coupled into a fiber (and will lose some power when fiber coupled), this is too small an output. Single pass efficiency is insufficient for the strontium repumping transition.

3.2.3 Spectral Parameters

A cavity has a spectral transmission, a plot in frequency space of the peaks of the resonant cavity. A spectral transmission is characterized by two parameters: the free spectral range (FSR, or $\Delta\nu_{FSR}$, in units of frequency), the full width half maximum (FWHM, or “linewidth,” also in units of frequency). These parameters together define a third parameter, the finesse (\mathcal{F} , unitless). Figs. 3.8 and 3.9 show the spectral transmission, indicating the FSR, the FWHM, and the \mathcal{F} .

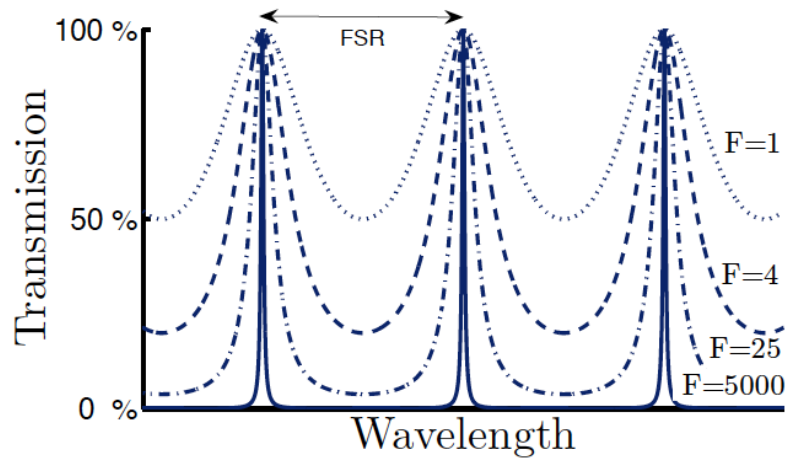


Figure 3.8: Plot of spectral transmission as a function of wavelength, for different values of the finesse \mathcal{F} [5].

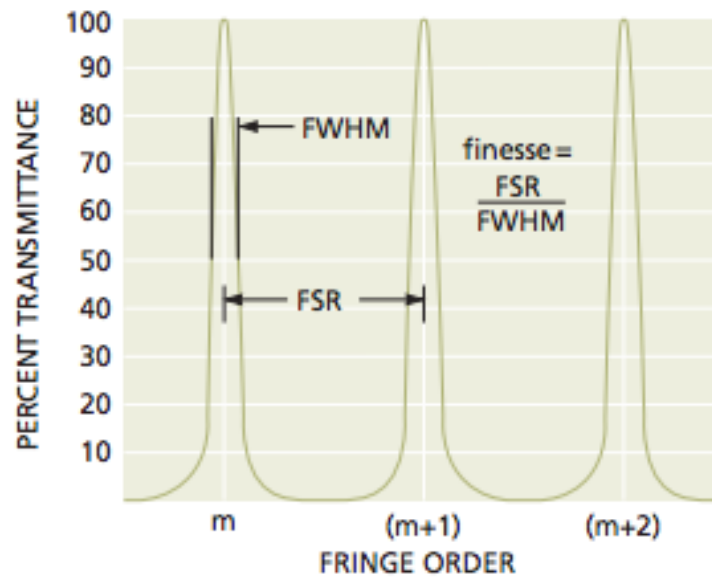


Figure 3.9: Plot of spectral transmission plot indicating the FSR and the FWHM [10].

The FSR describes the distance in frequency space between the resonant peaks. It is calculated for a cavity by:

$$FSR = \Delta\nu_{FSR} = \frac{c}{l_{opt}} \quad (3.34)$$

where l_{opt} is the the optical path length of one cavity round trip introducing losses. Note that the optical path length in the the crystal is $n_{crystal}L_{crystal}$. The linewidth and the FSR are related by:

$$\mathcal{F} = \frac{\Delta\nu_{FSR}}{FWHM} \quad (3.35)$$

where \mathcal{F} is the finesse of a resonator, characterized by the thickness of the peaks in frequency space:

$$\mathcal{F} = \frac{\pi\sqrt{g_{rt}}}{1 - g_{rt}} \quad (3.36)$$

where g_{rt} is the attenuation of the amplitude of the fundamental beam after one round trip in the cavity, defined by [5] to be:

$$g_{rt} = e^{i\phi} \sqrt{\prod_k r_k \cdot \prod_j t_j} \quad (3.37)$$

Here, k runs across all mirrors and j runs across the transmission of a media the beam has to cross in one round trip. t_1 is the transmission of the incoupling mirror. For mirrors with no absorption, power reflectivity r_a and t_a satisfy: $r_a + t_a = 1$. By decreasing the reflectivity of the resonator mirrors, r_i , these peaks in frequency space broaden.

Since the output light will be used to address a particular transition of strontium, a critical constraint is that the linewidth of the ECDL be at least narrower than the natural linewidth of the transition, but the linewidth of the cavity should be wider than that of the ECDL in order to accept all light from the ECDL. For this 3^P_2 to 3^D_J transition, the linewidth is 2.3 MHz [12]. The linewidth of the cavity, rearranging Eq. 3.35, is:

$$FWHM = \frac{\Delta\nu_{FSR}}{\mathcal{F}} \quad (3.38)$$

3.2.4 Cavity Power Enhancement

Ashkin, Boyd, and Dziedzic [19] provide the equations for calculating the power circulating in the cavity, P_c , and the power reflected from the cavity, P_r . Here, the subscript “1” refers to the first mirror through which the fundamental beam enters the cavity (the incoupling mirror), and subscript “2” to the second mirror. Ashkin, Boyd, and Dziedzic’s cavity consists of only two mirrors, creating a standing wave cavity in which the light travels bidirectionally. They define a reflectance parameter r_m to be: $r_m = t^2 r_2$ [19]. Extrapolating this to the most general case, one realizes that this reflectance parameter very closely related to g_{rt}^2 , the product of all the reflectances of all mirrors times the product of the transmissions of all media the beam will encounter in one round trip: $\prod_k r_k \cdot \prod_j t_j$, from Eq. 3.37. (However, r_m omits the reflectance of

the incoupling mirror, r_1 , but r_1 is then accounted for in the factors of $\sqrt{r_1 r_m}$ that are found in P_c and P_r .) These equations are:

$$P_c = P_F \frac{t_1}{(1 - \sqrt{r_1 r_m})^2 + 4\sqrt{r_1 r_m} \sin^2 \frac{\phi}{2}} \quad (3.39)$$

$$P_r = P_F \frac{(\sqrt{r_1} - \sqrt{r_m})^2 + 4\sqrt{r_1 r_m} \sin^2 \frac{\phi}{2}}{(1 - \sqrt{r_1 r_m})^2 + 4\sqrt{r_1 r_m} \sin^2 \frac{\phi}{2}} \quad (3.40)$$

where the incident fundamental beam is labeled P_F . In resonance, $\sin \frac{\phi}{2} = 0$ [19, 5], and these equations simplify to:

$$P_c = P_F \frac{t_1}{(1 - \sqrt{r_1 r_m})^2} \quad (3.41)$$

$$P_r = P_F \frac{(\sqrt{r_1} - \sqrt{r_m})^2}{(1 - \sqrt{r_1 r_m})^2} \quad (3.42)$$

Falkenau [5] uses g_{rt} (Eq. 3.37) to rewrite the circulating power as:

$$P_c = P_F \frac{t_1}{(1 - g_{rt})^2 + 4g_{rt} \sin^2 \frac{\phi}{2}} \xrightarrow{\text{in resonance}} P_F \frac{t_1}{(1 - g_{rt})^2} \quad (3.43)$$

3.2.5 Choice of Bow-tie Design

There are a few possible cavity geometries. The first is placing the crystal within the laser resonator, which minimizes the additional optics needed but significantly complicates the laser's cavity design. The second option is a linear, standing wave cavity which is external to the laser resonator. There are a few disadvantages to the linear cavity, however. First, the reflection on the incoupling mirror is aligned with the incident beam, and so the cavity provides unwanted optical feedback to the fundamental source. Second, the fundamental beam traverses the crystal in both directions, producing two SHG beams in opposite directions which can destructively interfere. The third cavity geometry option solves both these problems. This is a ring or bow-tie design, in which the fundamental beam circulates unidirectionally around the cavity. A diagram of a ring resonator is shown in Fig. 3.10, and of a bow-tie design in Fig. 3.11.

In choosing between the two unidirectional cavity geometries, the ring or bow-tie, it is important to note that the ring resonator's geometry and use of four plane mirrors require additional lenses to focus the beam. These are the two GRIN lenses in Fig. 3.10. These extra optical surfaces introduce additional losses to the cavity, which affect the finesse, as they are additional factors less than 1 in the $\prod_j t_j$ in Eq. 3.37.

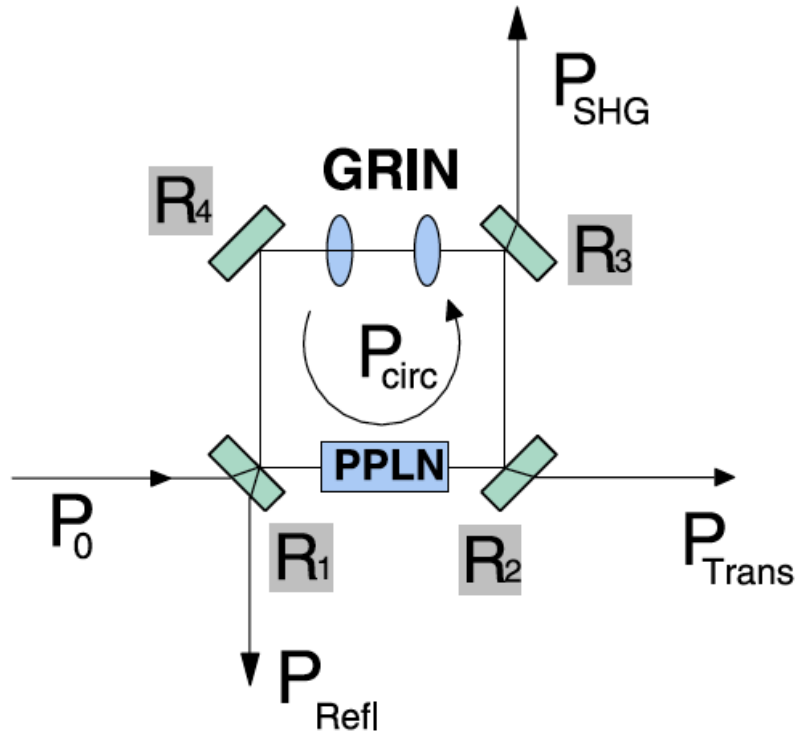


Figure 3.10: Ring resonator [11]

To avoid this problem, the bow-tie design allows the beam focusing to be done by two of the resonator's mirrors, and so two of its mirrors are concave, while the other two remain planar. Thus, for frequency doubling cavities that require a narrow linewidth, maximizing the finesse is important, and the bow-tie design is often preferred.

In the research process presented here, calculations were done based on the design and equations of Skoczowsky et. al.'s ring resonator before the conclusion to use a bow-tie design was reached. These ring resonator calculations are still applicable to the bow-tie design, and so will be worked through in the following section.

3.2.6 Impedance Matching

Impedance matching means that the input light is completely coupled into the cavity. This condition is satisfied when the reflectance of the incoupling mirror is set equal to the gain of one round trip of the cavity, and so P_c in Eq. 3.43 is maximized.

Skoczowsky, et. al. [11] use a PPLN crystal in a ring resonator SHG, a diagram of which can be found in Fig. 3.10. They define a loss factor, V :

$$V = 1 - V_0 - \eta P_{circ} \quad (3.44)$$

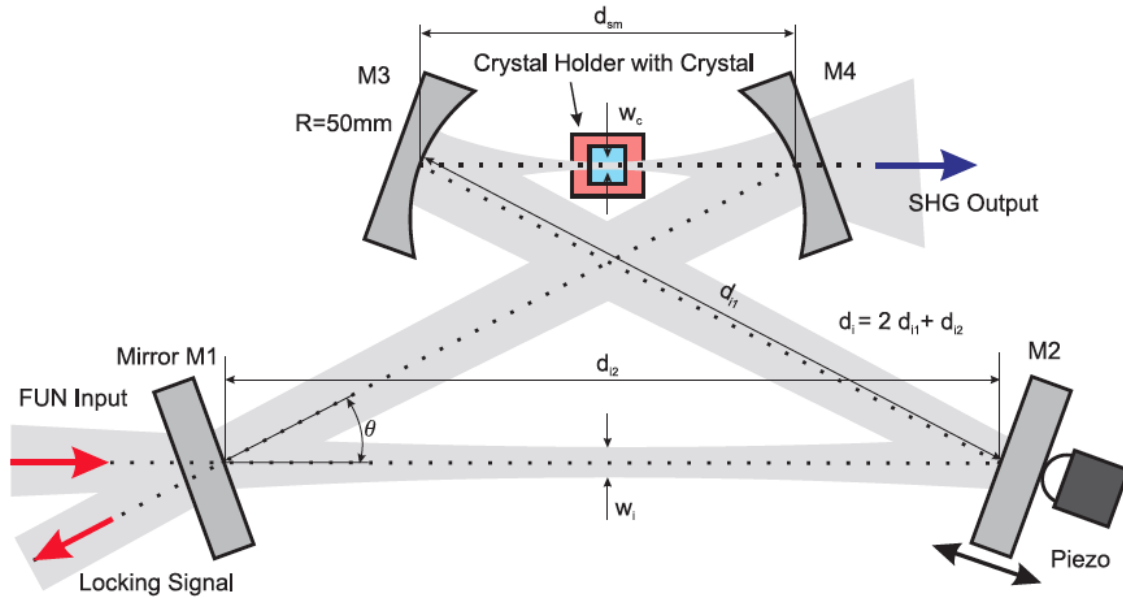


Figure 3.11: Bow-tie cavity [5]

where V_0 is the cavity loss, η is the nonlinear conversion efficiency (which we have been calling γ_{SH} , (recall Eq. 3.28, $P_{SHG} = \gamma_{SH} P_\omega^2$). This is similar to Eq. 3.37; both describe the losses of the system, where g_{rt} is roughly \sqrt{V} , except that V does not include factors of R_1 or R_2 . In Skoczowsky, et. al.'s convention, the square root and the factors of R_1 and R_2 are explicitly included in the equation for circulating power,

$$P_{circ} = P_0 \frac{(1 - R_1)R_2}{(1 - \sqrt{R_1 R_2 V})^2} \quad (3.45)$$

making it an iteration of Eq. 3.43, but specific to this cavity and using its own defined convention for including losses in the calculations. They also give an equation for the reflected power:

$$P_{refl} = P_0 \left(\frac{\sqrt{R_2 V} - \sqrt{R_1}}{1 - \sqrt{R_1 R_2 V}} \right)^2 \quad (3.46)$$

To impedance match the ring resonator, R_2 has to compensate the sum of all losses inside the resonator [11]. Eq. 3.46 shows a plot of the reflected power as a function of R_1 , the reflectivity of the incoupling mirror, for a few values of R_2 . This gets a little complicated because the loss factor, V , is a function of P_{circ} , which is, in turn, a function of V , and the coupled equations are not easily solved for using basic Mathematica solving commands.

Numerically solving for V obtains four solutions. Of these solutions, only two have physical meaning. Using these two solutions for V , P_{refl} can be plotted; the one that most closely resembles that from Skoczowsky, et. al. [11] is taken to be the correct

solution. Using the value of $\gamma_{SH} = 0.0237623$ (Eq. 3.29) specific to this crystal, the plot obtained differs slightly from Skoczowsky, et. al.'s [11], and is shown in Fig. 3.12.

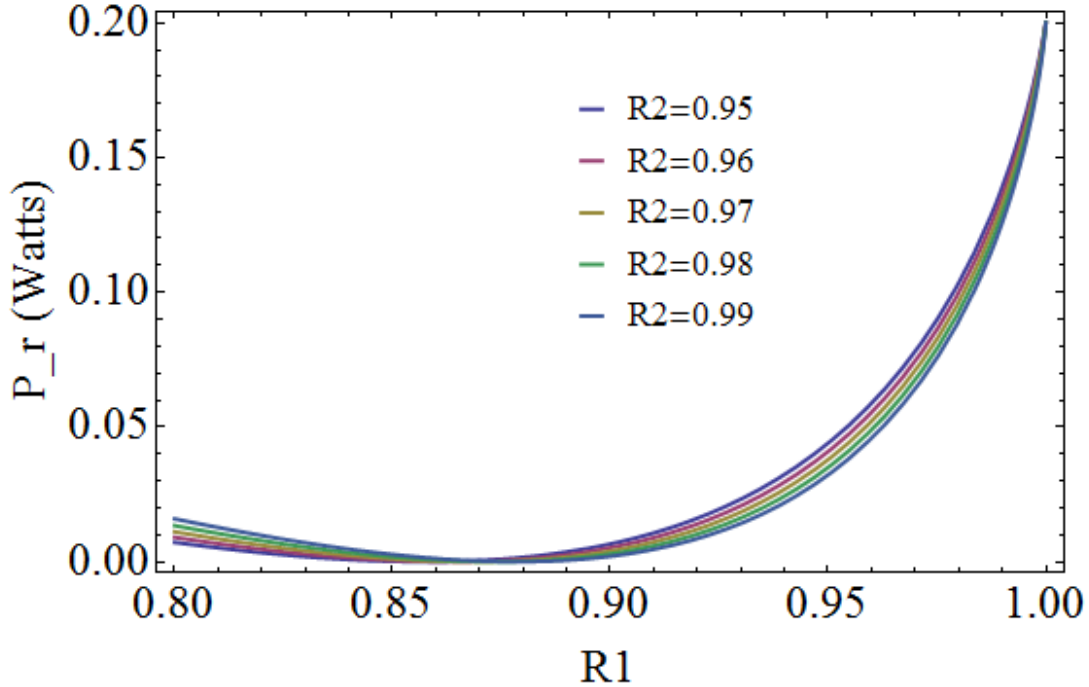


Figure 3.12: The reflected power as a function of reflectance of the incoupling mirror, for different values of the reflectance of the outcoupling mirror.

The value of R_1 at which P_{refl} is minimized for a given value of R_2 gives the value for which the cavity is impedance matched. As for choosing which R_2 line to use: since R_2 serves as the output coupler for the fundamental beam that will be used for locking the cavity, R_2 must be chosen low enough that some light is transmitted. Skoczowsky et. al. choose $R_2 = 0.96$. In Skoczowsky et. al.'s plot, the impedance matching condition is satisfied at $R_1 = 0.86$; mine is about the same, slightly higher.

However, $R_2 = 0.96$ is a relatively low reflectance, and significantly contributes to reducing the losses of the cavity (Eq. 3.37), which decreases the circulating power. The problem is that two mirrors are being used for coupling into and out of the cavity. Instead, the design can be modified such that the same mirror functions as both the incoupling and outcoupling mirror. By giving R_1 the job of transmitting both into and out of the cavity, R_2 can have high reflectance and not contribute to the losses.

This method is how many bow-tie resonators are designed. The SHG cavity described in N. Poli's dissertation thesis utilizes this idea. For the particular cavity designed in this thesis project, a bow-tie design is chosen. The variables designated to describe the geometry for the cavity of this thesis are indicated in Fig. 3.13. This diagram is a simplified version of Falkenau's diagram of Fig. 3.11.

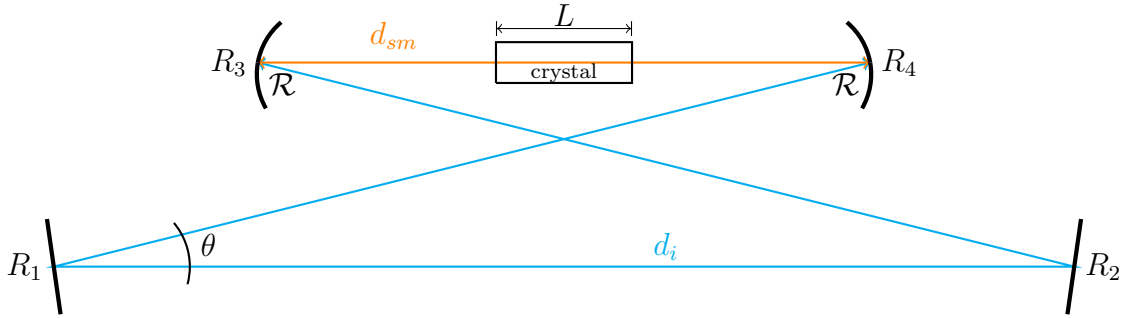


Figure 3.13: Cavity geometry. \mathcal{R} is the radius of curvature of the spherical mirrors; R_i is the reflectance of the i^{th} mirror; d_{sm} is the distance between the spherical mirrors (orange); d_i is the sum of the other three legs of the bow-tie (blue).

Similar to Skoczowsky, et. al.'s loss factor V , Poli defines a convention for the the losses after one pass. This loss factor is written as $1 - r_m$, where r_m is the “characteristic parameter,” defined to be:

$$r_m = TR_2R_3R_4(1 - \alpha_\omega L)(1 - \gamma_{SH}P_c) \quad (3.47)$$

where T is the transmission coefficient of the crystal, α_ω is the coefficient of linear losses for the fundamental beam, and $\gamma_{SH}P_c$ are the losses due to second harmonic conversion. In this notation, the g_{rt} used previously corresponds to $\sqrt{r_m R_1}$. However, the crystal is AR coated on both faces perpendicular to the beam propagation, and so the factor of T is included twice, such that r_m is:

$$r_m = T^2 R_2 R_3 R_4 (1 - \alpha_\omega L)(1 - \gamma_{SH}P_c) \quad (3.48)$$

Using the r_m notation instead of g_{rt} , the circulating and reflected powers are written as [13]:

$$P_c = \frac{1 - R_1}{(1 - \sqrt{R_1 r_m})^2} P_i \quad (3.49)$$

$$P_r = \frac{\sqrt{R_1} - \sqrt{r_m}}{(1 - \sqrt{R_1 r_m})^2} P_i \quad (3.50)$$

Impedance matching requires that the transmission of the input mirror is equal to the losses in the cavity. In the above equations, this corresponds to $P_r = 0$ for $R_1 = r_m$. This again leaves two coupled equations, Eq. 3.47 and Eq. 3.49. Solving these equations, the optimal value of R_1 can be determined.

These coupled equations turn out to be straightforward to solve. The AR curve for the crystal coating from Covesion, Inc. is shown in Fig. 3.14. From this curve, a value for the T in Eq. 3.47 can be approximated. In the range $\lambda=940\text{nm} - 1020\text{nm}$,

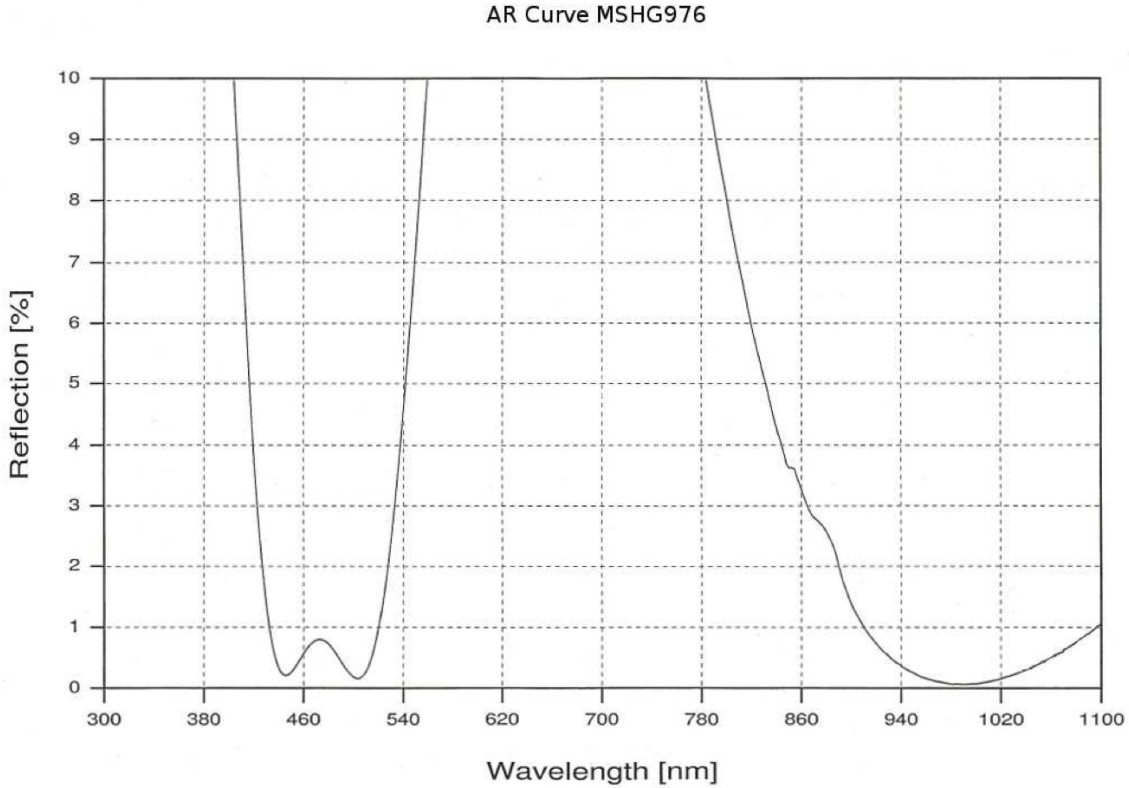


Figure 3.14: AR curve for MgO:LN [9]

R of the crystal is less than 0.5%, and around 994nm is closer to 0.01%. Therefore, the transmission T of the crystal is considered to be 99%.

The coefficient of linear losses of the crystal is obtained from Schwesyg, et. al. [20]. This paper provides absorption plots for an MgO:LN crystal in the ranges 340nm-800nm and 2000nm-3000nm. However, Schwesyg et. al. are unable to plot absorption between 800nm-2000nm, which they indicate are around 0.0005 cm^{-1} , due to the fact that their instrument is limited to about 0.003 cm^{-1} . For the calculations here, α_ω is taken to be 0.0005 cm^{-1} .

The value of γ_{SH} was calculated in Eq. 3.29 to be 50.54 mW^{-1} for a 20mm length crystal and a nonlinear coefficient of $d_{eff} = 14 \text{ pm/V}$. Since the input fundamental beam (the output from the ECDL discussed in the first half of this thesis) lases with about 220mW of power, this value is a good estimation of P_F .

Now, all the information needed to calculate R_1 for impedance matching has been collected. The parameters R_2 , R_3 , and R_4 are free to be varied. Starting with $R_2 = R_3 = R_4 = 0.99$, R_1 is set to $R_1 = r_m$, and Eq. 3.49 is simplified. This can be plugged in to Eq. 3.47, and Mathematica used to generate solutions. Two solutions for r_m are obtained: $r_m = 0.879497$ and 1.08052 . The second of these is not a physical result. The reflectance parameter cannot exceed 1, or it would indicate

that more than 100 percent of the incident light is coupled into the cavity. Therefore, the solution for impedance matching is $r_m (= R_1) = 0.879497$. This means that for $R_2 = R_3 = R_4 = 0.99$ and the other known values, the cavity will be impedance matched for $R_1 = 0.879$.

3.2.7 Astigmatism

Astigmatism in an optical beam is the phenomenon of a beam's having two components in planes perpendicular to its propagation with different focal points [5]. In resonators, this is caused by asymmetrical optical components. For instance, spherical mirrors reflect a collimated beam such that it has two foci: If f is the focal point for a collimated beam perpendicularly incident on the mirror, then for beams incident at some θ , the focal point in the tangential plane (f_t) and the focal point in the sagittal plane (f_s) vary according to:

$$\begin{aligned} f_t &= f \cos(\theta/2) = \frac{\mathcal{R}}{2} \cos(\theta/2) \\ f_s &= \frac{f}{\cos(\theta/2)} = \frac{\mathcal{R}}{2 \cos(\theta/2)} \end{aligned} \tag{3.51}$$

where \mathcal{R} is the radius of curvature of the convex mirrors. While a ring resonator with planar mirrors and convex lenses will be free of astigmatism, the problem of additional optical surfaces inducing more losses to the cavity outweighs the benefit of it being astigmatism-free. The issue of astigmatism can be solved in the case of spherical mirrors in a bow-tie cavity by making the incoming beam elliptical and by properly selecting the distance between the spherical mirrors of the cavity [5].

Solving with an equivalent setup of mirrors and lenses:

In order to determine this d_{sm} for which the effects of astigmatism are eliminated, the modes of the bow-tie cavity must be calculated. To do so, Falkenau [5] shows that the symmetrical bow-tie cavity can be described by an equivalent setup of lenses, as shown in Fig. 3.15. It can be further reduced to an equivalent resonator made of two flat mirrors with one lens in between, as depicted in Fig. 3.16 [5]. In this reduced configuration, the Gaussian mode is stable if the focal points reside on the surfaces of the mirrors [5].

Eq. 3.15, from the previous discussion of Gaussian beams, is a solution to Maxwell's wave equation $\nabla^2 u + k^2 u = 0$. It can be simplified for paraxial beams [5] as:

$$u(\vec{r}) = \frac{u_1}{q(z)} e^{-ik \frac{x^2 + y^2}{2q(z)}} \tag{3.52}$$

where

$$\frac{1}{q(z)} = \frac{1}{R(z)} - i \frac{\lambda}{\pi w^2(z)} \tag{3.53}$$

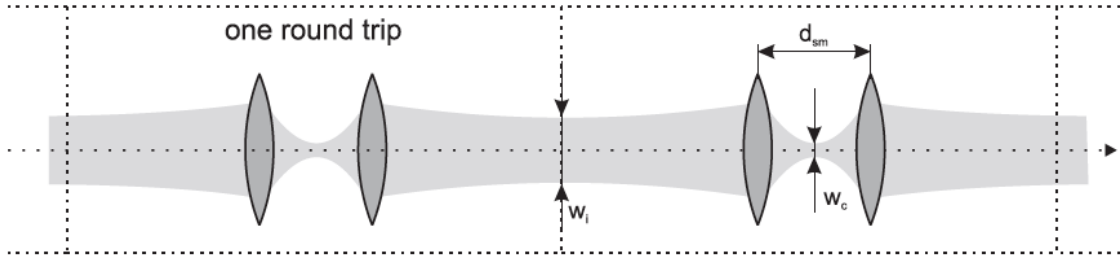


Figure 3.15: A bow-tie cavity reduced to an equivalent setup of lenses. [5]

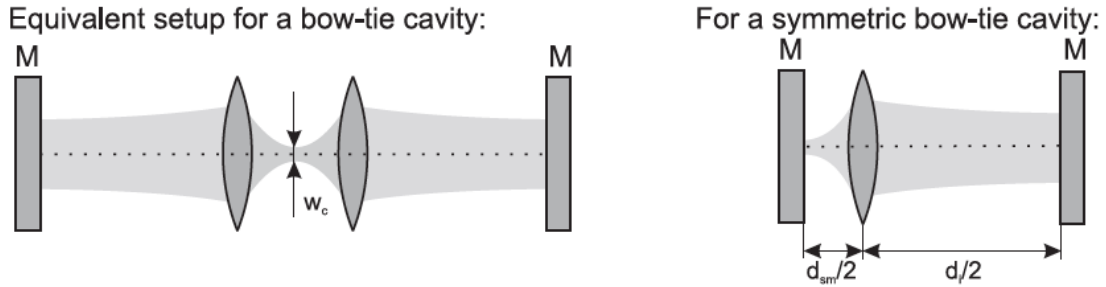


Figure 3.16: A bow-tie cavity reduced to an equivalent setup of lenses and mirrors. [5]

and $w(z)$ and $R(z)$ are as previously defined (Eq. 3.16). At a focal point, the wavefront of a Gaussian beam is a plane wave; this therefore reduces to:

$$\begin{aligned} \frac{1}{q(z)} &= -i \frac{\lambda}{\pi w^2(z)} \\ q(z) &= \frac{i\pi w^2(z)}{\lambda} \end{aligned} \quad (3.54)$$

The beam is altered as it propagates through the cavity and encounters the various optical components. These transformations can be represented by 2×2 matrices, which, for the symmetric equivalent cavity of Fig. 3.16, are:

$\begin{pmatrix} 1 & d_{sm}/2 \\ 0 & 1 \end{pmatrix}$ This represents the propagation from the left mirror of the symmetric equivalent cavity to its lens, along the distance $d_{sm}/2$.

$\begin{pmatrix} 1 & 0 \\ -1/f & 1 \end{pmatrix}$ is the lens of the equivalent cavity, with focal length f , which will differ for the tangential and sagittal components of the beam.

$\begin{pmatrix} 1 & d_i/2 \\ 0 & 1 \end{pmatrix}$ is the propagation from the lens to the right mirror of the symmetric equivalent cavity, along the distance $d_i/2$.

These transformations can be matrix multiplied to result in the total matrix, M , of

the cavity on the beam:

$$M = \begin{pmatrix} A & B \\ C & D \end{pmatrix} = \begin{pmatrix} 1 & d_{sm}/2 \\ 0 & 1 \end{pmatrix} \cdot \begin{pmatrix} 1 & 0 \\ -1/f_1 & 1 \end{pmatrix} \cdot \begin{pmatrix} 1 & d_i/2 \\ 0 & 1 \end{pmatrix} \quad (3.55)$$

To include the effect of the crystal as well, one must include:

$$\begin{pmatrix} 1 & L/2 \\ 0 & 1 \end{pmatrix} \text{ is the propagation along half the length of the crystal.}$$

$$\begin{pmatrix} 1 & 0 \\ 0 & 1/n_\omega \end{pmatrix} \text{ is the effect on the beam when the beam crosses from air, of refractive index 1, to the crystal, of refractive index } n_\omega.$$

Since the equivalent cavity of mirrors and lenses is symmetric, only half of the cavity is considered in these matrix transformations. The transformation matrix M for this half-cavity becomes:

$$\begin{aligned} M &= \begin{pmatrix} A & B \\ C & D \end{pmatrix} \\ &= \begin{pmatrix} 1 & L/2 \\ 0 & 1 \end{pmatrix} \cdot \begin{pmatrix} 1 & 0 \\ 0 & 1/n_\omega \end{pmatrix} \cdot \begin{pmatrix} 1 & \frac{(d_{sm}-L)}{2} \\ 0 & 1 \end{pmatrix} \cdot \begin{pmatrix} 1 & 0 \\ -1/f & 1 \end{pmatrix} \cdot \begin{pmatrix} 1 & d_i/2 \\ 0 & 1 \end{pmatrix} \end{aligned} \quad (3.56)$$

where L has been subtracted from d_{sm} to keep the total path length fixed.

The overall matrix M acts on the beam parameter $q(z)$, transforming it from an initial parameter q_1 to a final parameter q_2 :

$$q_2 = \frac{Aq_1 + B}{Cq_1 + D} \quad (3.57)$$

Since a resonator mode is self-consistent, the Gaussian beam parameter $q(z)$ must return to its original state after one trip through the cavity, requiring that $q_1 = q_2$. However, this matrix M does not represent a full trip around the cavity, but rather starts at the center of the crystal and ends halfway between the planar mirrors. Thus q_1 does not equal q_2 for this half-cavity matrix. Defining q_1 to be the beam parameter that corresponds to achieving the beam waist w_i (between the two planar mirrors), and q_2 to be the beam parameter corresponding to w_c , (the waist between the concave mirrors, i.e., the beam waist in the crystal), the beam parameters can be written in terms of the waists:

$$q_1 = q_i = \frac{i\pi w_i^2(z)}{\lambda}, \quad \text{and} \quad q_2 = q_c = \frac{i\pi w_c^2(z)}{\lambda} \quad (3.58)$$

which can be plugged into matrix M (Eqn. 3.57) to get two coupled equations¹, one from the real part and one from the imaginary part, in terms of A, B, C , and D , the

¹The same equations have been obtained as found in [5] with the exception of an extra factor of π in the $w_i^2 w_c^2$ coefficient of the second equation.

components of M :

$$\begin{aligned} Aw_i^2 - Dw_c^2 &= 0 \\ B\lambda^2 + C\pi^2 w_i^2 w_c^2 &= 0 \end{aligned} \tag{3.59}$$

A, B, C , and D are functions of the cavity parameters d_{sm} , f , d_i , L , and n_ω . The values L , n_ω , and λ are known: $L = 20$ mm, $n_\omega = 2.216768$ (calculated from $n_e[994\text{nm}, 211^\circ\text{K}]$, see Eq. 3.26), and $\lambda = 994\text{nm}$. f is either the sagittal or tangential focus, from Eq. 3.51. Using \mathcal{R} , θ , and d_i as variable parameters, the coupled equations can be solved for w_c and w_i in terms of d_{sm} .

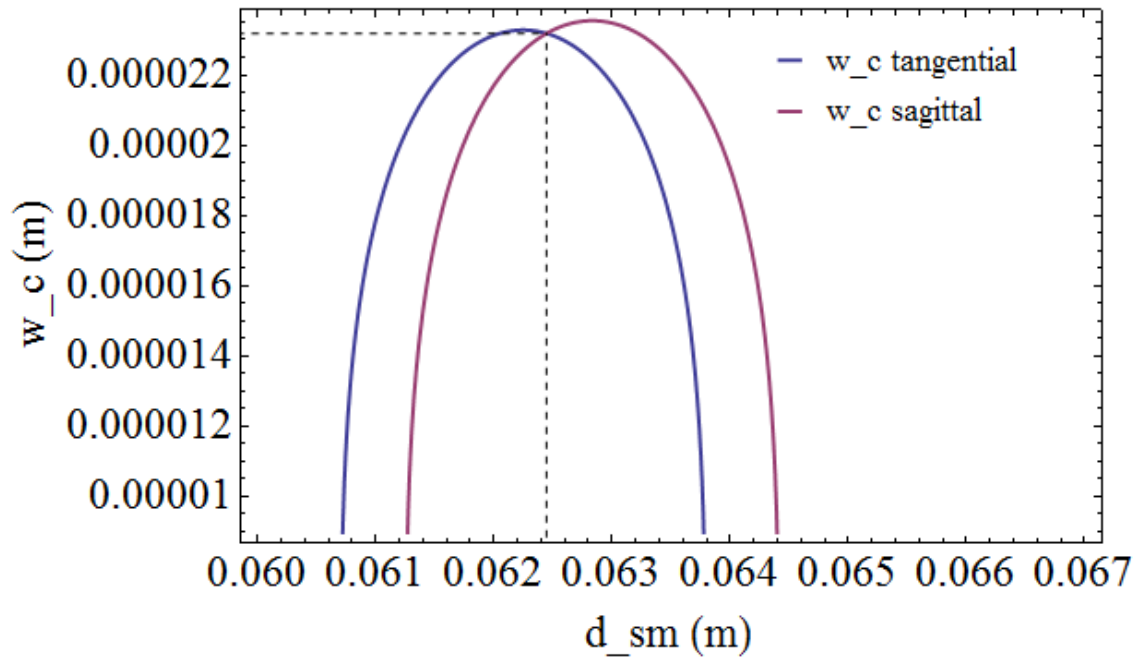
Solving these equations results in a total of eight solutions for each w_c and w_i . After determining which of these corresponded to the physical situation, w_c can be plotted for the tangential and sagittal components of the beam on the same plot, and w_i for both components on another, as shown in Fig. 3.17.

These plots very closely resemble the results achieved by Falkenau [5]. The intersection point of the two w_c curves indicates the d_{sm} for which the tangential and sagittal beam waists are located at the same point in the crystal. w_c . The intersection can then be solved; this intersection point is the location in the crystal at which a circular beam profile can be achieved [5].

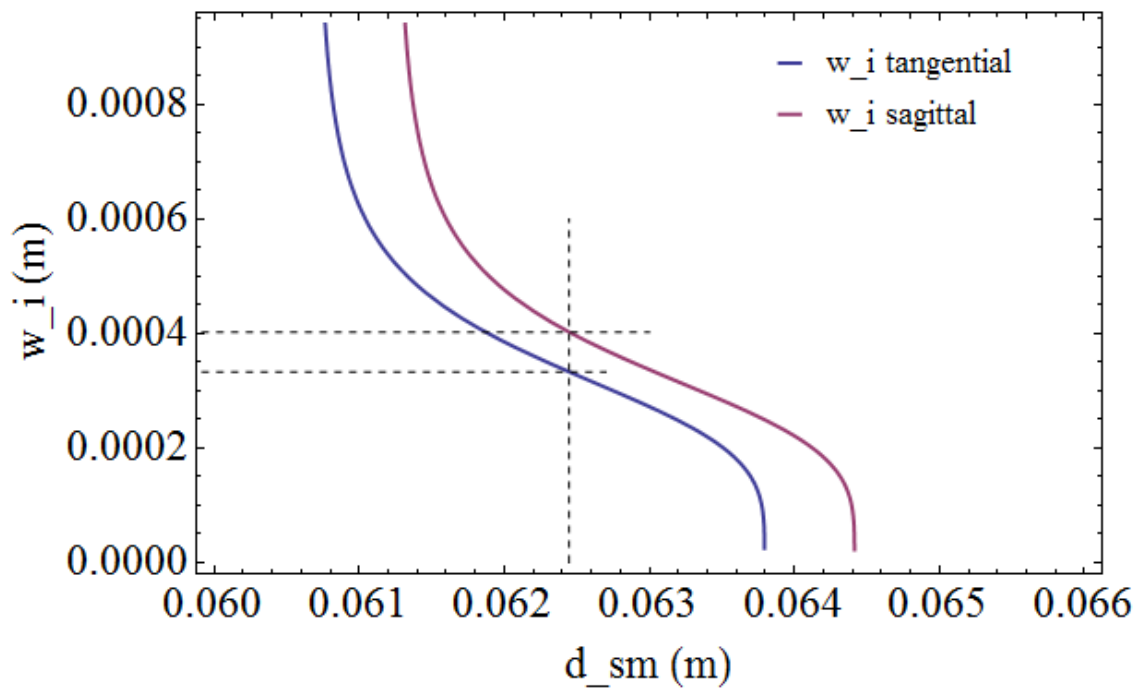
At this intersection, both beam waist curves are fairly flat, meaning that the intersection is stable: small changes of the mirrors' position and angle as the cavity is aligned will not change the beam waist significantly. This also makes the cavity more stable long-term against mechanical and acoustic vibrations. If d_{sm} is perturbed, the components of the beam waist will remain matched.

Note that the bow-tie configuration minimizes astigmatism. As the angle θ is increased, the beams approach the same angle of incidence on the mirrors as in a ring cavity. When θ is increased from 12° to 22° , the angle of incidence of the beam on the convex mirrors increases, and the astigmatism is far worse: the foci of the tangential and sagittal components of the beam get farther away from each other, as shown in Fig. 3.18. This also affects the stability. At higher values of θ , the intersection of the waists in the crystal of the tangential and sagittal beam components moves out of a stable region.

This same computation can be done for the cavity in the absence of the crystal. To do so, Eq. 3.55 is used to determine the coefficients of Eq. 3.59, and the coupled equations are solved. Plotting the solutions to w_c both with and without crystal, as shown in Fig. 3.19, it is clear that there is a lensing effect due to the interaction of the curved wavefront of the incident beam and the planar crystal surface, such that the beam waist is much larger with the crystal inserted in the cavity.



(a)



(b)

Figure 3.17: Plots of (a) the beam waist in the crystal, w_c , and (b) the beam waist between the planar mirrors, w_i , for both the tangential and sagittal components of the beam, as functions of the distance between the spherical mirrors, d_{sm} .

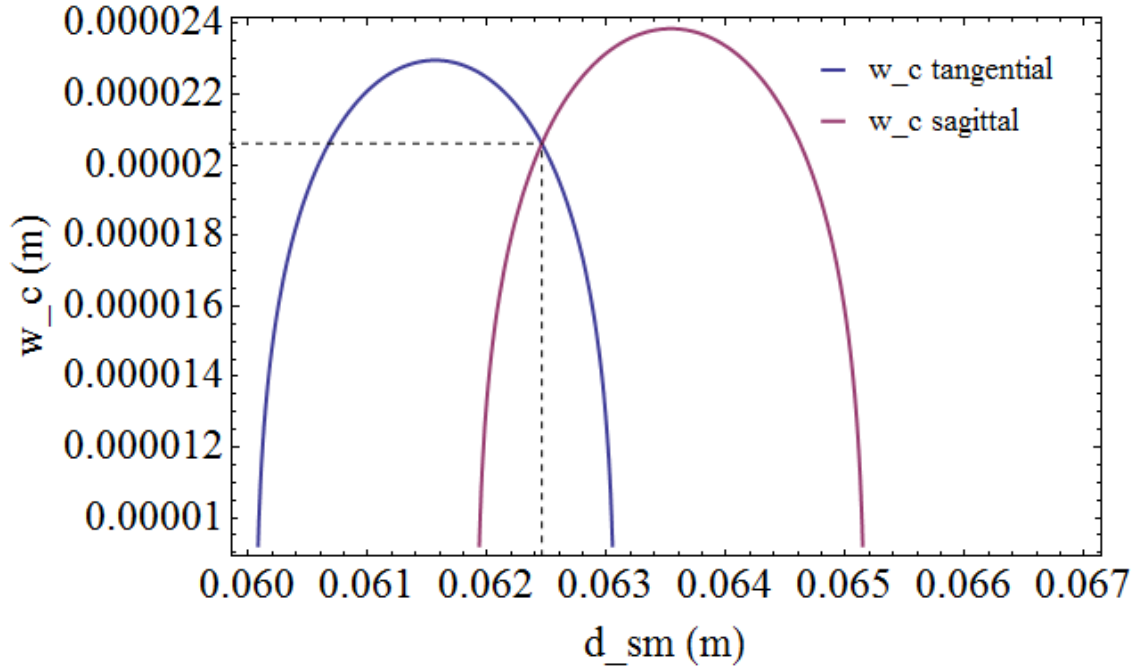


Figure 3.18: The beam waist in the crystal as a function of d_{sm} , for $\theta = 22^\circ$. This illustrates how the folded beam path minimizes astigmatism.

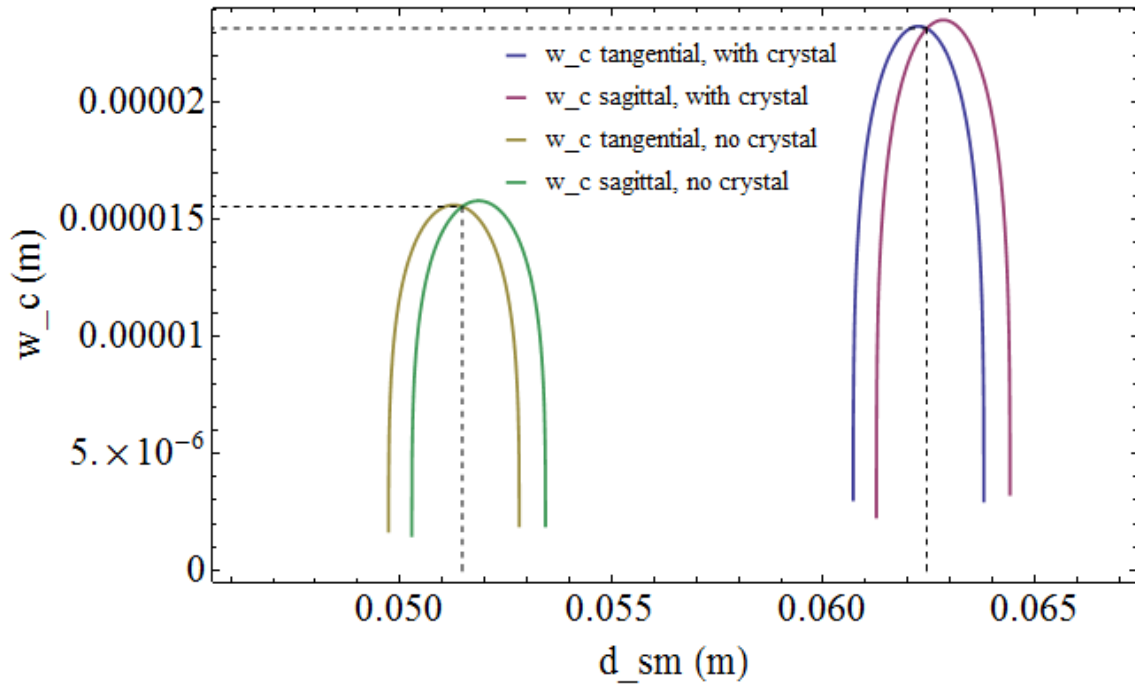


Figure 3.19: w_c plotted for both the tangential and sagittal beam components as a function of d_{sm} , for the cavity with and without a crystal.

The crystal will be easier to align perpendicularly to the beam if these two sets of curves (with and without the crystal) have overlapping stable regions [5]. However, with a crystal length of 20 mm, this overlap has not been found possible to achieve; no reason has been found to indicate that it is absolutely necessary to the crystal alignment.

Solving without the equivalent setup of mirrors/lenses:

It is informative to show how to solve without the equivalent setup of mirrors and lenses, and instead, to simply do the same matrix type calculation around the full cavity. Fig. 3.20 shows the geometry of the bow-tie cavity for reference.

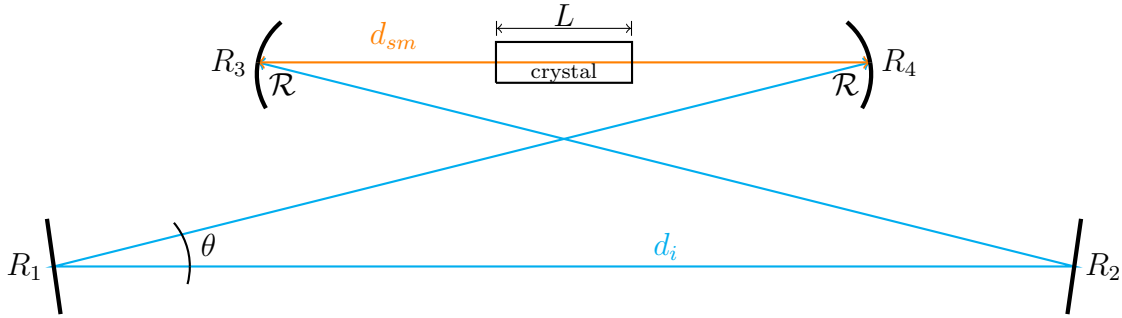


Figure 3.20: Cavity geometry. Figure reproduced from Fig. 3.13 for reference.

Starting at the center of the crystal, one can follow the beam path around the bow-tie:

$\begin{pmatrix} 1 & L/2 \\ 0 & 1 \end{pmatrix}$	propagation from the center of the crystal to one end of the crystal,
$\begin{pmatrix} 1 & 0 \\ 0 & 1/n_\omega \end{pmatrix}$	change index of refraction at the boundary between crystal and air,
$\begin{pmatrix} 1 & (d_{sm} - L)/2 \\ 0 & 1 \end{pmatrix}$	propagation from the end of the crystal to the first concave mirror,
$\begin{pmatrix} 1 & 0 \\ -1/f & 1 \end{pmatrix}$	focusing due to the concave mirror,
$\begin{pmatrix} 1 & d_i \\ 0 & 1 \end{pmatrix}$	propagation along d_i , the other three legs of the bow-tie, from one concave mirror to the other concave mirror,
$\begin{pmatrix} 1 & 0 \\ -1/f & 1 \end{pmatrix}$	focusing by the second concave mirror,
$\begin{pmatrix} 1 & (d_{sm} - L)/2 \\ 0 & 1 \end{pmatrix}$	propagation from the concave mirror to the crystal,

$$\begin{pmatrix} 1 & 0 \\ 0 & n_\omega/1 \end{pmatrix} \quad \text{change of refractive index at boundary between air and crystal,}$$

$$\begin{pmatrix} 1 & L/2 \\ 0 & 1 \end{pmatrix} \quad \text{propagation from the end of the crystal back to the center.}$$

Matrix multiplying these, the total matrix transformation is:

$$\begin{aligned} M &= \begin{pmatrix} A & B \\ C & D \end{pmatrix} \\ &= \begin{pmatrix} 1 & L/2 \\ 0 & 1 \end{pmatrix} \cdot \begin{pmatrix} 1 & 0 \\ 0 & 1/n_\omega \end{pmatrix} \cdot \begin{pmatrix} 1 & (d_{sm} - L)/2 \\ 0 & 1 \end{pmatrix} \cdot \begin{pmatrix} 1 & 0 \\ -1/f & 1 \end{pmatrix} \cdot \begin{pmatrix} 1 & d_i \\ 0 & 1 \end{pmatrix} \\ &\quad \cdot \begin{pmatrix} 1 & 0 \\ -1/f & 1 \end{pmatrix} \cdot \begin{pmatrix} 1 & (d_{sm} - L)/2 \\ 0 & 1 \end{pmatrix} \cdot \begin{pmatrix} 1 & 0 \\ 0 & n_\omega/1 \end{pmatrix} \cdot \begin{pmatrix} 1 & L/2 \\ 0 & 1 \end{pmatrix} \end{aligned} \quad (3.60)$$

In this case, M *does* represent propagation around the entire cavity; the beam returns to its initial point, and so $q_1 = q_2$. Acting this matrix on the beam parameter and solving as done for the case of the equivalent setup, plotting the waist between the two concave mirrors (i.e., the waist in the crystal) gives the same curves and same intersection point as obtained with the equivalent setup (shown in Fig. 3.17a). This reinforces the point that the symmetric setup is equivalent to the full cavity, and clarifies how each matrix corresponds to each beam-altering element of the cavity.

3.2.8 Thermal Lensing

Due to the high circulating power in the cavity, some of the fundamental radiation is dissipated in the crystal, creating a temperature gradient that has a lensing effect. This must be accounted for in the previous cavity geometry calculations. The thermal lens has a focal length, f , and a lensing power, p , (in Diopters, or inverse meters), given by [21, 22]:

$$p = \frac{1}{f} = \frac{\alpha_\omega (\partial n / \partial T) P_c}{\pi K_c} \int_{-L/2}^{L/2} \frac{1}{w^2(z)} dz \quad (3.61)$$

where α_ω is the previously determined linear absorption coefficient, $\partial n / \partial T|_{T \rightarrow 211^\circ\text{C}}$ is the partial derivative of the refractive index with respect to temperature, evaluated at the temperature at which the crystal will be held (211°C, in this case), P_c is the circulating power, K_c is the thermal conductivity, and $w(z)$ is the $1/e^2$ beam radius along the length of the crystal, $w(z) = w_0 \sqrt{1 + (z/(\pi n w_0^2 / \lambda))^2}$, where w_0 is the desired 22.41 μm beam waist. From [22], the thermal conductivity for PPLN is given to be $K_c = 4.6 \text{ W/m } ^\circ\text{C}$.

Solving with values specific to this cavity, $p = 1.017 \times 10^{-16}$ Diopters (1/m). This corresponds to a thermal lensing focal length of $f = 9.83 \times 10^{15}$ m.

To take this lensing into account, the crystal can be considered as a thick lens, which can be represented by additional matrices in the overall matrix operating on the beam parameter. To account for the axially varying beam radius $w(z)$ in the crystal, the lensing can be approximated by slicing the crystal into N thin gradient-index lenses of infinitesimal thickness Δz , and a matrix M_T represents each of these lenses acting on the beam. M_T can be multiplied in the limit $N \rightarrow \infty$. M_T is defined as [21]:

$$M_T = \begin{pmatrix} 1 & L/2n_0 \\ 0 & 1 \end{pmatrix} \cdot \begin{pmatrix} 1 & 0 \\ -p & 1 \end{pmatrix} \cdot \begin{pmatrix} 1 & L/2n_0 \\ 0 & 1 \end{pmatrix} \quad (3.62)$$

where n_0 is the on-axis index of refraction (the value of the index of refraction without the effects of thermal lensing). This factor of the index of refraction is not included in propagation in the crystal in the calculations done by either [22, 5]. Following their calculations, the calculations in this thesis likewise do not include the index of refraction in the corresponding matrix.

For simplification, this set of N lenses can be approximated by a finite number of lenses along the crystal. Following the method of [22], the thermal lensing can be approximated as 8 ideal thin lenses spaced equally along the crystal, as illustrated in Fig. 3.21.

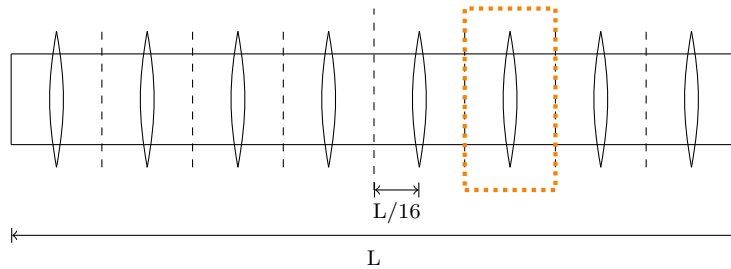


Figure 3.21: Thermal lensing modeled in the crystal as 8 thin lenses evenly spaced along the crystal. The orange dotted box indicates the section represented by one M_{lens} .

The matrix representing each of these 8 lenses is:

$$M_{lens} = \begin{pmatrix} 1 & L/16 \\ 0 & 1 \end{pmatrix} \cdot \begin{pmatrix} 1 & 0 \\ -p/8 & 1 \end{pmatrix} \cdot \begin{pmatrix} 1 & L/16 \\ 0 & 1 \end{pmatrix} \quad (3.63)$$

where the first matrix in M_{lens} represents propagation along a sixteenth of the crystal, the second represents the lens, and the third propagation along the next sixteenth. Therefore, starting in the center of the crystal and following the beam around the

bow-tie cavity, the overall matrix operation becomes:

$$\begin{aligned}
M &= \begin{pmatrix} A & B \\ C & D \end{pmatrix} \\
&= M_{lens} \cdot M_{lens} \cdot M_{lens} \cdot M_{lens} \cdot \begin{pmatrix} 1 & 0 \\ 0 & 1/n_\omega \end{pmatrix} \cdot \begin{pmatrix} 1 & (d_{sm} - L)/2 \\ 0 & 1 \end{pmatrix} \\
&\quad \cdot \begin{pmatrix} 1 & 0 \\ -1/f & 1 \end{pmatrix} \cdot \begin{pmatrix} 1 & d_i \\ 0 & 1 \end{pmatrix} \cdot \begin{pmatrix} 1 & 0 \\ -1/f & 1 \end{pmatrix} \cdot \begin{pmatrix} 1 & (d_{sm} - L)/2 \\ 0 & 1 \end{pmatrix} \cdot \begin{pmatrix} 1 & 0 \\ 0 & n_\omega/1 \end{pmatrix} \\
&\quad \cdot M_{lens} \cdot M_{lens} \cdot M_{lens} \cdot M_{lens}
\end{aligned} \tag{3.64}$$

which is consistent with the beam propagation with the thermal lensing as modeled as the eight lenses in Fig. 3.21: Beginning at the center of the crystal, the light first propagates through four of these ‘‘lenses.’’ Then, it crosses the boundary between the crystal and air, at which the refractive index changes from n_ω to 1. The next matrix element represents the propagation of the beam from the end of the crystal to the curved mirror, which is followed by a matrix representing the curved mirror’s effect on the beam, focusing it. The following is the propagation along d_i , all three other legs of the bow-tie. Then, again, the beam hits a curved mirror and is focused. It then traverses the distance between that curved mirror and the end of the crystal, where it changes to a medium of a different refractive index. (Note that here the beam is moving from refractive index 1 to n_ω rather than n_ω to 1, and so the matrix has a factor of $n_\omega/1$ rather than $1/n_\omega$ in it.) Finally the beam propagates along the other half of the crystal, through the other four lenses that represent the thermal lensing, returning to the starting location.

Once again, this represents the beam propagating full circle, so $q_1 = q_2$. Acting the matrix M on the beam parameter as done previously, and plotting $w_c(d_{sm})$ yields a plot negligibly different from that without accounting for thermal lensing. It therefore appears that with the thermal lens calculated here, the beam waist in the crystal is not altered to a noticeable degree.

3.2.9 Acceptance Bandwidths

It is important to determine the acceptance bandwidths of the cavity in order to determine the sensitivity of the cavity to small variations in the phase matching parameters. These small variations are $\delta\lambda$ and δT , as defined by [5] and found in Eqs. 3.65 and 3.66. Acceptance is defined as the value at which the conversion efficiency diminishes by a factor of two compared to the phase matching condition. For critical and noncritical phase matching, the angular acceptance $\delta\alpha$ (which can be found in [5]), must also be considered, since the angular position of the crystal determines the phase matching. For quasi-phase matching, as used here, the beam is directed along the crystal perpendicular to the poling, and is built on an optical

table so any vibrations that affect this alignment are suppressed. The acceptance bandwidths are:

$$\delta\lambda = \frac{1.39\lambda_\omega}{2\pi L} \left(\frac{\partial n_\omega}{\partial \lambda_\omega} - \frac{1}{2} \frac{\partial n_{2\omega}}{\partial \lambda_{2\omega}} \right)^{-1} \quad (3.65)$$

$$\delta T = \frac{1.39\lambda_\omega}{2\pi L} \left(\frac{\partial}{\partial T_\omega} (n_\omega - n_{2\omega}) \right)^{-1} \quad (3.66)$$

where, λ_ω and $\lambda_{2\omega}$ are the fundamental and second harmonic wavelengths and n_ω and $n_{2\omega}$ are the indices of refraction at the fundamental and second harmonic wavelengths, respectively. Taking partial derivatives of the best fit equation for the index of refraction for PPLN (Eq. 3.26), the angular bandwidth is calculated to be $\delta\lambda=51.067\mu\text{m}$, which corresponds to a δf of 5.87 THz, and the temperature bandwidth is calculated to be $\delta T = 0.277^\circ\text{C}$.

The wavelength should be tunable by several linewidths of the transition [5], which corresponds to an order of tens of MHz. The acceptance bandwidth of $\delta f= 5.87$ THz is a factor of 10^5 larger than the required tuning range of the transition, and so the SHG will remain phase matched within this detuning range.

The temperature controller from Covesion is specified with a stability of $\pm 0.01^\circ\text{C}$. Therefore, the crystal temperature will be controlled to within a range that is a factor of 10 times smaller than the required temperature acceptance of $.277^\circ\text{C}$. Thus, the phase matching will remain fixed with the temperature control of the crystal oven.

3.2.10 Optimizing the Cavity

Now that the various parameters of the cavity are described and can be calculated, they must be considered collectively. The resonator should approach the optimum focusing condition (L/z_R) while being impedance matched, minimizing astigmatism, and also taking into consideration thermal lensing effects and satisfying acceptance bandwidths. The relationships between all the variables and the characteristics of the cavity are summarized in the flowchart of Fig. 3.22. The following discussion presents the results of the calculations for this particular doubling cavity.

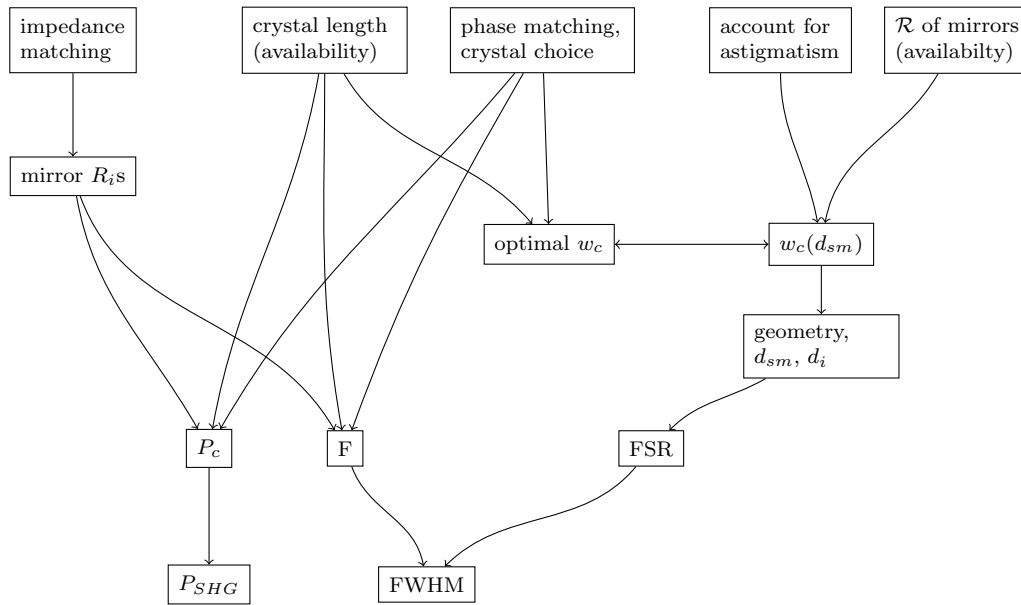


Figure 3.22: Flowchart illustrating the relationships between the variables and calculable quantities characterizing the cavity.

The optimal reflectance of the incoupling mirror (R_1) is determined in order to impedance match the cavity. Minimizing the circulating power, the optimal reflectance is calculated to be $R_1 = 0.8825$. The reflectances for the other mirrors (R_2 , R_3 , and R_4) are chosen: from availability of concave spherical mirrors from various vendors, it is determined reasonable to purchase mirrors with reflectances of 99.5%, so $R_2 = R_3 = R_4 = 0.995$. g_{rt} (Eq. 3.37) is then calculable given these values. For this particular cavity, summing over the indices k and j , g_{rt} becomes:

$$g_{rt} = \sqrt{\prod_k r_k \cdot \prod_j t_j} = \sqrt{T^2 R_1 R_2 R_3 R_4 (1 - \alpha_\omega L) (1 - \gamma_{SH} P_c)} \quad (3.67)$$

which agrees with r_m from N. Poli's dissertation, where $g_{rt} = \sqrt{r_m R_1}$ as previously discussed (except for T^2 to account for loss at both perpendicular faces of the crystal). The values of T , α_ω , L , and γ_{SH} are known, and the circulating power, P_c can be calculated from Eq. 3.49. These are then used to calculate \mathcal{F} of the resonator (Eq. 3.36). For this cavity, the finesse is calculated to be $\mathcal{F} = 24.0985$.

The geometry of the bow-tie cavity is then determined in order to compensate for the astigmatism introduced by the spherical mirrors. The variable parameters d_i , R , and θ , can be varied until the tangential and sagittal components of the beam waist in the crystal intersect at a value of w_c , which matches the value of w_c determined in Section 3.2.1 to be optimal for phase matching in a crystal of a given length. (Recall that this has been shown for this cavity to be $w_0(20\text{mm}) = 22.4\mu\text{m}$ in Eq. 3.32, for a crystal length of 20mm. Had the crystal not already been purchased, its length would

be an additional parameter to be adjusted in these calculations). For this cavity, this intersection occurs for $\mathcal{R} = 50\text{mm}$, $\theta = 12^\circ$, and $d_i = 850\text{mm}$.

The intersection of the beam waists indicates the necessary d_{sm} . In this case the intersection is at $w_c = 23.18\mu\text{m}$, $d_{sm} = 62.45\text{mm}$. With d_{sm} and d_i , the FSR is calculated (Eq. 3.34):

$$FSR = \frac{c}{l_{opt}} = \frac{c}{d_i + (d_{sm} - L) + n_c L} \quad (3.68)$$

where $n_c = n_e(994\text{nm}, 211^\circ\text{K}) = 2.216768$, and $L = 20\text{mm}$. The FSR is calculated to be 320 MHz. This FSR and \mathcal{F} give a linewidth of 13.28 MHz.

Once the reflectances and geometries are selected, the circulating power (calculated from Eq. 3.49, or more generally, from Eq. 3.41), can be used to calculate the second harmonic output power, from Eq. 3.28. With the cavity, the incident beam on the crystal is P_c rather than P_ω , and so the equation for the second harmonic power becomes: $P_{SHG} = \gamma_{SH} P_c^2$. With all values calculated for this cavity, $P_{SHG} = 139.21\text{mW}$. This is plenty of output second harmonic power; only a few mW are needed for the strontium repumper.

Since for these values the astigmatism does not alter the curves for the beam waist, and calculating the acceptance bandwidths and determining that small variations in wavelength and temperature will not be problematic, the conditions thus calculated are satisfactory for the cavity.

3.3 Cavity Components

To date, the crystal, oven, and temperature controller have been purchased. Still to be purchased are the two planar and two concave mirrors, the piezo, and mounts. Product numbers for the purchased components can be found in Appendix B.

3.4 Future Doubling Cavity Work

This project will be passed on for completion to a new member of the Weld Lab. The next task to be completed will be to test the single-pass, no cavity SHG efficiency, which has a predicted value of:

$$P_{SHG} = \gamma_{SH} P_F^2 = 2.02 \text{ mW} \quad (3.69)$$

All other cavity components will need to be purchased, including the mirrors, piezo, and mounts. The cavity will then be ready for assembly and alignment. Then the cavity-enhanced SHG efficiency can be tested, to see if its predicted value of

$$P_{SHG} = \gamma_{SH} P_c^2 = 139.21 \text{ mW} \quad (3.70)$$

is achieved. Finally, the cavity can be locked and stabilized.

Once this cavity is completed and successful frequency doubling is achieved with output power sufficient to address the 497nm strontium transition, this information on SHG and cavity design can be used for other frequency doubling projects. These projects will be used to achieve wavelengths to address other atomic transitions in future strontium and lithium experiments of the Weld Lab. Ultimately, a unibody design, much like that for the ECDL of the first half of this thesis, would be ideal for the doubling cavity as well. Using the work presented in the past chapter as a platform for understanding the principles and calculations describing a cavity for enhancement of a nonlinear optical process, future cavity designs can go further to incorporate stability and other benefits into the design.

Chapter 4

Conclusions

This thesis has described two components of the overall project to develop a stable light source for ultracold strontium experiments. Of the many narrow linewidth wavelengths needed for the cooling, trapping and imaging of strontium, this particular project worked toward the development of the 497nm repumper, used to capture the atoms lost to a metastable state of the strontium cooling process.

The first part of this project described the construction of the first ECDL built in-house for the Weld Lab: a 994nm, narrow linewidth, stable light source. In addition to having successfully produced stable lasing at 994nm with 220mW of output power, the description presented in this thesis meant to serve as an instructive guide for ECDL construction. These future projects will be wavelength adaptable so that light stable, narrow linewidth light sources can be produced for other wavelengths to address other necessary atomic transitions. Currently, a second ECDL for the Weld Lab, to produce a 403nm light source, is under construction with guidance from this work.

The second part of this thesis regarded research into the method of frequency doubling, the process used to convert this 994nm light to the 497nm necessary for the strontium repumper. The second chapter explained some basic nonlinear optics theory, discussed the physics of the process of second harmonic generation, and provided discussion and examples of calculations of the geometry and properties of stable cavities. The particular design for the cavity-enhanced 994nm to 497nm SHG process is determined through this thesis. This work is intended to provide a foundation for the Weld Lab's future frequency doubling projects.

Appendix A

Product numbers for ECDL components

A.1 Epoxies

Item	Vendor, P/N
Epo-Tek 353ND, (8 oz. kit)	Epoxy Technology, Inc. P/N 353ND
Torrseal, Loctite 1C Hysol (4 oz. EPK kit)	Amazon.com, P/N B004VODQ0M
GCElectronics 10114 Quik Stik 5m epoxy, 2.5 oz	Allied Electronics, Inc. P/N 70159772
Escali high precision lab scale, 125 g × .01 g	Amazon.com P/N B000LPLI6Y
Plastic mixing sticks	
Plastic syringes w/ taper tip, .20oz, .024"	McMaster-Carr P/N 7510A661
Toaster oven (Black & Decker TRO480BS), large capacity	Amazon.com P/N B002CVTT3Y

A.2 Diffraction gratings

Item	Vendor, P/N
Holographic reflection grating, Au-coated, 1350 g/mm, 3.2mm thick \times 6mm length \times 12mm width	Newport Corporation Richardson Gratings P/N 33999FL02-229H
Ruled reflection grating, Au-coated, 1200 g/mm, 3.2mm thick \times 6mm length \times 12mm width	Newport Corporation Richardson Gratings P/N 33999FL02-530R
Holographic reflection grating, Au-coated, 1350 g/mm, 3.2mm thick \times 10mm length \times 12mm width	Newport Corporation Richardson Gratings P/N 33999FL02-229H

A.3 Electrical: protection circuit and wiring

Item	Vendor, P/N
Laser Diode and Temperature Controller 6305 ComboSource Controller 500mA	Arroyo Instruments, LLC.
10 Ω 1206 pkg resistor	Digi-Key P/N ERJ-8GEYJ100V
2 Ω 1206 pkg resistor	purchased from UCSB Electrical Engineering storeroom
0.1 μ F 1206 pkg capacitor	Digi-Key P/N 490-1775-1-ND
1000pF (1nF) 1206 pkg capacitor	(I accidentally purchased 100pF capacitors (from Digi-Key); to avoid waiting for the correct order to ship, I purchased the 1000pF capacitors from the UCSB EE storeroom)
EMI filter Murata ferrite bead 1206 pkg	Mouser P/N 81-BLM31A700S
SOD-323 pkg 1N5711 schottky diode	Mouser P/N 621-1N5711WS-F
printed circuit board	
Box for cable connections	purchased from UCSB Physics storeroom
(2) DB15HD connector, 3 rows, shell size E	Digi-Key P/N 17EHD015PAA
DB15 connector	Digi-Key P/N L717SDA15P-ND
DB9 connector	Digi-Key P/N L717SDE09P-ND
BNC connector	[found in Prof. Cannell's supplies]
6 ft. DB15HD extension cable	Deep Surplus P/N CB370-MM-6

6 ft. DB15 extension cable	Winford Engineering, LLC P/N EXT15-6
6 ft. DB9 extension cable	Winford Engineering, LLC P/N EXT9-6
BNC cable	(The Weld Lab already had an extra, I didn't need to purchase one)
Soldering iron with fine-point tip	
Solder	
Solder wick	
Solder fume extractor	Parts Express P/N 370-358
Helping hands with magnifying glass, flexible arms, locking base	
Fine-tipped tweezers, high grade tapered bent	McMaster-Carr P/N 8384A49
Kapton-coated (polyimide) round magnet wire, 23AWG heavy-build	MWS Wire Industries P/N 40633
23 AWG standard PVC-insulated electrical wire	
heat shrink tubing	
Heat gun	P/N

A.4 Diode laser

Item	Vendor, P/N
Ridge Waveguide Laser AR coated 980nm 50mW	Eagleyard Market Tech. Inc. P/N EYP-RWE-0980
980nm IR laser diode D5.6mm	Egismos P/N D6-4-980-100-N
Single mode laser diode 300mW 970-990nm (980)	QPhotonics, LLC P/N QLD-980-300S
3-pin socket for diode laser	Thorlabs P/Ns S8060 and S7060R
Collimation tube with optic	Thorlabs P/N LT230P-B
SM9 spanner wrench for a M9×0.5 optics housing	Thorlabs P/N SPW301
985nm laser diodes, bare, 200mW, 4 pins, 9mm pkg.	Power Technology P/N LD1715

A.5 O-rings

Item	Vendor, P/N
(3) Viton O-rings, ID 3/8, thickness 1/16	McMaster-Carr P/N 9464K17
(2) Viton O-rings, 3/32 width, ID 4.5	McMaster-Carr P/N 9464K115
Viton O-rings, 1/16 width, ID 5/64	McMaster-Carr P/N 9464K104

A.6 Screws/nuts/washers

Item	Vendor, P/N
(8) 4-40 jack screws, male thread, 3/16" hex length, 3/16" or 1/4" screw length	McMaster-Carr P/N 92710A215
(6) 4-40 hex nuts	
(2) 8-32×3/8" ss ^a socket head	McMaster-Carr P/N 92196A192
(15) 8-32×1" ss socket head	McMaster-Carr P/N 92196A199
(2) flat washers, stainless steel 301/302/304, OD .310, ID .206	Superior Washer P/N 300-966-031
(3) 3/8"-24×1/2" ss socket head	McMaster-Carr P/N 92196A355
4/40×1/4" ss socket head	McMaster-Carr P/N 92196A106
(6) 8-32×1" nylon screws	McMaster-Carr P/N 93135A199
(2) 4-40×1" ss socket head (length > 0.78)	
(4) 1/4-20×5/8" (length arbitrary) ss socket head	
Fine adjust screw 1/4-100 sleeve of Ø 0.343"±0.001", hole cut 0.345"±0.001"	Newport P/N 9376-K
1-72 ss socket head ^b , (length > 0.37)	

^a"ss" denotes stainless steel

^bThis screw is only necessary if one is machining a jig.

A.7 Cleaning supplies

Item	Vendor, P/N
Sonicator, Branson 2510 Ultrasonic Cleaner with mechanical timer	Cleanosonic P/N B2510MT
Alconox powdered cleaner, 1×4 lb. box	Alconox, Inc. P/N 1104-1
Acetone	
Methanol	
Isopropanol	
Plastic bags	
Chemical waste disposal jars	
Lens cleaning wipes	McMaster-Carr P/N 52465T7
Kim wipes	
Gloves	

A.8 Piezo modulation

Item	Vendor, P/N
Piezo actuator, stacked ceramic multi-layer, low-voltage, 5mm×5mm×10mm, 60V max, 1000N blocking force	Noliac North America, Inc. P/N SCMAP02-H10-A01
Function Generator, 4MHz sweep	Digi-Key P/N BK4001A-ND
(2) Sapphire windows	Swiss Jewel Company P/N W7.87
Clamp	

A.9 Temperature control

Item	Vendor, P/N
(2) TECs, ceramic plate Peltier solid-state thermoelectric coolers,	Laird Technology P/N 56460-501, Sager P/N 263388, item CP10,127,05,L1,W4.5
Arctic Silver 5 thermal paste	
Thermistor 50k	EPCOS P/N B57861S0503F040
AD590 temperature transducer	Thorlabs P/N AD590

A.10 Components for beam output

Item	Vendor, P/N
Microscope slides for Brewster window	
Diamond-tipped scribe, fixed point	McMaster-Carr P/N 2018A51
anamorphic prism pair, AR-coated, B coating for 650-1050nm, unmounted	Thorlabs P/N PS871-B, N-SF11
prism alignment etching	
Optical isolator, fixed band, body type II	Thorlabs P/N IO-2.5D-994-VLP
Fiber couple assembly	
IR viewing card	Thorlabs P/N VRC2
Optomechanical components (clamps, mounts, etc.)	
Optomechanical v-clamp, small with PM3 clamping arm	Thorlabs P/M VC1
plastic tweezers	

A.11 Vacuum

Item	Vendor, P/N
Vacuum seal-off valve, 1/4" aluminum,	DLH Industries Inc. P/N V1021-1
Valve operator, 25mm ISO flange, 1/4"	DLH Industries Inc. P/N V1025-3-25

Appendix B

Product numbers for cavity components

Item	Vendor, P/N
MgO:PPLN, 20mm long crystal	Covesion P/N MSHG976-0.5-20
PPLN oven	Covesion P/N PV20
Temperature controller	Covesion P/N OC1
mirror 1 (incoupling)	
mirror 2	
mirror 3	
mirror 4	
piezo	
mirror mounts	

Bibliography

- [1] S. Stellmer, M. K. Tey, B. Huang, R. Grimm, and F. Schreck. Bose-einstein condensation of strontium. *Physical Review Letters*, 103, 2009.
- [2] A. G. Truscott, N. R. Heckenberg, and H. Rubinsztein-Dunlop. ? *Optical and Quantum Electronics*, 31:417–430, 1999.
- [3] Steck Group. Steck group web page. <http://atomoptics.uoregon.edu/unilaser/>.
- [4] E. C. Cook, P. J. Martin, T. L. Brown-Heft, J. C. Garman, and D. A. Steck. High passive-stability diode-laser design for use in atomic-physics experiments. *Review of Scientific Instruments*, 83, 2012.
- [5] M. Falkenau. *Chromium atoms in a deep optical dipole trap*. PhD thesis, Universität Stuttgart, 2008.
- [6] I. Biaggio, P. Kerkoc, L. S. Wu, P. Gunter, and B. Zysset. Refractive indices of orthorhombic knbo3 ii. phase-matching configurations for nonlinear-optical interactions. *Journal of the Optical Society of America B*, 9(4):507–517, 1992.
- [7] Eksma Optics Inc. Eksma optics web page. <http://eksmaoptics.com/formulas-and-tools/>.
- [8] R. W. Boyd. *Nonlinear optics*. Academic Press, Boston, San Diego, 1992.
- [9] Covesion, Inc. Covesion web page. <http://www.covesion.com/support/ppln-tutorial.html>.
- [10] CVI Melles Griot Inc. Cvi melles griot web page. https://www.cvimellesgriot.com/Products/Documents/TechnicalGuide/Spectral_Analysis.pdf.
- [11] D. Skoczowsky, A. Jechow, H. Sturmer, T. Possner, J. Sacher, and R. Menzel. Quasi-monolithic ring resonator for efficient frequency doubling of an external cavity diode laser. *Applied Physics B*, 98:751–757, 2010.

- [12] S. Stellmer. *Degenerate quantum gases of strontium*. PhD thesis, University of Innsbruck, 2013.
- [13] N. Poli. *Raffreddamento ed intrappolamento di atomi stronzio: verso un nuovo standard di frequenza nella regione ottica*. PhD thesis, Università Degli Studi di Firenze, 2005.
- [14] Newport Richardson Inc. Newport richardson online handbook. <http://gratings.newport.com/information/handbook/handbook.asp>.
- [15] Peter Powers. *Fundamentals of Nonlinear Optics*. CRC Press, Taylor and Francis Group, 2011.
- [16] G. D. Boyd and D. A. Kleinman. Parametric interaction of focused gaussian light beams. *Journal of Applied Physics*, 39, 1968.
- [17] B. Zysset, I. Biaggio, and P. Gunter. Refractive indices of orthorhombic knbo₃. i. dispersion and temperature dependence. *Journal of the Optical Society of America B*, 9(3):380–386, 1992.
- [18] O. Gayer, Z. Sacks, E. Galun, and A. Arie. Temperature and wavelength dependent refractive index equations for mgo-doped congruent and stoichiometric linbo₃. *Appl. Phys. B*, 91, 2008.
- [19] A. Ashkin, G.D. Boyd, and J.M. Dziedzic. Resonant optical second harmonic generation and mixing. *IEEE Journal of Quantum Electronics*, 2:109–124, 1966.
- [20] J.R. Schwesyg, A. Markosyan, M. Falk, M.C.C. Kajiyama, D.H. Jundt, K. Buse, and M.M. Fejer. Optical loss mechanisms in magnesium-doped lithium niobate crystals in the 300 to 2950 nm wavelength range. In *Advances in Optical Materials*, volume Nonlinear Crystals and Processes II, 2011.
- [21] A. Douillet, J. J. Zondy, A. Yelisseyev, S. Lobanov, and L. Isaenko. Stability and frequency tuning of thermally loaded continuous-wave aggas₂ optical parametric oscillators. *J. Opt. Soc. Am. B*, 16, 1999.
- [22] Ulrich Ströbner. *Development of Optical Synthesizers*. PhD thesis, Universitat Konstanz, 2001.